Dynamics and control of full-body humanoid robots for contact tasks

State-of-the-art seminar
by
Vyankatesh Raghav Ashtekar
(20105279)
under the supervision of
Dr. Ashish Dutta, Professor

Department of Mechanical Engineering
Indian Institute of Technology Kanpur
Kanpur, UP 208016, India

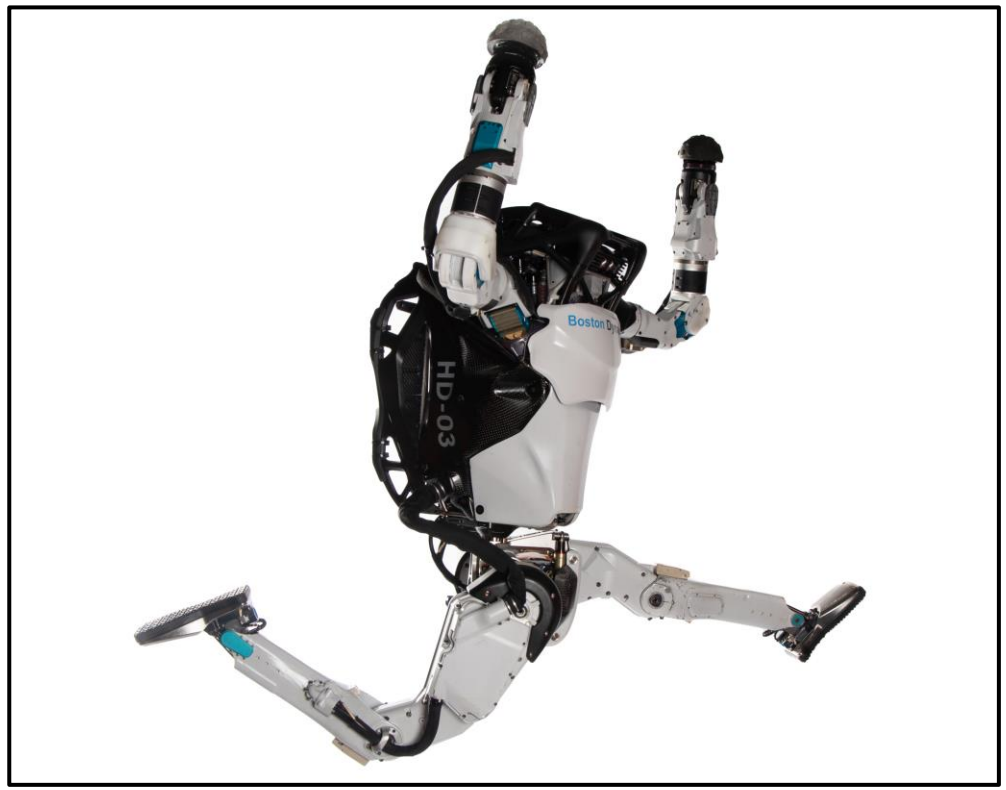
HD-03


HONDA

Outline:

- Background and introduction
- Overview: rigid body kinematics & dynamics
- Simplified models of humanoids for walking and balancing
- Dynamics of full-body humanoids
- Platforms for simulation
- Literature summary and gaps
- Proposed work

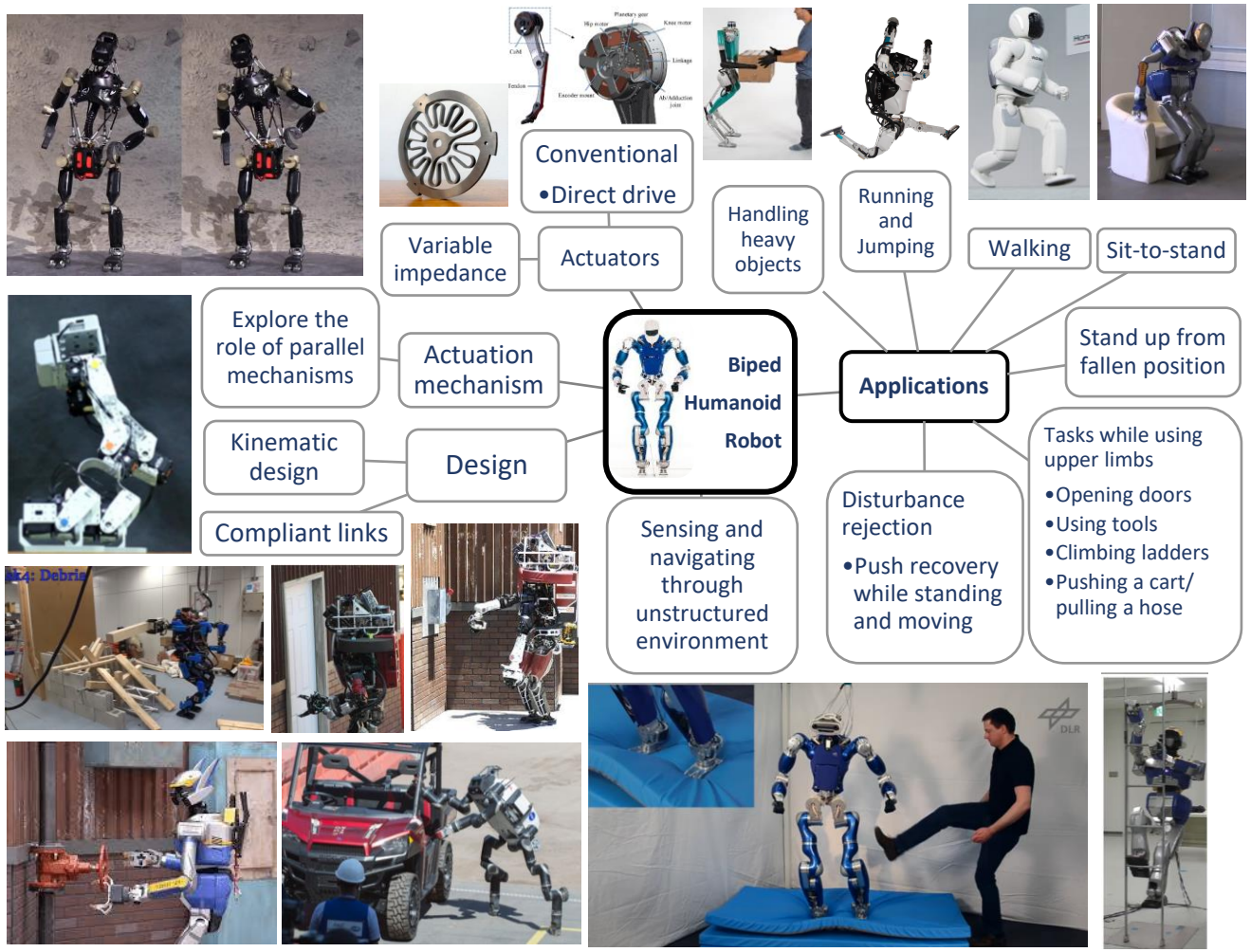

Before we start,

Why 'humanoid' robots?
Why walking machines?
Why biped walking machines?

Events that spur innovation in humanoid robots

- DARPA Robotics Challenge 2013-15
  - Tasks:
    1. Drive a utility vehicle at the site.
    2. Travel dismounted across the rubble.
    3. Remove debris blocking an entryway.
    4. Open a door and enter a building.
    5. Climb an industrial ladder and traverse an industrial walkway.
    6. Use a tool to break through a concrete panel.
    7. Locate and close a valve near a leaking pipe.
    8. Connect a fire hose to a standpipe and turn on a valve.

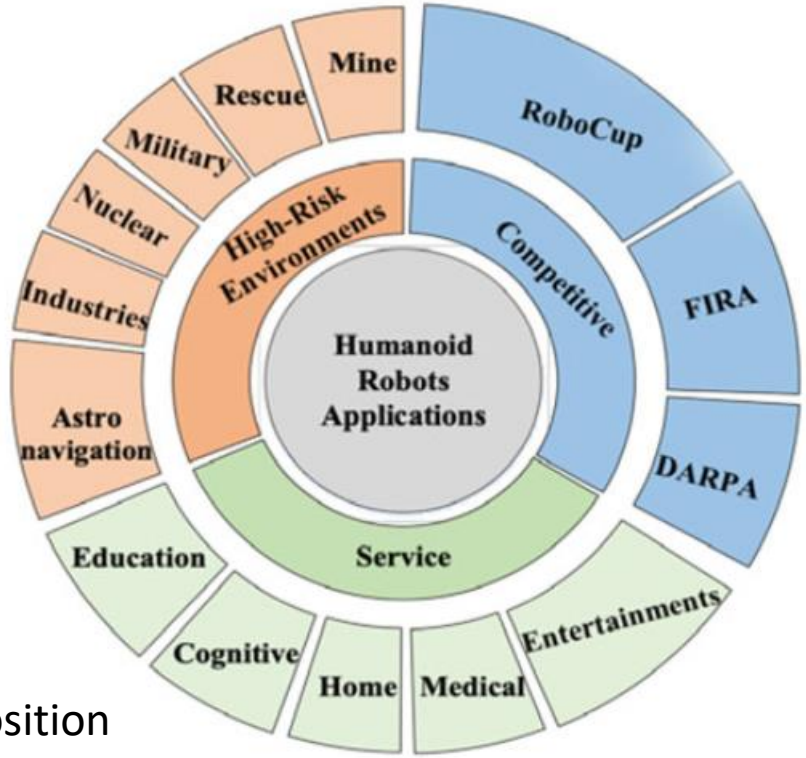

- 'Robocup AdultSize League' teams
  - Notably, all the participating robots have the ability to stand up from a fallen position
  - Conference: https://link.springer.com/conference/robocup
- FIRA
  - Robot sports
  - Founded by Prof. Jong-Hwan Kim, KAIST, Korea in 1996 – is the oldest robot soccer competition in the world.

Saeedvand, S., Jafari, M., Aghdasi, H., & Baltes, J. (2019). A comprehensive survey on humanoid robot development. *The Knowledge Engineering Review, 34*, E20. doi:10.1017/S0269888919000158

State-of-the-art humanoids

	ASIMO	**HRP-5/4/3/2**	**ATLAS**	**TORO**	**LOLA**	**Valkyrie**	
	Honda, Japan	Kawada Robotics, AIST Japan	Boston Dynamics, USA	DLR RM, Germany	TU Munich, Germany	NASA, USA	• **CoMAN** • (iit, Italy) • **SARCOS** (CMU) • **HUBO** (KAIST) • **TALOS** (Spain) • **RH5**(DFKI, Germany) • **WABIAN - 2R** (U. Waseda, Japan) • **AR-600** (RUSSIA)
DOF	57 (31+26)	30 (28+2)	28	39 (27+12)	26 (has toe)	44	
Actuation	Electric	Electric	Hydraulic	Electric	Electric	Electric	
Height	1.3 m	1.54 m	1.5 m	1.74 m	1.76 m	1.90 m	
Weight	50 kg	58 kg	89 kg	76 kg	68 kg	125 kg	
Speciality	The first high DOF full-body humanoid	Open-source project. Oldest robot to stand up from fall on flat ground	Amazing acrobatic skills, high power: weight ratio	Torque controlled, Safe to work along with humans	Multi-contact locomotion (locomotion while taking support)	Compliant actuators with series elastic actuators	
							

Source: https://robots.ieee.org/robots/

Bipedal Humanoid Hardware Design: a Technology Review

Table 1 recently developed bipedal humanoid robots with a full humanoid body plan

Name	Height (cm)	Weight (kg)	Actuation	No. of actuators	Sensing	Manufacture	Year	Tentative price
Asimo (2011 model)	130	48	Electric Harmonic Drive	57	Joints: position IMU, 2x F/T, Camera	Magnesium alloy	2011	2500000 USD
Atlas (Next Generation)	150	75	Hydraulic Servo-valves	28	Joints: position, force Lidar, Stereo vision	Metal, 3D-printed	2016	N/A
Atlas-Unplugged	188	182	Hydraulic Servo-valves	30	Joints: position, force Lidar, Stereo vision	Aluminium Titanium	2015	2000000 USD
Digit	155	42.2	Electric Cycloid Drive	16	Joints: position IMU, Lidar, 4x Depth Cam.	Aluminium, milled Carbon fiber	2019	250000 USD
HRP-5P	183	101	Electric Harmonic Drive	37	Joints: position 4x F/T, IMU, Lidar Stereo Vision	Metal (unspecified)	2018	N/A
Hydra	185	135	Hydraulic EHA	41	Joints: position, force IMU, 2x F/T, Lidar, Stereo	Aluminium milled	2016	N/A
Kengoro	167	55.9	Electric Muscle /w Tendons	106	Joints: position, tension IMU, 2x F/T, Stereo Vision	Aluminium 3D-printed	2016	N/A
NimbRo-OP2(X)	135	19	Electric DC Servo-motors	34	Joints: position IMU, Stereo Vision	PA12 Nylon 3D-printed	2017	25000 EUR
TALOS	175	95	Electric Harmonic Drive	32	Joints: position, torque IMU, RGBD camera	Metal (unspecified)	2017	900000 EUR
Toro	174	76.4	Electric Harmonic Drive	39	Joints: position, torque 2x IMU, RGB&D cameras	Aluminium milled	2014	N/A
Valkyrie	187	129	Electric SEA	44	Joints: position, force, torque 7x IMU, 2xF/T, Multiple cameras	Metal (unspecified)	2013	2000000 USD
WALK-MAN	191	132	Electric SEA	29	Joints: position, torque 2x IMU, 4x F/T, Lidar Stereo Vision	Aluminium milled	2015	N/A

Prime movers:

1. Electric motor
2. Hydraulic actuator
3. Pneumatic actuator
4. Pneumatic muscle

Transmission:

1. Gearbox
2. Harmonic drive
3. Series elastic element
4. Tendon drive
5. Mechanism

Sensing:

1. Joint encoder
2. Torque sensors
3. Force sensors
4. IMU
5. Lidar
6. Stereo camera
7. RGB&D camera

Ficht, G., Behnke, S. Bipedal Humanoid Hardware Design: a Technology Review. *Curr Robot Rep* **2,** 201–210 (2021). https://doi.org/10.1007/s43154-021-00050-9

Kinematics & Dynamics

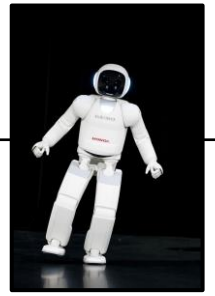

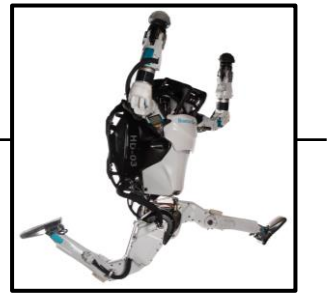

- Humanoids can be described either as an **open-loop/tree-type** or **closed-loop** or a **floating multi-body system** (with possible internal closed loops)
- Kinematics
  - Open-loop / tree-type
    - Forward kinematics (FK) has a unique solution, expressions in closed form
    - Inverse kinematics (IK) has multiple branches
  - Closed-loop
    - FK has multiple branches
    - IK has multiple branches

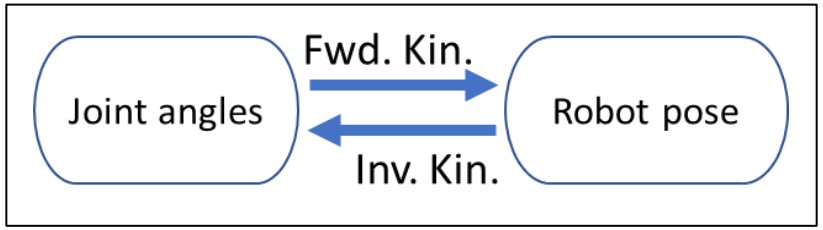

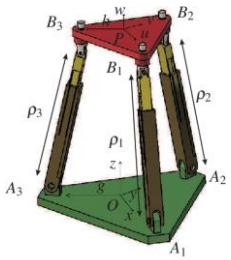

Single support phase (SSP)	Serial/ tree type open chain	#DOF =#Actuators
Double/ multiple support phase	Closed single/ multiple loop chain	Redundantly actuated
Flight phase	Floating body	Underactuated

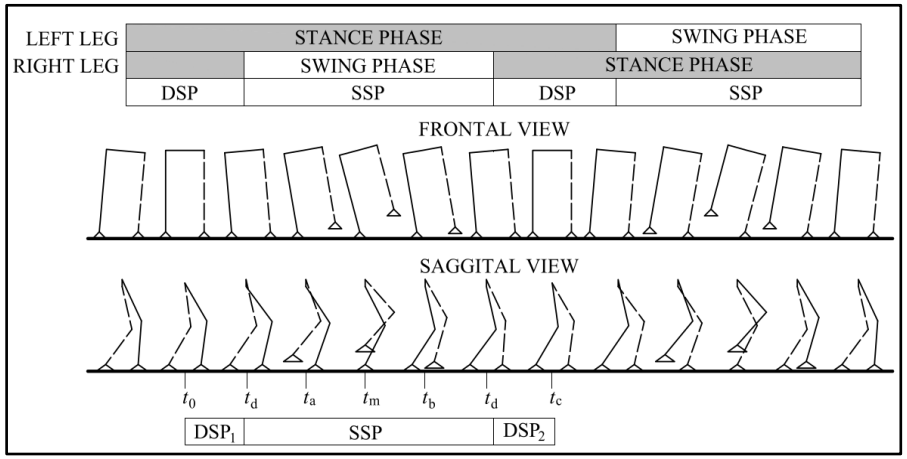

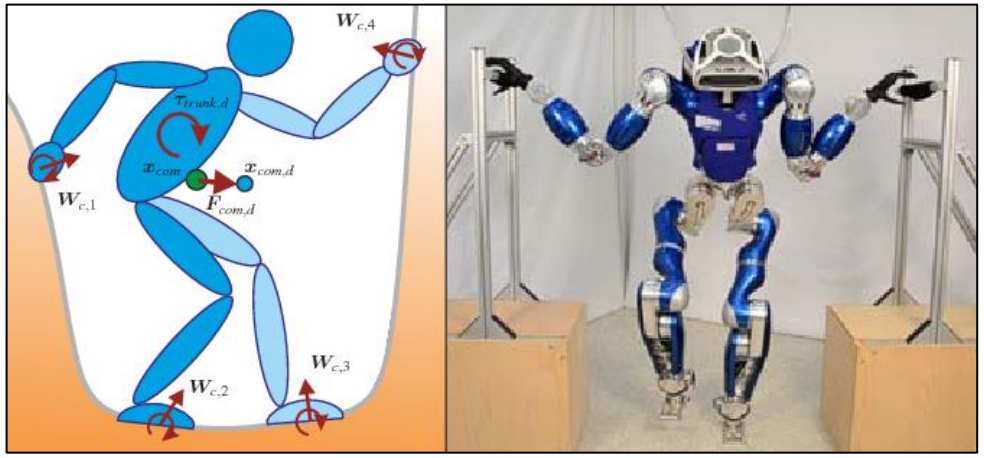

Sarkar, A., & Dutta, A. (2015). 8-DoF biped robot with compliant-links. Robotics and Autonomous Systems, 63, 57-67.
Ghosal A. (2006) Robotics: Fundamental Concepts and Analysis (pp. 151-219), New Delhi, Oxford University Press.

Kinematics & Dynamics

- The problem can be classified as a hybrid dynamics problem

- Equations are presented here in the Lagrangian form.

1. Fixed base system
   - The humanoid has different equations in different phases
   - Single stance phase

$$\boldsymbol{M}(\boldsymbol{q})\ddot{\boldsymbol{q}} + \boldsymbol{C}(\boldsymbol{q},\dot{\boldsymbol{q}})\dot{\boldsymbol{q}} + \boldsymbol{G}(\boldsymbol{q}) = \boldsymbol{\tau}^{nc}$$

$$\text{where } \boldsymbol{\tau}^{nc} = \boldsymbol{\tau}_m \text{ or } \boldsymbol{\tau}^{nc} = \boldsymbol{J}^T\boldsymbol{F}$$

   - Double stance/ multi-contact phase

$$\boldsymbol{M}(\boldsymbol{q})\ddot{\boldsymbol{q}} + \boldsymbol{C}(\boldsymbol{q},\dot{\boldsymbol{q}})\dot{\boldsymbol{q}} + \boldsymbol{G}(\boldsymbol{q}) = \boldsymbol{J}_{\eta q}^T\boldsymbol{\lambda} + \boldsymbol{\tau}^{nc}$$

$$\boldsymbol{\eta}(\boldsymbol{q}) = \boldsymbol{0}$$

$$\boldsymbol{J}\dot{\boldsymbol{q}} + \boldsymbol{\Phi}(t) = \boldsymbol{0}$$

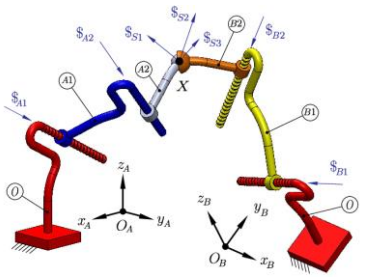

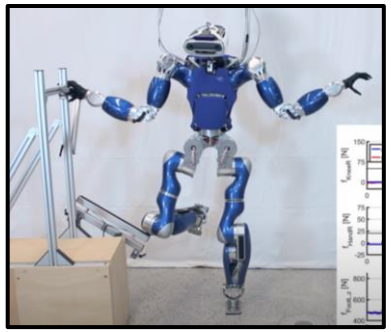

   - Rheonomic constraints $\Phi(t)$ are encountered in the case of compliant bodies
   - Above equations are derived assuming <u>bilateral constraints</u>
   - An *n*-DOF system holonomic constraints only can be modelled in *n* generalised coordinates
   - An *n*-DOF system non-holonomic constraints need *n*+1 generalised coordinates

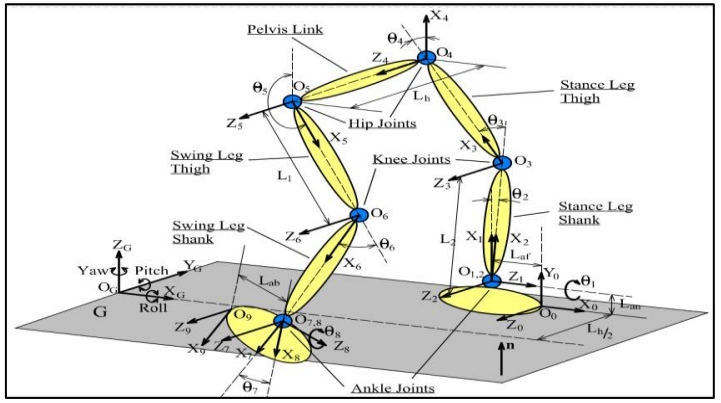

2. Floating base system
   - Suitable for tree-type systems
   - We will see more on this later in the presentation

Ghosal. (2006) Robotics: Fundamental Concepts and Analysis (pp. 151-219), New Delhi, Oxford University Press.
Greenwood, D. T. (1988). *Principles of dynamics* (pp. 239-298). Englewood Cliffs, NJ: Prentice-Hall.

Kinematics & Dynamics

Inverse dynamics

- Estimating required actuator torques/ forces for a planned motion
- Required in feed-forward control strategies
- Algorithms
  - Recursive NE algorithm

Forward dynamics

- Simulate physics without conducting physical experiments
- Predict motion faster than real-time (to avoid falls?)
- Required in computed torque control
- Algorithms
  - Inertia Matrix methods: Joint-space Inertia Matrix method, Composite Rigid Body algorithm
  - Propagation methods: Articulated Rigid-Body algorithm

- Best of the algorithms for forward and inverse dynamics are documented in the book 'Rigid Body Dynamics Algorithms' by Prof Roy Featherstone.

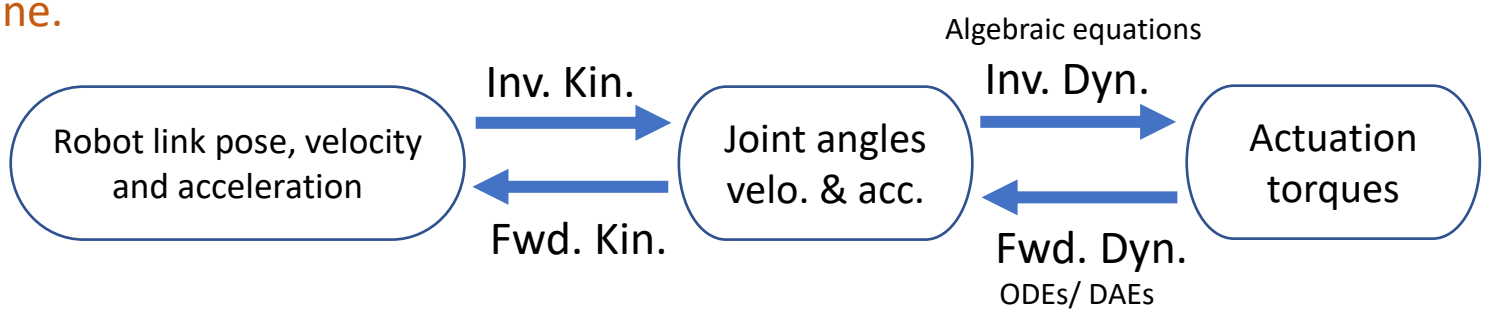

Luh, J. Y. S., Walker, M. W., and Paul, R. P. C. (June 1, 1980). "On-Line Computational Scheme for Mechanical Manipulators." ASME. J. Dyn. Sys., Meas., Control. June 1980; 102(2): 69–76. https://doi.org/10.1115/1.3149599

Featherstone R. (2008) Dynamics of Rigid Body Systems. In: Rigid Body Dynamics Algorithms. Springer, Boston, MA. https://doi.org/10.1007/978-1-4899-7560-7_3

Closed-Form Inverse Kinematic Joint Solution for Humanoid Robots

Inputs: Position and orientation of end effector w.r.t hip/reference frame

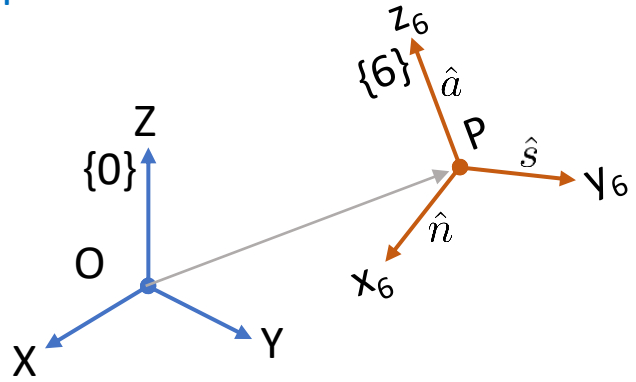

$$
{}^0\mathbf{T}_6 = \prod_{i=1}^{6} {}^{i-1}\mathbf{A}_i = {}^0\mathbf{A}_1 {}^1\mathbf{A}_2 {}^2\mathbf{A}_3 {}^3\mathbf{A}_4 {}^4\mathbf{A}_5 {}^5\mathbf{A}_6
$$

$$
= \begin{bmatrix} \mathbf{x}_6 & \mathbf{y}_6 & \mathbf{z}_6 & \mathbf{p}_6 \\ 0 & 0 & 0 & 1 \end{bmatrix} = \begin{bmatrix} \mathbf{n} & \mathbf{s} & \mathbf{a} & \mathbf{p} \\ 0 & 0 & 0 & 1 \end{bmatrix}
$$

Forward Kinematics using (original)DH convention

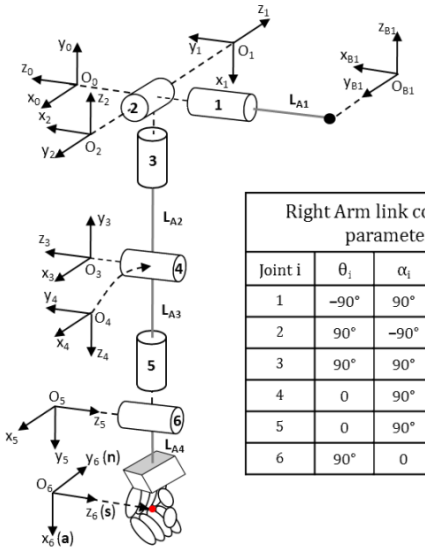

Right Arm link coordinate parameters				
Joint i	θ_i	α_i	a_i	d_i
1	−90°	90°	0	0
2	90°	−90°	0	0
3	90°	90°	0	$-L_{A2}$
4	0	90°	0	0
5	0	90°	0	L_{A3}
6	90°	0	L_{A4}	0

Fig. 2. Link Coordinate Frames of the Right Arm of a Hubo KHR-4 Robot and its D-H Parameters.

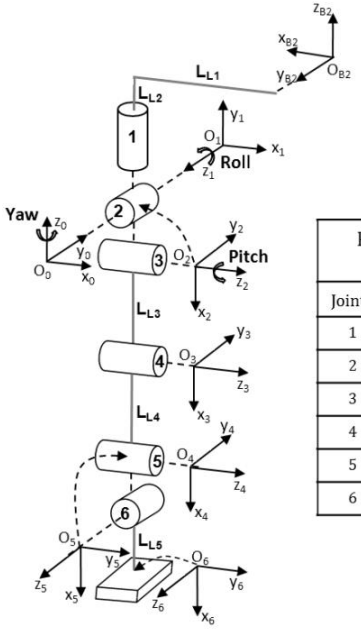

Right Leg link coordinate parameters				
Joint i	θ_i	α_i	a_i	d_i
1	0	90°	0	0
2	−90°	−90°	0	0
3	0	0	L_{L3}	0
4	0	0	L_{L4}	0
5	0	90°	0	0
6	0	0	L_{L5}	0

Fig. 3. Link Coordinate Frames of the Right Leg of a Hubo KHR-4 Robot and its D-H Parameters.

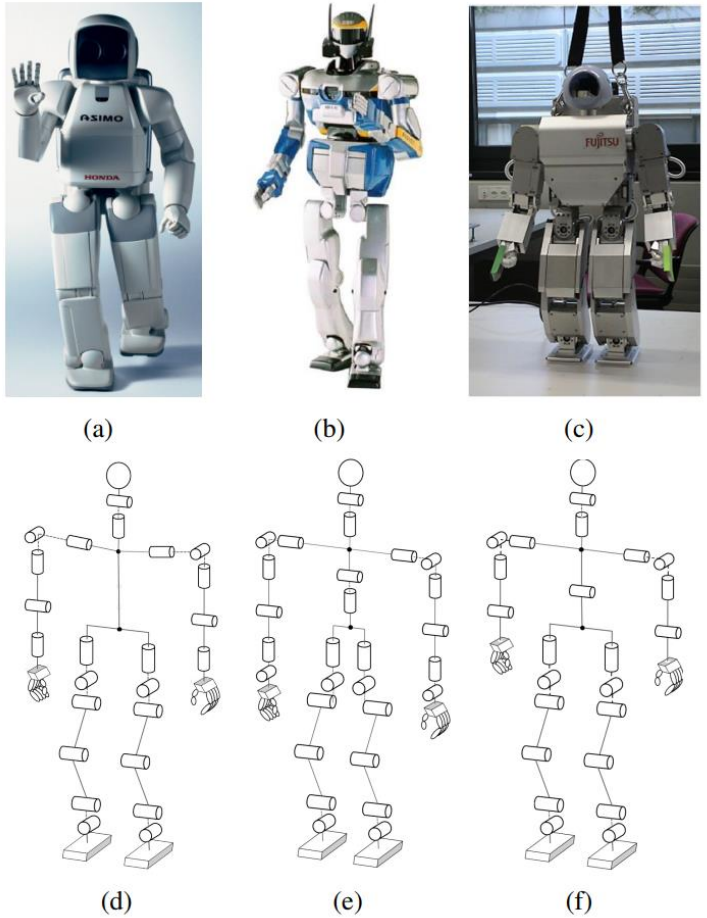

Fig. 4. (a) HONDA ASIMO Robot and its associated kinematic diagram in (d), (b) AIST HRP-2 Robot and its associated kinematic diagram in (e), and (c) Fujitsu HOAP-2 Robot and its associated kinematic diagram in (f).

M. A. Ali, H. Andy Park and C. S. G. Lee, "Closed-form inverse kinematic joint solution for humanoid robots," *2010 IEEE/RSJ International Conference on Intelligent Robots and Systems*, 2010, pp. 704-709, doi: 10.1109/IROS.2010.5649842.

Closed-Form Inverse Kinematic Joint Solution for Humanoid Robots

Contribution:

- Closed-form inverse kinematics for certain full-body humanoids
- "The novelty here is to observe the intersection of 3 adjacent joint axes in the kinematic chain for decoupling the robotic arm/leg system into positioning and orientation subsystems for solving its joint solution."
- Steps to the solution
  1. Provide ${}^0A_6$
  2. Compute $T' = ({}^0A_6)^{-1}$
  3. Solve the simple inverse kinematics problem to find out actuation variables θ_i
  4. Detect singularities
     1. $\theta_2 = 0$ or π
     2. $\theta_4 = 0$
     3. Above two cases occurring together
  5. Choose the proper branch of solution

$$\mathtt{KNEE} = \mathrm{sign}(\mathbf{z}_3 \cdot (\mathbf{x}_3 \times \mathbf{x}_4)) = \mathrm{sign}(\mathrm{S}_4)$$
$$\mathtt{HIP} = \mathrm{sign}(\mathbf{z}_1 \cdot (\mathbf{x}_1 \times \mathbf{x}_2) = \mathrm{sign}(\mathrm{S}_2)$$

6. $$\mathtt{ANKLE} = \mathrm{sign}(\mathbf{p}' \cdot \mathbf{x}_5) = \mathrm{sign}(\mathrm{C}_{5\psi}),$$

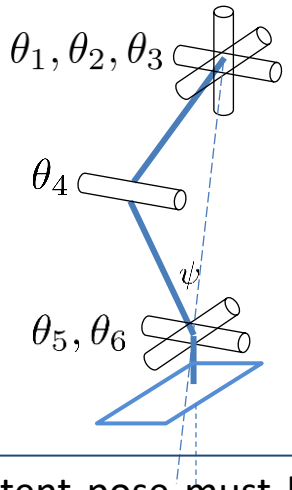

In the double support phase/ multi-contact phase, a consistent pose must be supplied for the IK problem satisfying the loop closure constraints.

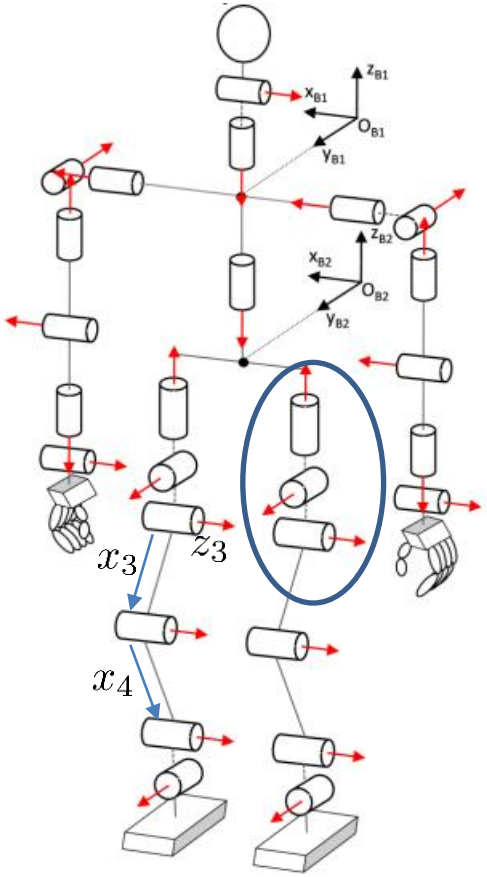

(a)

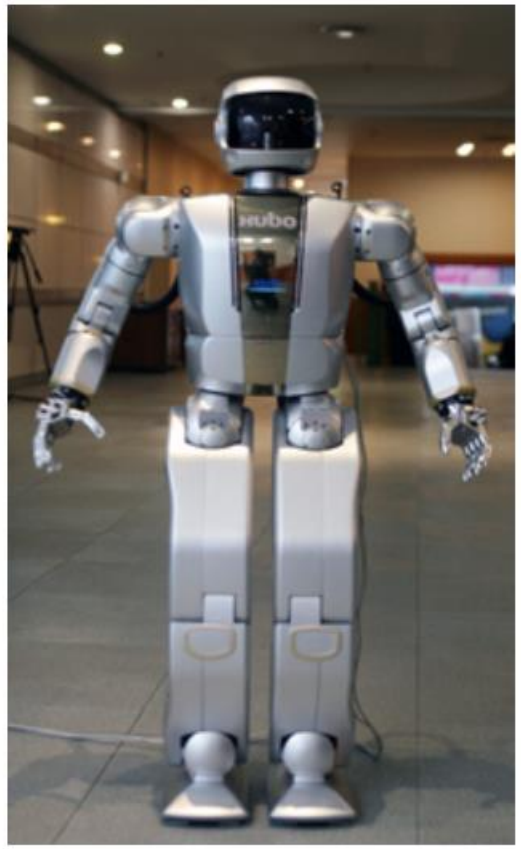

(b)

Fig. 1. A Hubo KHR-4 Humanoid Robot.

M. A. Ali, H. Andy Park and C. S. G. Lee, "Closed-form inverse kinematic joint solution for humanoid robots," *2010 IEEE/RSJ International Conference on Intelligent Robots and Systems*, 2010, pp. 704-709, doi: 10.1109/IROS.2010.5649842.

A survey: dynamics of humanoid robots

Kinematics

$$\boldsymbol{q} \stackrel{\text{def}}{=} \begin{bmatrix} \boldsymbol{q}_{\mathrm{B}}^{\mathrm{T}} & \boldsymbol{q}_{\mathrm{J}}^{\mathrm{T}} \end{bmatrix}^{\mathrm{T}}$$

$$\boldsymbol{q}_{\mathrm{J}} \stackrel{\text{def}}{=} \begin{bmatrix} \boldsymbol{q}_0^{\mathrm{T}} & \boldsymbol{q}_1^{\mathrm{T}} & \boldsymbol{q}_2^{\mathrm{T}} & \boldsymbol{q}_3^{\mathrm{T}} & \boldsymbol{q}_4^{\mathrm{T}} & \boldsymbol{q}_5^{\mathrm{T}} \end{bmatrix}^{\mathrm{T}}$$

Trunk | L arm | R arm | L leg | R leg | Head

$$\boldsymbol{J}_{\mathrm{CB}}(\boldsymbol{p},\boldsymbol{q})\dot{\boldsymbol{q}}_{\mathrm{B}} + \boldsymbol{J}_{\mathrm{CJ}}(\boldsymbol{p},\boldsymbol{q})\dot{\boldsymbol{q}}_{\mathrm{J}} = \dot{\boldsymbol{p}}.$$

$$\boldsymbol{J}_{\mathrm{CB}k}\dot{\boldsymbol{q}}_{\mathrm{B}} + \boldsymbol{J}_{\mathrm{CJ}k}\dot{\boldsymbol{q}}_{\mathrm{J}} = \dot{\boldsymbol{p}}_{\mathrm{C}k}$$

Corners of the support polygon

The equation of motion

$$\begin{bmatrix} \boldsymbol{H}_{\mathrm{BB}} & \boldsymbol{H}_{\mathrm{BJ}} \\ \boldsymbol{H}_{\mathrm{BJ}}^{\mathrm{T}} & \boldsymbol{H}_{\mathrm{JJ}} \end{bmatrix} \begin{bmatrix} \ddot{\boldsymbol{q}}_{\mathrm{B}} \\ \ddot{\boldsymbol{q}}_{\mathrm{J}} \end{bmatrix} + \begin{bmatrix} \boldsymbol{b}_{\mathrm{B}} \\ \boldsymbol{b}_{\mathrm{J}} \end{bmatrix} = \begin{bmatrix} \boldsymbol{0} \\ \boldsymbol{\tau}_{\mathrm{J}} \end{bmatrix} + \begin{bmatrix} \boldsymbol{\tau}_{\mathrm{CB}} \\ \boldsymbol{\tau}_{\mathrm{CJ}} \end{bmatrix}$$

(6+n) x 1

$$\begin{bmatrix} \boldsymbol{\tau}_{\mathrm{CB}} \\ \boldsymbol{\tau}_{\mathrm{CJ}} \end{bmatrix} = \sum_{i=0}^{5} \int_{\boldsymbol{p}\in\mathcal{S}_i} \begin{bmatrix} \boldsymbol{J}_{\mathrm{CB}}^{\mathrm{T}}(\boldsymbol{p},\boldsymbol{q}) \\ \boldsymbol{J}_{\mathrm{CJ}}^{\mathrm{T}}(\boldsymbol{p},\boldsymbol{q}) \end{bmatrix} \boldsymbol{\sigma}(\boldsymbol{p})\mathrm{d}s,$$

Discretize

$$\begin{bmatrix} \boldsymbol{\tau}_{\mathrm{CB}} \\ \boldsymbol{\tau}_{\mathrm{CJ}} \end{bmatrix} = \sum_{k=1}^{N_{\mathrm{C}}} \begin{bmatrix} \boldsymbol{J}_{\mathrm{CB}k}^{\mathrm{T}} \\ \boldsymbol{J}_{\mathrm{CJ}k}^{\mathrm{T}} \end{bmatrix} \boldsymbol{f}_{\mathrm{C}k}$$

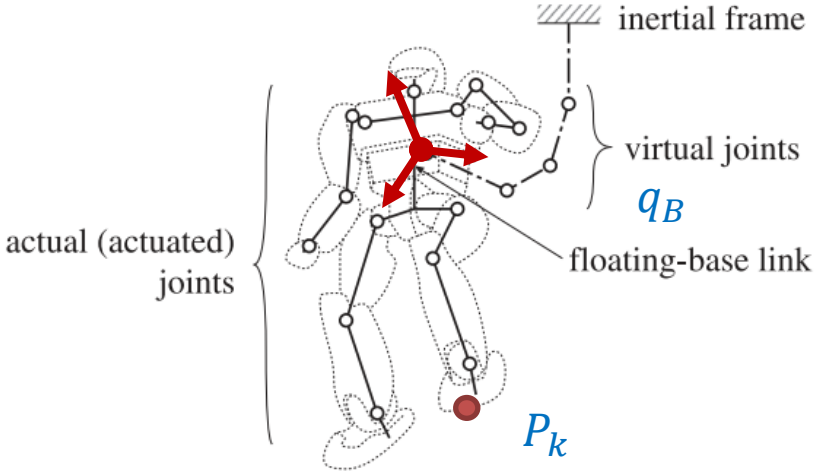

$$\left[\begin{array}{cc|ccc|ccc} \boldsymbol{H}_{\mathrm{BB}} & \boldsymbol{H}_{\mathrm{BJ}} & -\boldsymbol{J}_{\mathrm{CB1}}^{\mathrm{T}} & \cdots & -\boldsymbol{J}_{\mathrm{CB}N_{\mathrm{C}}}^{\mathrm{T}} & \boldsymbol{O} & \cdots & \boldsymbol{O} \\ \boldsymbol{H}_{\mathrm{BJ}}^{\mathrm{T}} & \boldsymbol{H}_{\mathrm{JJ}} & -\boldsymbol{J}_{\mathrm{CJ1}}^{\mathrm{T}} & \cdots & -\boldsymbol{J}_{\mathrm{CJ}N_{\mathrm{C}}}^{\mathrm{T}} & \boldsymbol{O} & \cdots & \boldsymbol{O} \\ \hline \boldsymbol{J}_{\mathrm{CB1}} & \boldsymbol{J}_{\mathrm{CJ1}} & \boldsymbol{O} & \cdots & \boldsymbol{O} & -\boldsymbol{1} & & \boldsymbol{O} \\ \vdots & \vdots & \vdots & & \vdots & & \ddots & \\ \boldsymbol{J}_{\mathrm{CB}N_{\mathrm{C}}} & \boldsymbol{J}_{\mathrm{CJ}N_{\mathrm{C}}} & \boldsymbol{O} & \cdots & \boldsymbol{O} & \boldsymbol{O} & & -\boldsymbol{1} \end{array}\right] \left[\begin{array}{c} \ddot{\boldsymbol{q}}_{\mathrm{B}} \\ \ddot{\boldsymbol{q}}_{\mathrm{J}} \\ \boldsymbol{f}_{\mathrm{C1}} \\ \vdots \\ \boldsymbol{f}_{\mathrm{C}N_{\mathrm{C}}} \\ \hline \ddot{\boldsymbol{p}}_{\mathrm{C1}} \\ \vdots \\ \ddot{\boldsymbol{p}}_{\mathrm{C}N_{\mathrm{C}}} \end{array}\right] = \left[\begin{array}{c} -\boldsymbol{b}_{\mathrm{B}} \\ \boldsymbol{\tau}_{\mathrm{J}} - \boldsymbol{b}_{\mathrm{J}} \\ -\dot{\boldsymbol{J}}_{\mathrm{CB1}}\dot{\boldsymbol{q}}_{\mathrm{B}} - \dot{\boldsymbol{J}}_{\mathrm{CJ1}}\dot{\boldsymbol{q}}_{\mathrm{J}} \\ \vdots \\ -\dot{\boldsymbol{J}}_{\mathrm{CB}N_{\mathrm{C}}}\dot{\boldsymbol{q}}_{\mathrm{B}} - \dot{\boldsymbol{J}}_{\mathrm{CJ}N_{\mathrm{C}}}\dot{\boldsymbol{q}}_{\mathrm{J}} \end{array}\right]$$

(6+n+3Nc) x (6+n+3Nc +**3Nc**)

(6+n+3Nc) x 1

(6+n+3Nc +**3Nc**) x 1

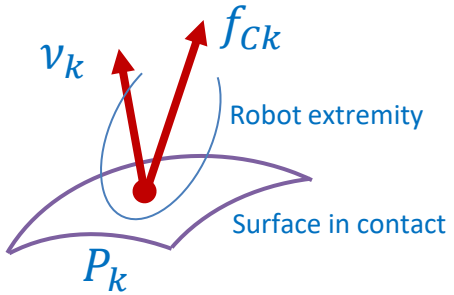

- Time evolution is described by a differential inclusion
- The problem can be converted to LCP (when $\mu_s = \mu_k$) and solved
- The field of study is: Non-smooth/ hybrid mechanics (e.g. a bouncing ball)

Rigid surfaces in contact

(I: stationary contact)

$$\begin{cases} \dot{\boldsymbol{p}}_{\mathrm{C}k} = \boldsymbol{0} \\ \boldsymbol{\nu}_{\mathrm{k}}^{\mathrm{T}}\boldsymbol{f}_{\mathrm{C}k} \geq 0 \\ \|\boldsymbol{f}_{\mathrm{C}k} - (\boldsymbol{\nu}_{\mathrm{k}}^{\mathrm{T}}\boldsymbol{f}_{\mathrm{C}k})\boldsymbol{\nu}_k\| \leq \mu_{\mathrm{S}k}\boldsymbol{\nu}_{\mathrm{k}}^{\mathrm{T}}\boldsymbol{f}_{\mathrm{C}k} \end{cases}$$

3Nc independent equalities

(II: sliding)

$$\begin{cases} \dot{\boldsymbol{p}}_{\mathrm{C}k} \neq \boldsymbol{0}, \quad \boldsymbol{\nu}_k^{\mathrm{T}}\dot{\boldsymbol{p}}_{\mathrm{C}k} = 0 \\ \boldsymbol{f}_{\mathrm{C}k} \times \left(\boldsymbol{\nu}_k - \mu_{\mathrm{K}k}\frac{\dot{\boldsymbol{p}}_{\mathrm{C}k}}{\|\dot{\boldsymbol{p}}_{\mathrm{C}k}\|}\right) = \boldsymbol{0} \end{cases}$$

(III: separation)

$$\begin{cases} \boldsymbol{\nu}_k^{\mathrm{T}}\dot{\boldsymbol{p}}_{\mathrm{C}k} > 0 \\ \boldsymbol{f}_{\mathrm{C}k} = \boldsymbol{0} \end{cases},$$

Tomomichi Sugihara & Mitsuharu Morisawa (2020) A survey: dynamics of humanoid robots, Advanced Robotics, 34:21-22, 1338-1352, DOI: 10.1080/01691864.2020.1778524

A survey: dynamics of humanoid robots

Centroidal dynamics

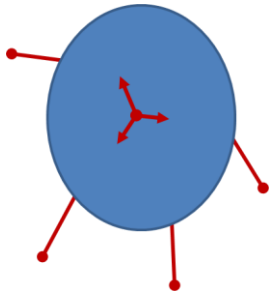

$$\begin{bmatrix} \dot{\boldsymbol{h}}_{\mathrm{L}} \\ \dot{\boldsymbol{h}}_{\mathrm{A}} \end{bmatrix} + \begin{bmatrix} m\boldsymbol{g} \\ \boldsymbol{0} \end{bmatrix} = \begin{bmatrix} \boldsymbol{f}_{\mathrm{C}} \\ \boldsymbol{n}_{\mathrm{C}} - \boldsymbol{p}_{\mathrm{G}} \times \boldsymbol{f}_{\mathrm{C}} \end{bmatrix}$$

$$\boldsymbol{h}_{\mathrm{L}} = \boldsymbol{H}_{\mathrm{L}}\dot{\boldsymbol{q}}$$

$$\boldsymbol{h}_{\mathrm{A}} = \boldsymbol{H}_{\mathrm{A}}\dot{\boldsymbol{q}}$$

Centroidal Momentum Matrices (CMM)

$$\begin{bmatrix} \boldsymbol{H}_{\mathrm{L}} \\ \boldsymbol{H}_{\mathrm{A}} \end{bmatrix} \equiv \begin{bmatrix} \boldsymbol{H}_{\mathrm{BB}} & \boldsymbol{H}_{\mathrm{BJ}} \end{bmatrix}$$

$$\begin{bmatrix} \dot{\boldsymbol{H}}_{\mathrm{L}}\dot{\boldsymbol{q}} + m\boldsymbol{g} \\ \dot{\boldsymbol{H}}_{\mathrm{A}}\dot{\boldsymbol{q}} \end{bmatrix} \equiv \boldsymbol{b}_{\mathrm{B}}$$

$$\boxed{\begin{bmatrix} \boldsymbol{H}_{\mathrm{BB}} & \boldsymbol{H}_{\mathrm{BJ}} \\ \boldsymbol{H}_{\mathrm{BJ}}^{\mathrm{T}} & \boldsymbol{H}_{\mathrm{JJ}} \end{bmatrix} \begin{bmatrix} \ddot{\boldsymbol{q}}_{\mathrm{B}} \\ \ddot{\boldsymbol{q}}_{\mathrm{J}} \end{bmatrix} + \begin{bmatrix} \boldsymbol{b}_{\mathrm{B}} \\ \boldsymbol{b}_{\mathrm{J}} \end{bmatrix} = \begin{bmatrix} \boldsymbol{0} \\ \boldsymbol{\tau}_{\mathrm{J}} \end{bmatrix} + \begin{bmatrix} \boldsymbol{\tau}_{\mathrm{CB}} \\ \boldsymbol{\tau}_{\mathrm{CJ}} \end{bmatrix}}$$

When the robot is in air:

$$\boldsymbol{H}_{\mathrm{BB}}\dot{\boldsymbol{q}}_{\mathrm{B}} + \boldsymbol{H}_{\mathrm{BJ}}\dot{\boldsymbol{q}}_{\mathrm{J}} = \boldsymbol{h}_{\mathrm{B0}} : \text{const.}$$

$$\dot{\boldsymbol{q}}_{\mathrm{B}} = \boldsymbol{H}_{\mathrm{BB}}^{-1}\boldsymbol{h}_{\mathrm{B0}} - \boldsymbol{H}_{\mathrm{BB}}^{-1}\boldsymbol{H}_{\mathrm{BJ}}\dot{\boldsymbol{q}}_{\mathrm{J}}$$

$$\dot{\boldsymbol{q}}_{\mathrm{J}} = \boldsymbol{H}_{\mathrm{BJ}}^{\#}(\boldsymbol{h}_{\mathrm{B0}} - \boldsymbol{H}_{\mathrm{BB}}\dot{\boldsymbol{q}}_{\mathrm{B}}) + (\boldsymbol{1} - \boldsymbol{H}_{\mathrm{BJ}}^{\#}\boldsymbol{H}_{\mathrm{BJ}})\boldsymbol{\eta}$$

- These relations are important for full-body motion planning and control without affecting the gross motion of the robot

Overview of humanoid motion resolution:

- Dynamical requirements keep changing due to varying structure
- All motion requirements may not be satisfiable due to limitation on contact forces
- Stack of Tasks (SoT): Motions need to be prioritized. E.g., balancing vs performing a task
- Prioritized Motion Resolution: Computing joint torque requirements based on SoT

(A) Conserved linear/angular momentum
(B) Mechanical constraint (e.g. closed kinematic structure)
(C) Desired contact with the environment
(D) Desired (non-conserved) linear/angular momentum
(E) Desired motions of effectors in free-space

Tomomichi Sugihara & Mitsuharu Morisawa (2020) A survey: dynamics of humanoid robots, Advanced Robotics, 34:21-22, 1338-1352, DOI: 10.1080/01691864.2020.1778524

A survey: dynamics of humanoid robots

Control frameworks for the synthesis of full-body motion:

A. Method I: Generalized Inverse dynamics/ dynamics filter
   - Define trajectories of CoM and joints based on SoT. Generate the required values of accelerations
   - **Compute joint torques** and contact forces using EoM.

B. Method II
   - Desired contact force is determined.
   - They are considered as intermediate i/p to the system and **joint torques are determined** (either using EoM or its simplifications)

C. Method III: Resolved motion rate control/ momentum control
   - CoM trajectory is determined using the CoM-ZMP model taking into account bounds on contact forces
   - **Consistent joint angle trajectories are resolved** and joint torques required for tracking the same are computed

- A and B need torque controllable actuators.
- C has a longer history of implementation and low-back drivable position-controlled actuators can be used

Challenges and active areas of research

- Exhaustive dynamic modelling of the humanoid robot including all non-linear effects
- Handling the transition from contact to non-contact
- Exploring motion resolution methods
- Understanding humans' motion skill and implementing the same

Tomomichi Sugihara & Mitsuharu Morisawa (2020) A survey: dynamics of humanoid robots, Advanced Robotics, 34:21-22, 1338-1352, DOI: 10.1080/01691864.2020.1778524

Hybrid Dynamics: Solving Equations of Motion with Contact and Impact

Equations of motion of a rigid-body system in joint space, subject to multiple frictionless point contact constraints

$$\boldsymbol{H}\ddot{\boldsymbol{q}} + \boldsymbol{C} = \boldsymbol{\tau} + \boldsymbol{T}\boldsymbol{\lambda}$$

$$\dot{\boldsymbol{\zeta}} = \boldsymbol{M}\boldsymbol{\lambda} + \boldsymbol{d}, \quad \dot{\boldsymbol{\zeta}} \geq \boldsymbol{0}, \quad \boldsymbol{\lambda} \geq \boldsymbol{0}, \quad \dot{\boldsymbol{\zeta}}^{\mathrm{T}}\boldsymbol{\lambda} = 0$$

Constraint eq. double differentiated.

$$\begin{array}{ll} \text{minimize} & \frac{1}{2}\boldsymbol{\lambda}^{\mathrm{T}}\boldsymbol{M}\boldsymbol{\lambda} + \boldsymbol{\lambda}^{\mathrm{T}}\boldsymbol{d} \\ \text{subject to} & \boldsymbol{\lambda} > \boldsymbol{0}. \end{array}$$

Where,

$$\boldsymbol{M} = \boldsymbol{T}^{\mathrm{T}}\boldsymbol{H}^{-1}\boldsymbol{T}$$

$$\boldsymbol{T} = \begin{bmatrix} \boldsymbol{t}_1 & \boldsymbol{t}_2 & \cdots & \boldsymbol{t}_{n_c} \end{bmatrix}$$

$$\boldsymbol{t}_i = \left(\boldsymbol{J}^{\mathrm{T}}_{sc(i)} - \boldsymbol{J}^{\mathrm{T}}_{pc(i)}\right)\boldsymbol{n}_i$$

$$\zeta_i = \boldsymbol{n}_i \cdot \left(\boldsymbol{v}_{sc(i)} - \boldsymbol{v}_{pc(i)}\right)$$

Where,

ζ_i is the contact separation velocity

$\boldsymbol{H}$ is the joint space/ generalized inertia matrix

$\boldsymbol{q}$ is a vector of (independent) joint space/generalized variables

$\boldsymbol{C}$ is the vector of joint space/ generalized bias force

$\boldsymbol{\tau}$ is the vector of generalized (non-conservative) forces

$\boldsymbol{n}_i$ is the 6D unit force acting along the contact normal

$\boldsymbol{t}_i$ is $\boldsymbol{n}_i$ contact normal transformed in the joint space

$\boldsymbol{\lambda}$ is the vector of scalars (Lagrange multipliers)

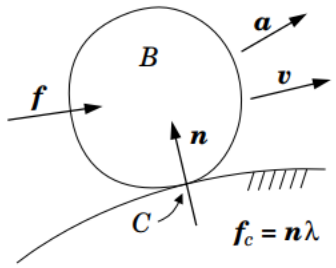

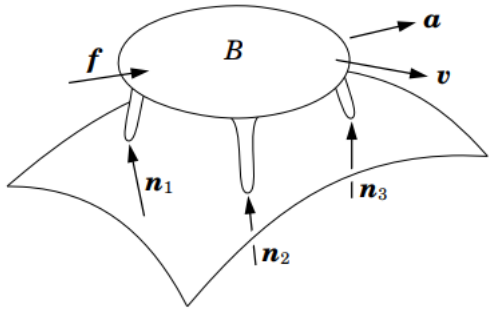

Simulation procedure:

1. Integrate forward in time, treating active contacts as equality constraints
2. Monitor the system for two kinds of events: geometric events (contact gains and losses) and negative contact forces.
3. If one or more such events are detected during the most recent integration step, then interpolate the system back to the moment of the earliest event.
   - If the event is a **contact gain** (e.g. a collision), then apply impulsive dynamics and identify the new set of current contacts and the new set of active contacts.
   - If the event is a **negative contact force**, then formulate and solve and identify the new sets of current and active contacts.
   - If the event is a geometric **contact loss**, then remove the lost contacts from the sets of current and active contacts.
4. Go to step 1.

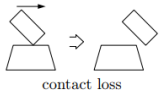

Featherstone R. (2008) Contact and Impact. In: Rigid Body Dynamics Algorithms. Springer, Boston, MA. https://doi.org/10.1007/978-1-4899-7560-7_11

Zero-Moment Point - Thirty Five Years of its Life

***Definition 1 (The notion of the ZMP)**: The pressure under supporting foot can be replaced by the appropriate reaction force acting at a certain point of the mechanism's foot. Since the sum of all moments of active forces with respect to this point is equal to zero, it is termed the zero-moment point (ZMP).*

(Vukobratović and Juričić 1969, Vukobratović *et al.* 1990)

***Interpretation 1**: ZMP is the point on the walking ground surface at which the horizontal components of the resultant moment generated by active forces and moments acting on human/humanoid links are equal to zero.*

***Interpretation 2**: ZMP is the point on the floor at which the moments around x and y axes generated by reaction force and moment are zero.*

Background:

- Biped humanoid robot is a tree type open-chain mechanism with all joints actuated except the one joint-- between the foot and the ground
- It can topple in presence of strong disturbances
- The foot cannot be controlled with a DOF, but indirectly by ensuring the appropriate dynamics of the mechanism above the foot.
- Thus, the overall indicator of the mechanical behaviour is the point where the influence of all forces acting on the mechanism can be replaced by one single force. This point was termed the *Zero-Moment Point* (*ZMP*).

Active forces & moments

- ✓ Gravitational force
- ✓ External disturbance
- ✓ Inertial force at CoM of the humanoid ($-m\boldsymbol{a}$)

- × Joint torques
- × Any other internal forces & moments

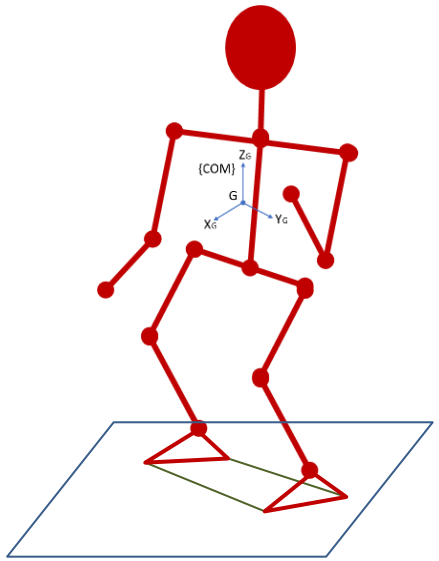

Vukobratović, Miomir, and Branislav Borovac. "Zero-moment point—thirty five years of its life." International journal of humanoid robotics 1, no. 01 (2004): 157-173.
Vukobratović, Miomir, Branislav Borovac and Dragoljub Surdilović, "Zero-Moment Point – Proper Interpretation." USC Neuroscience, 1/19/2004

Zero-Moment Point - Thirty Five Years of its Life

Assumptions:

1. Single-support phase (for this derivation)
2. Contact area is planar
3. Complete foot is in contact with the ground
4. Enough static friction is available so that the foot is at rest

Equations of static equilibrium for the foot

Find **OP**

$$\mathbf{R} + \mathbf{F}_\mathrm{A} + \mathbf{m}_\mathrm{s}\mathbf{g} = 0$$

$$\overrightarrow{\mathbf{OP}} \times \vec{\mathbf{R}} + \overrightarrow{\mathbf{OG}} \times \mathbf{m}_\mathrm{s}\mathbf{g} + \mathbf{M}_\mathrm{A} + M_\mathrm{z} + \overrightarrow{\mathbf{OA}} \times \mathbf{F}_\mathrm{A} = 0$$

$$(\overrightarrow{\mathbf{OP}} \times \vec{\mathbf{R}})^\mathrm{H} + \overrightarrow{\mathbf{OG}} \times \mathbf{m}_\mathrm{s}\mathbf{g} + \mathbf{M}_\mathrm{A}^\mathrm{H} + (\overrightarrow{\mathbf{OA}} \times \mathbf{F}_\mathrm{A})^\mathrm{H} = 0$$

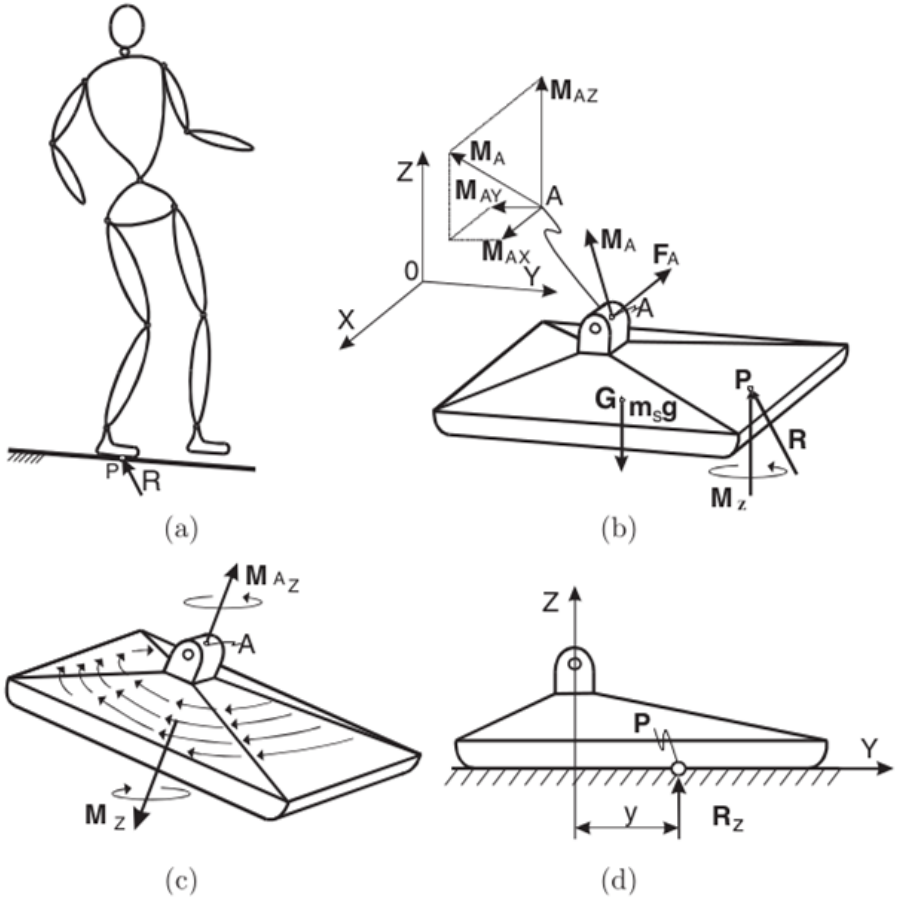

Bottom view

Schematic
First angle projection

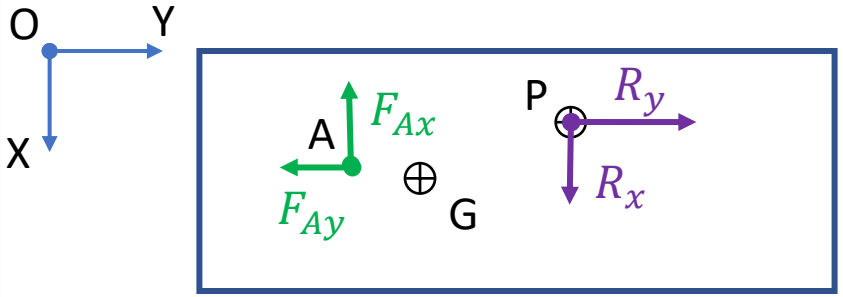

$$R_z = \max\{F_{Az} + m_S g, 0\}$$

$$R_x = F_{Ax}$$

$$R_y = F_{Ay}$$

$$\boxed{(\boldsymbol{GP} \times \boldsymbol{R}) = -\boldsymbol{M}_\mathrm{A} - (\mathbf{GA} \times \boldsymbol{F}_A)}$$

$$M_\mathrm{z} = M_\mathrm{fr} = -(M_\mathrm{A}^\mathrm{z} + (\overrightarrow{\mathbf{OA}} \times \mathbf{F}_\mathrm{A})^\mathrm{z})$$

Front view

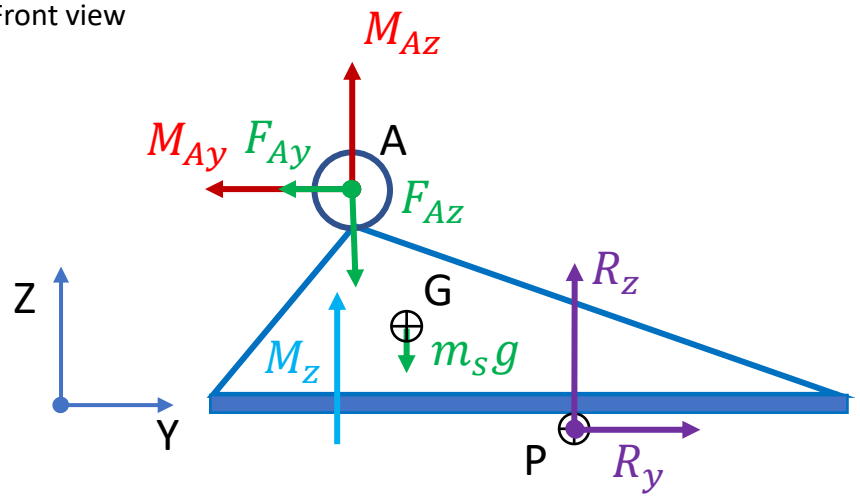

LHS view

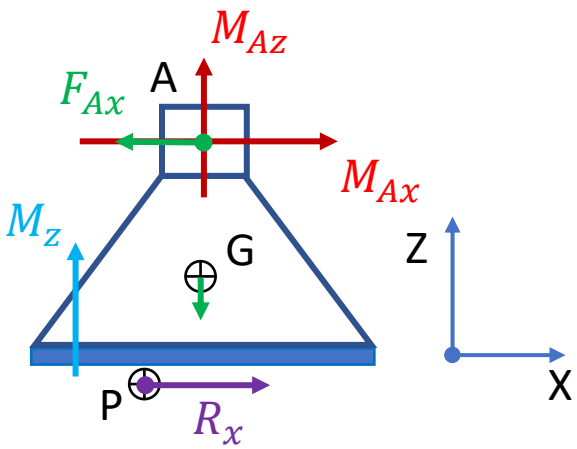

Vukobratović, Miomir, and Branislav Borovac. "Zero-moment point—thirty five years of its life." International journal of humanoid robotics 1, no. 01 (2004): 157-173.

Forces Acting on a Biped Robot. Center of Pressure—Zero Moment point

Consider any point P on the sole
Moment of the forces acting at P about Q

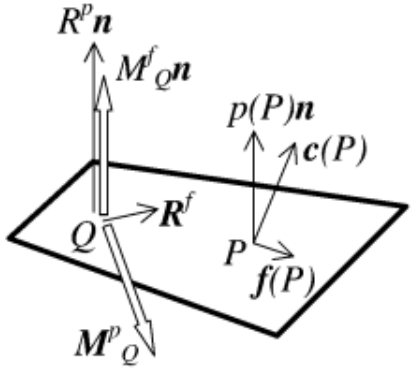

Total normal GRF and its moment about Q

$$\boldsymbol{R}^p = \left(\int_S p(P)dS\right)\boldsymbol{n} \equiv R^p\boldsymbol{n}, \qquad R^p > 0$$

$$\boldsymbol{M}^p_Q = \left(\int_S p(P)\boldsymbol{QP}dS\right) \times \boldsymbol{n}$$

Always in plane (Tilting moment)

Total tangential GRF and its moment about Q

$$\boldsymbol{R}^f = \int_S \boldsymbol{f}(P)dS, \qquad \boldsymbol{R}^f \cdot \boldsymbol{n} = 0$$

$$\boldsymbol{M}^f_Q = \int_S \boldsymbol{QP} \times \boldsymbol{f}(P)dS$$

Always ⊥ to the plane

A point Q where M^P is zero, $Q \to C$

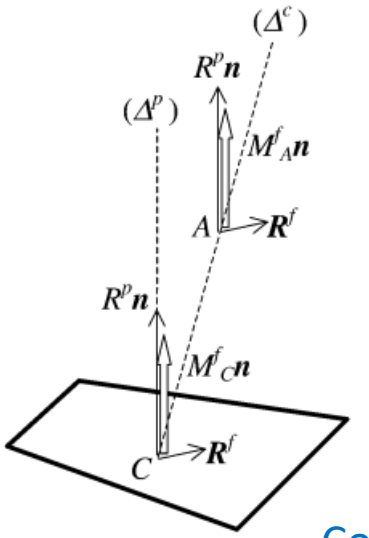

Contact wrench

$$\boldsymbol{R}^c = R^p\boldsymbol{n} + \boldsymbol{R}^f, \qquad R^p > 0, \qquad \boldsymbol{R}^f \cdot \boldsymbol{n} = 0$$

$$\boldsymbol{M}^c_C = \boldsymbol{M}^f_C\boldsymbol{n} + \cancel{M^P_C}$$

COP C (Δ^c) can be defined as a point (axis) where the moment of contact forces is purely perpendicular to the sole (no tilting component)

D is the ZMP

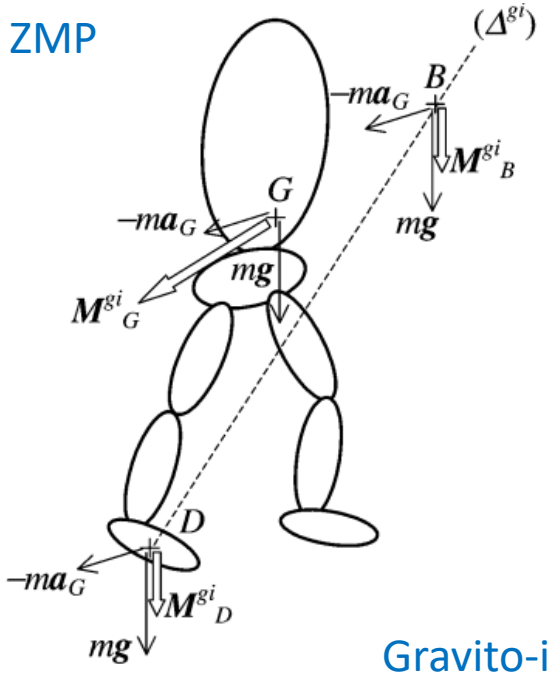

Gravito-inertial wrench

$$\boldsymbol{R}^{gi} = m\boldsymbol{g} - m\boldsymbol{a}_G$$

$$\boldsymbol{M}^{gi}_Q = \boldsymbol{QG} \times m\boldsymbol{g} - \boldsymbol{QG} \times m\boldsymbol{a}_G - \dot{\boldsymbol{H}}_G$$

$$\boldsymbol{M}^{gi}_D = \boldsymbol{DG} \times m\boldsymbol{g} - \boldsymbol{DG} \times m\boldsymbol{a}_G - \dot{\boldsymbol{H}}_G,$$

$$\boldsymbol{M}^{gi}_D \times \boldsymbol{n} = \boldsymbol{0}.$$

Horizontal component of GIW is zero

Δ^{gi} is an axis where the moment of gravito-inertial forces is purely ⊥ the sole

P. Sardain and G. Bessonnet, "Forces acting on a biped robot. Center of pressure-zero moment point," in *IEEE Transactions on Systems, Man, and Cybernetics - Part A: Systems and Humans*, vol. 34, no. 5, pp. 630-637, Sept. 2004, doi: 10.1109/TSMCA.2004.832811.

Forces Acting on a Biped Robot. Center of Pressure—Zero Moment point

Newton-Euler equations of motion (about CoM):

$$\boldsymbol{R}^c + m\boldsymbol{g} = m\boldsymbol{a}_G$$

$$\boldsymbol{M}_Q^c + \boldsymbol{QG} \times m\boldsymbol{g} = \dot{\boldsymbol{H}}_G + \boldsymbol{QG} \times m\boldsymbol{a}_G$$

Moments are written about general point Q

$$\boldsymbol{R}^c + (m\boldsymbol{g} - m\boldsymbol{a}_G) = \boldsymbol{0}$$

$$\boldsymbol{M}_Q^c + (\boldsymbol{QG} \times m\boldsymbol{g} - \boldsymbol{QG} \times m\boldsymbol{a}_G - \dot{\boldsymbol{H}}_G) = \boldsymbol{0}$$

Dynamic equilibrium
D'Alembert's form

$$\boldsymbol{R}^c + \boldsymbol{R}^{gi} = \boldsymbol{0}$$

$$\boldsymbol{M}_Q^c + \boldsymbol{M}_Q^{gi} = \boldsymbol{0}.$$

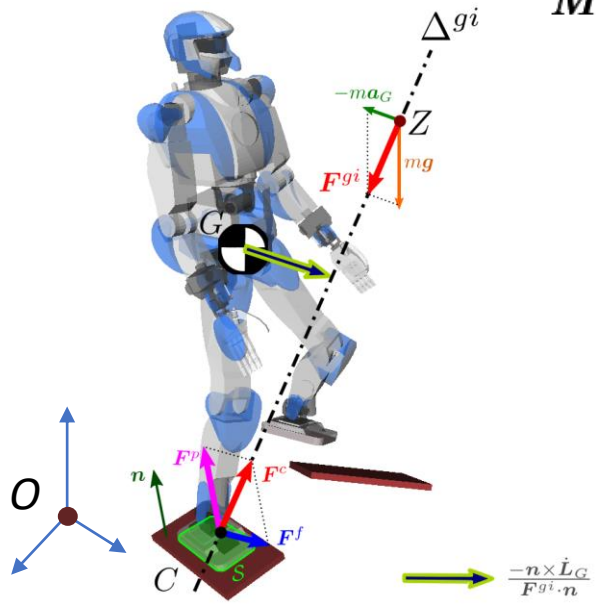

Computation of COP-ZMP

We have sensors providing us R_P and we can compute M_O^P.
Find CoP using this data--
Using vector triple product identity:

$$\boldsymbol{M}_O^p = \boldsymbol{OC} \times \boldsymbol{R}^p$$

$$\boldsymbol{OC} = \frac{\boldsymbol{n} \times \boldsymbol{M}_O^p}{R^p} = \frac{\boldsymbol{n} \times \boldsymbol{M}_O^c}{\boldsymbol{R}^c \cdot \boldsymbol{n}}$$

Similarly, coordinates of ZMP can be derived as:

$$\boldsymbol{OD} = \frac{\boldsymbol{n} \times \boldsymbol{M}_O^{gi}}{\boldsymbol{R}^{gi} \cdot \boldsymbol{n}}$$

COP-ZMP coincidence can be seen easily from the N-E equations

The result is true even when multiple contacts are made with the same flat surface.

The biped is dynamically balanced if the contact forces and the gravity-inertia forces are strictly opposite

P. Sardain and G. Bessonnet, "Forces acting on a biped robot. Center of pressure-zero moment point," in *IEEE Transactions on Systems, Man, and Cybernetics - Part A: Systems and Humans*, vol. 34, no. 5, pp. 630-637, Sept. 2004, doi: 10.1109/TSMCA.2004.832811.

Zero-Moment Point - Thirty Five Years of its Life

How to use ZMP in biped motion?

1. Gait synthesis
2. Gait analysis
   - Compute the position of the ZMP using the expressions
   - If the ZMP belongs to the interior of the support polygon, it exists. Distance of the ZMP from the polygon boundary is a measure of stability of the humanoid

- If ZMP exists at all times during a gait, then the gait is 'dynamically balanced.' In such cases ZMP == CoP.
- ZMP is generally computed from the 'other side,' i.e., CoP is easy to compute
- Emergency strategies in the case foot areal contact shifts only to an edge:
  - Generate internal moment such that the value of **R** shoots up. This requires huge real-time computations.
  - Extend other limbs (stepping ahead & lean against the help of arms)

Other cases:

- Ballet gait
- Unbalanced gait

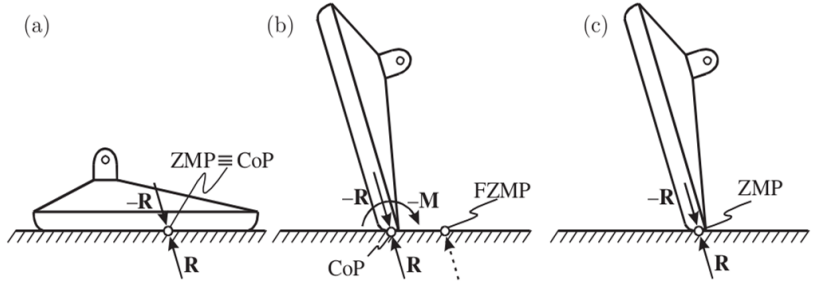

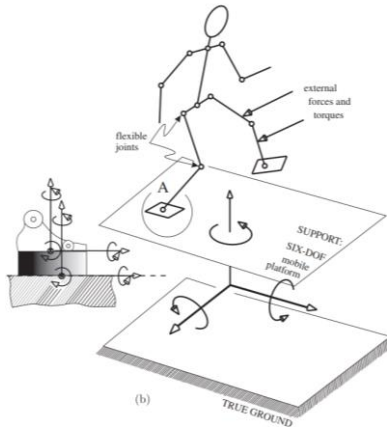

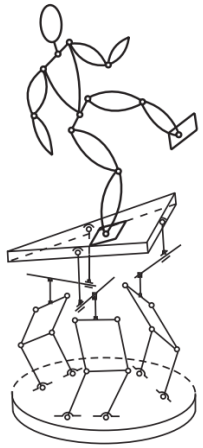

ZMP cannot be used:

- to detect foot slip
- when the ground is not flat
- when the arms of the robot are in contact with the environment

Future directions:

- Assume more realistic high DOF models
- Model the simplified dynamics phenomena in greater detail
- Better foot-ground contact modelling
- Foot split in two links with a stiff connection rather than a single rigid foot
- Incorporate elasticity in joint actuation. Inclusion of active stiffness.
  - Achieve force-position control of the elastic actuators
- Generate continuous transition of ZMP from SSP to DSP and vice versa.
- Strategies to tackle dynamically interacting ground.
- Progress in building General Humanoid Dynamics simulators like V-HRP

Vukobratović, Miomir, and Branislav Borovac. "Zero-moment point—thirty five years of its life." International journal of humanoid robotics 1, no. 01 (2004): 157-173.
Kajita S., Hirukawa H., Harada K., Yokoi K. (2014) ZMP and Dynamics. In: Introduction to Humanoid Robotics. Springer Tracts in Advanced Robotics, vol 101. Springer, Berlin, Heidelberg. https://doi.org/10.1007/978-3-642-54536-8_3

The 2D inverted pendulum model of humanoid

Assumptions:

- Robot mass concentrated at the CoM, masses legs, passive pivot joint at ground
- The robot motion is constrained to the *sagittal plane X-Z*
- The **inputs** of the pendulum are the **torque τ** at the pivot and the kick **force f** at the prismatic joint along the leg.

Key concepts:

- **Gravity compensation** to the ideal model of a biped
- Linear trajectory (not necessarily horizontal) of the CoM leads to a linear differential equation describing the system.
- A conserved quantity named Orbital Energy is derived for the linear trajectories

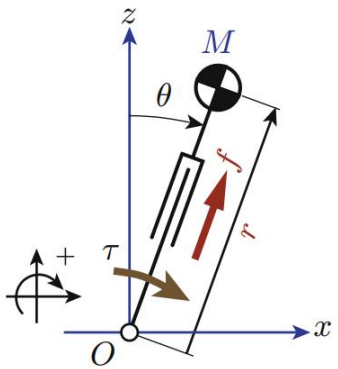

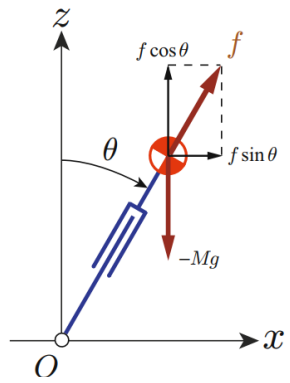

EoM in polar coordinates:

$$r^2\ddot{\theta} + 2r\dot{r}\dot{\theta} - gr\sin\theta = \tau/M$$
$$\ddot{r} - r\dot{\theta}^2 + g\cos\theta = f/M.$$

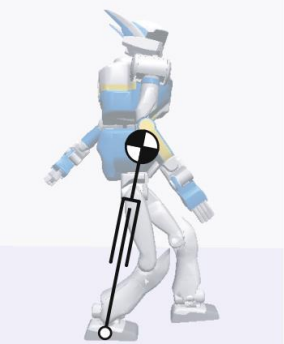

Intuitively, we can say the pendulum is keeping the CoM height by extending its leg as fast as it is falling. We call this the Linear Inverted Pendulum mode

$$M\ddot{x} = f\sin\theta$$

$$\boxed{f = \frac{Mg}{\cos\theta}.}$$

(Condition for horizontal linear motion of CoM)

$$M\ddot{x} = \frac{Mg}{\cos\theta}\sin\theta = Mg\tan\theta = Mg\frac{x}{z}$$

$$\ddot{x} = \frac{g}{z}x$$

(Linear motion of CoM, zero ankle torque)

$$x(t) = x(0)\cosh(t/T_c) + T_c\dot{x}(0)\sinh(t/T_c)$$

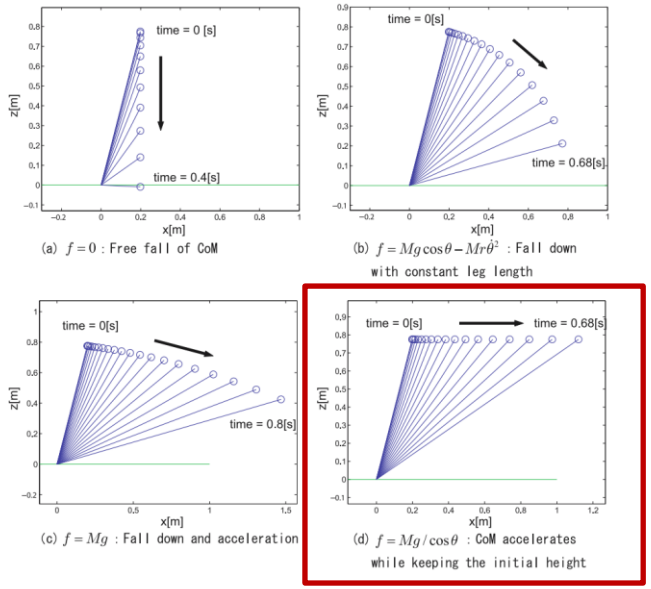

Kajita S., Hirukawa H., Harada K., Yokoi K. (2014) Biped Walking. In: Introduction to Humanoid Robotics. Springer Tracts in Advanced Robotics, vol 101. Springer, Berlin, Heidelberg. https://doi.org/10.1007/978-3-642-54536-8_4

The 2D inverted pendulum model of humanoid

Orbital energy

$$\dot{x}(\ddot{x} - \frac{g}{z}x) = 0$$

$$\int \{\ddot{x}\dot{x} - \frac{g}{z}x\dot{x}\}dt = constant.$$

$$\frac{1}{2}\dot{x}^2 - \frac{g}{2z}x^2 = constant \equiv E.$$

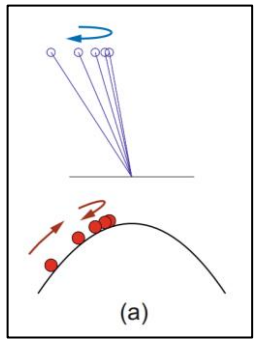

$$E = -\frac{g}{2z}x_{rev}^2 \quad \text{or} \quad E = \frac{1}{2}\dot{x}_{top}^2$$

$$|x_{rev}| = \sqrt{-\frac{2zE}{g}} \qquad |\dot{x}_{top}| = \sqrt{2E}$$

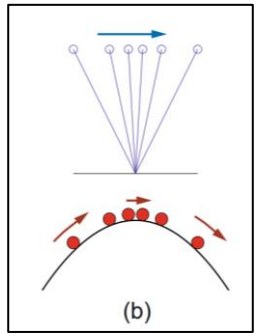

- The sign of orbital energy can tell whether a step will be successful or not (CoM will pass through or not).

Planning a simple biped gait:

- Support leg exchange happens instantaneously
- The final speed of the previous support phase = the initial speed of the new support phase.
- Orbital energy may not be necessarily conserved during stepping

$$E_0 = -\frac{g}{2z}x_s^2. \longrightarrow E_1 = \frac{1}{2}v_1^2. \longrightarrow E_2 = -\frac{g}{2z}x_e^2.$$

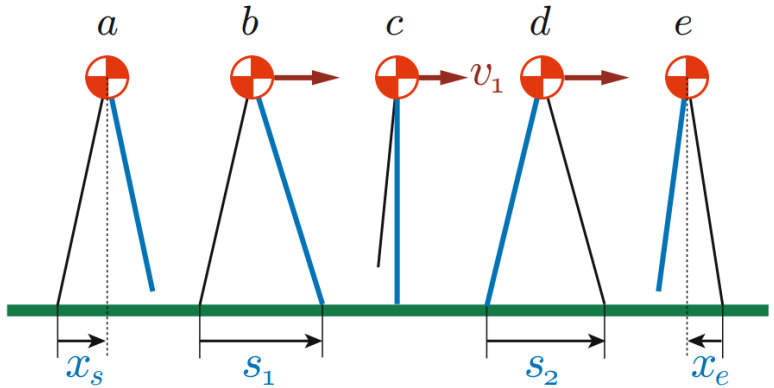

Fig. 4.9 Specification for a walk of one step forward. We need support leg exchanges twice.

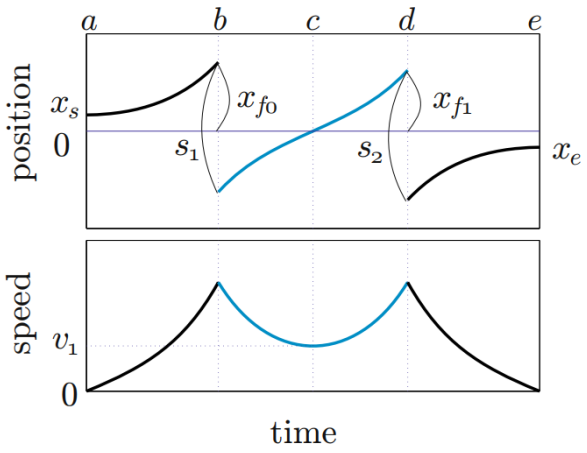

Fig. 4.10 Planned trajectory of the center of mass, position and velocity

Kajita S., Hirukawa H., Harada K., Yokoi K. (2014) Biped Walking. In: Introduction to Humanoid Robotics. Springer Tracts in Advanced Robotics, vol 101. Springer, Berlin, Heidelberg. https://doi.org/10.1007/978-3-642-54536-8_4

The 3D inverted pendulum model of humanoid

Assumptions:

- Modelling for single support phase
- The supporting point is a <u>passive</u> spherical joint. This
- The pendulum consists of a point mass

Observations:

- A 3D LIP is a mere concatenation of two 2D LIP. This allows separate controller design for the Sagittal and the Lateral planar motions

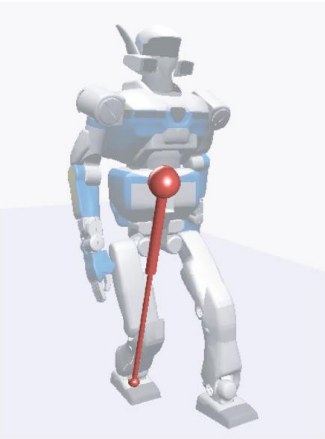

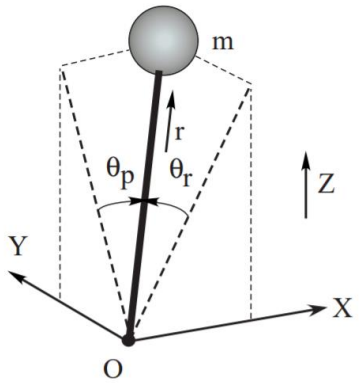

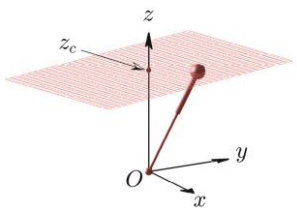

$$\boldsymbol{p} = (x, y, z)^{\mathrm{T}}$$
$$\boldsymbol{q} = (\theta_r, \theta_p, r)^{\mathrm{T}}$$
$$\boldsymbol{\tau}^a = (\tau_r, \tau_p, f)^{\mathrm{T}}$$

Motion constraint

$$z = k_x x + k_y y + z_c$$

Acceleration constraint

$$[f(\frac{x}{r}) \quad f(\frac{y}{r}) \quad f(\frac{z}{r}) - Mg] \begin{bmatrix} -k_x \\ -k_y \\ 1 \end{bmatrix} = 0$$

Force required to maintain the constraints

$$f = \frac{Mgr}{z_c}$$

Equations of motion
In cartesian coordinates
In the most general case

$$m(-z\ddot{y} + y\ddot{z}) = \frac{D}{C_r}\tau_r - mgy,$$

$$m(z\ddot{x} - x\ddot{z}) = \frac{D}{C_p}\tau_p + mgx,$$

$$C_r \equiv \cos\theta_r, C_p \equiv \cos\theta_p,$$

$$D \equiv \sqrt{{C_r}^2 + {C_p}^2 - 1},$$

$$mS_p\ddot{x} - mS_r\ddot{y} + mD\ddot{z} = f - mgD \quad \bigstar$$

Equations of motion:
(3D LIP with zero ankle torque)

$$\ddot{x} = \frac{g}{z_c}x,$$
$$\ddot{y} = \frac{g}{z_c}y.$$

Equations of motion:
(With zero ankle torque)

$$M\ddot{x} = (x/r)f$$
$$M\ddot{y} = (y/r)f$$
$$M\ddot{z} = (z/r)f - Mg$$

Kajita S., Hirukawa H., Harada K., Yokoi K. (2014) Biped Walking. In: Introduction to Humanoid Robotics. Springer Tracts in Advanced Robotics, vol 101. Springer, Berlin, Heidelberg. https://doi.org/10.1007/978-3-642-54536-8_4

S. Kajita, F. Kanehiro, K. Kaneko, K. Yokoi and H. Hirukawa, "The 3D linear inverted pendulum mode: a simple modeling for a biped walking pattern generation," Proceedings 2001 IEEE/RSJ International Conference on Intelligent Robots and Systems, 2001, pp. 239-246 vol.1, doi: 10.1109/IROS.2001.973365.

The 3D inverted pendulum model of humanoid

Generating walking pattern in 3D

- Assume simultaneous support exchange in x as well as y directions

Walk primitive

- A trajectory symmetric about y axis is generated
- With $\boldsymbol{E_y}$ **negative and** $\boldsymbol{E_x}$ **positive** it turns out to be a segment of hyperbola
- It is defined by the terminal position $(\bar{x}, \bar{y})$

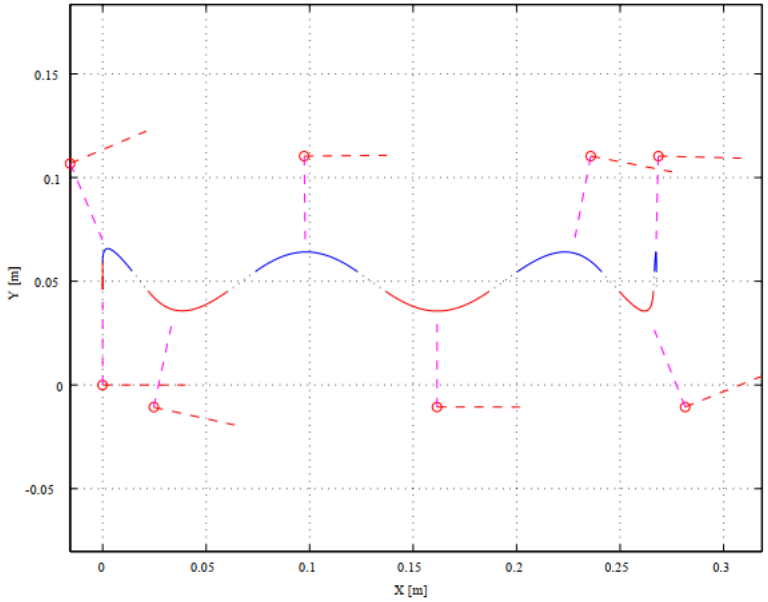

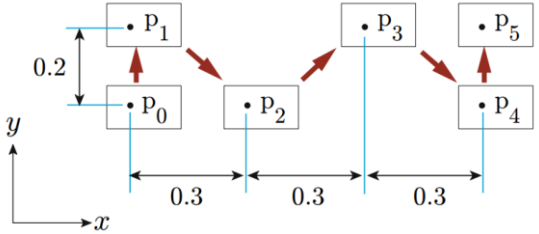

n	1	2	3	4	5
$s_x^{(n)}$	0.0	0.3	0.3	0.3	0
$s_y^{(n)}$	0.2	0.2	0.2	0.2	0.2

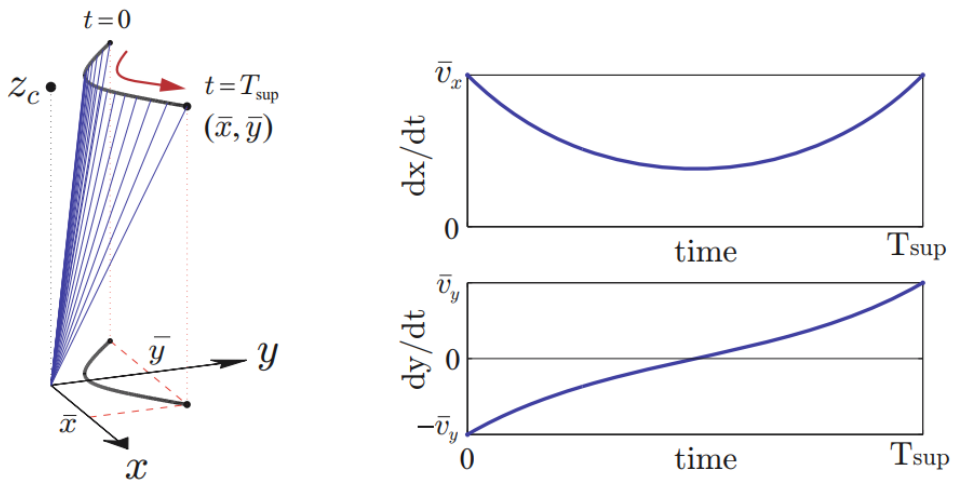

(a) View in 3D space

(b) time profile the velocity

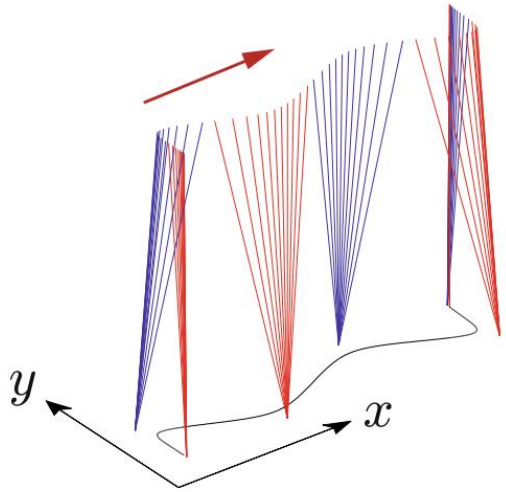

Kajita S., Hirukawa H., Harada K., Yokoi K. (2014) Biped Walking. In: Introduction to Humanoid Robotics. Springer Tracts in Advanced Robotics, vol 101. Springer, Berlin, Heidelberg. https://doi.org/10.1007/978-3-642-54536-8_4

S. Kajita, F. Kanehiro, K. Kaneko, K. Yokoi and H. Hirukawa, "The 3D linear inverted pendulum mode: a simple modeling for a biped walking pattern generation," Proceedings 2001 IEEE/RSJ International Conference on Intelligent Robots and Systems, 2001, pp. 239-246 vol.1, doi: 10.1109/IROS.2001.973365.

Control of Walking Robots Based on Manipulation of the Zero Moment Point

Control dynamic walking of a biped without prescribing the ZMP trajectory. Instead, the reference position of the trunk of the robot is specified. The objective of the proposed method is to obtain a smooth and soft motion based on real-time feedback control.

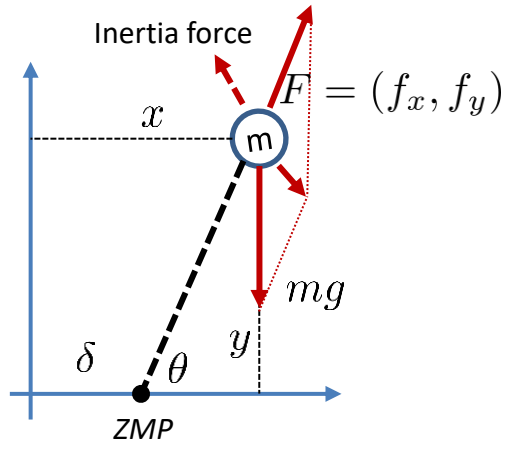

Biped approximated as a 2D inverted pendulum

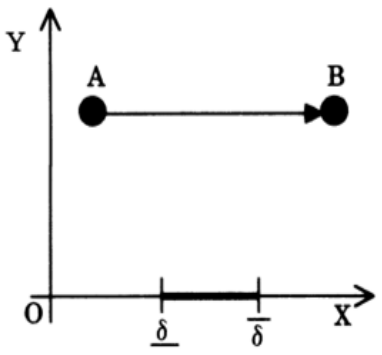

A possible trajectory of the point mass and the ZMP during dynamic walking

Equations of motion of the point mass are:

$$m\ddot{x} = f_x$$

$$m\ddot{y} = f_y - mg$$

Definition of ZMP gives us:

$$M_\delta^{gi} = -(x-\delta)(m)(g+\ddot{y}) + (x)(m\ddot{x}) = 0$$

$$\delta = \frac{x(\ddot{y}+g) - y\ddot{x}}{\ddot{y}+g}.$$

Consider ZMP motion *δ(t)* at a constant velocity given by:

$$\delta(t) = \underline{\delta} + \frac{\overline{\delta} - \underline{\delta}}{T} t$$

LIPM case:

Recall the homogeneous solution:

$$\boxed{x(t) = x(0)\cosh(t/T_c) + T_c\dot{x}(0)\sinh(t/T_c)}$$

Particular solution:

$$x(t) = (x_0 - \underline{\delta})\cosh\frac{1}{\alpha}t + \alpha\left(\nu_0 - \frac{\overline{\delta} - \underline{\delta}}{T}\right)\sinh\frac{1}{\alpha}t + \frac{\overline{\delta} - \underline{\delta}}{T}t + \underline{\delta},$$

Control: $y = h_{ref}$ and $x = x_{ref}$

Actuation signal: ZMP (δ)

Assumptions:

1. ZMP can lie anywhere in the contact patch
2. Arbitrarily positive force f_x and f_y can be applied once ZMP is inside some bounded stable region.

Control law: $f_y = h_{ref} - y - \dot{y} + mg$

$$m\ddot{y} + \dot{y} + y = h_{ref}$$

$$m\ddot{x} = f_x = f_y \tan\theta$$

$$\beta\ddot{x} - x + \delta = 0 \qquad \left(\lim_{y \to h_{ref}} \beta = \frac{h_{ref}}{g}\right)$$

Control law: $\delta = 2x - x_{ref} + \dot{x}$

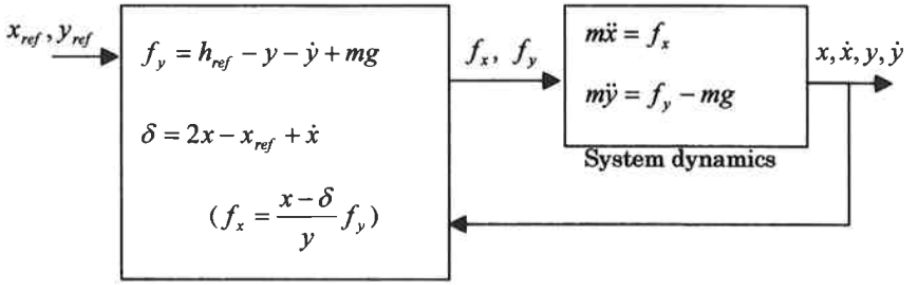

Mitobe, K., Capi, G., & Nasu, Y. (2000). Control of walking robots based on manipulation of the zero moment point. *Robotica, 18*(6), 651-657. doi:10.1017/S0263574700002708

Control of Walking Robots Based on Manipulation of the Zero Moment Point

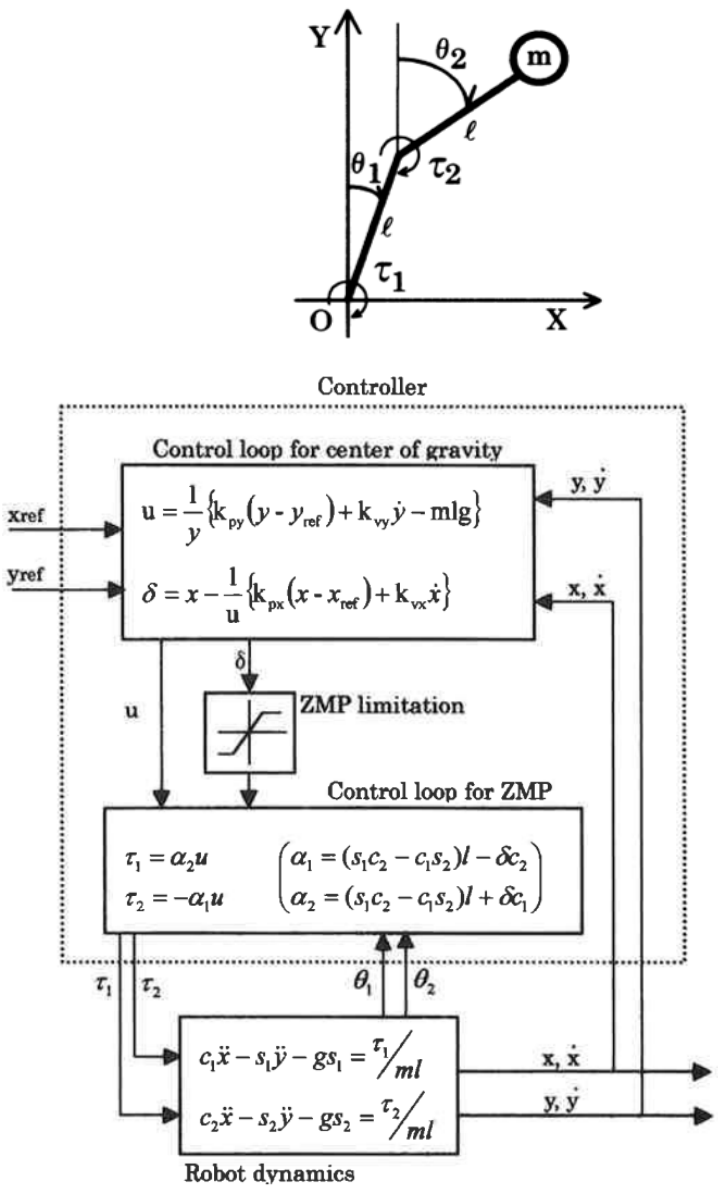

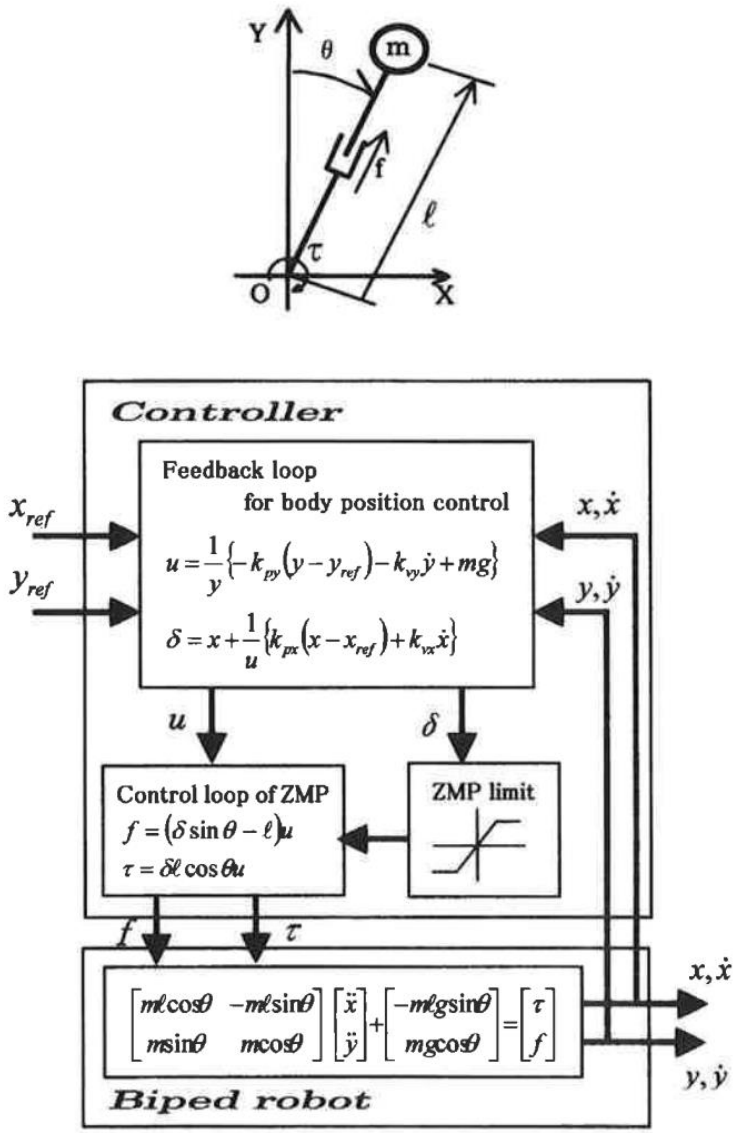

Mitobe, K., Capi, G., & Nasu, Y. (2000). Control of walking robots based on manipulation of the zero moment point. *Robotica, 18*(6), 651-657. doi:10.1017/S0263574700002708

Control of Walking Robots Based on Manipulation of the Zero Moment Point

A biped model with two motors with encoders in each leg

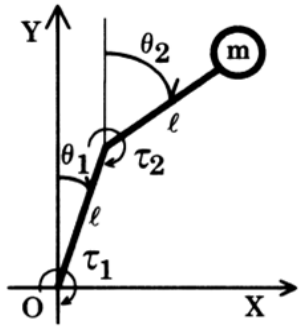

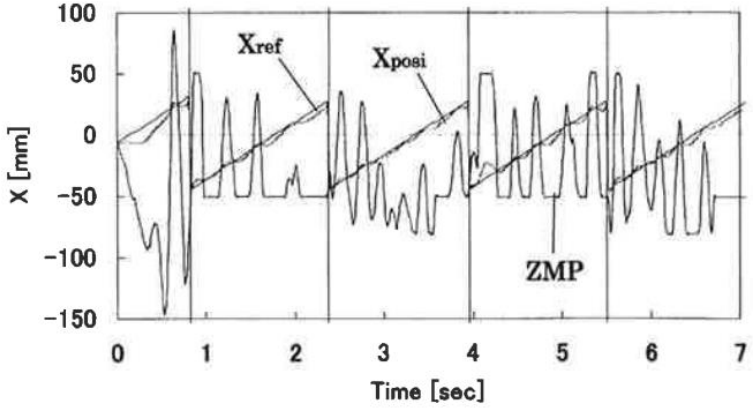

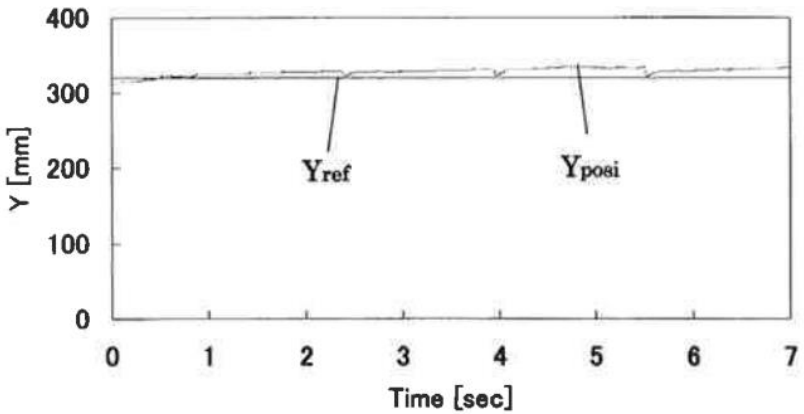

A biped model with prismatic actuation with rack-and-pinion and a motor at the ankle

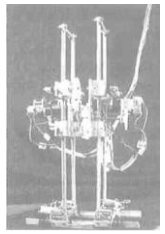

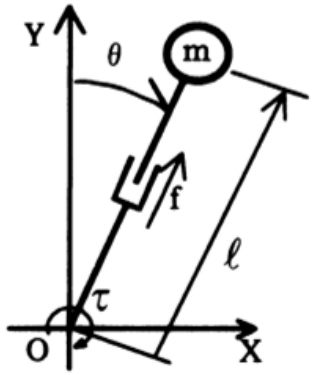

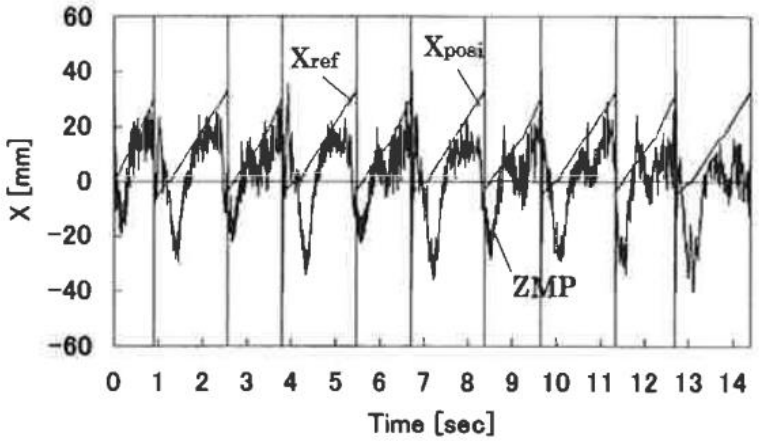

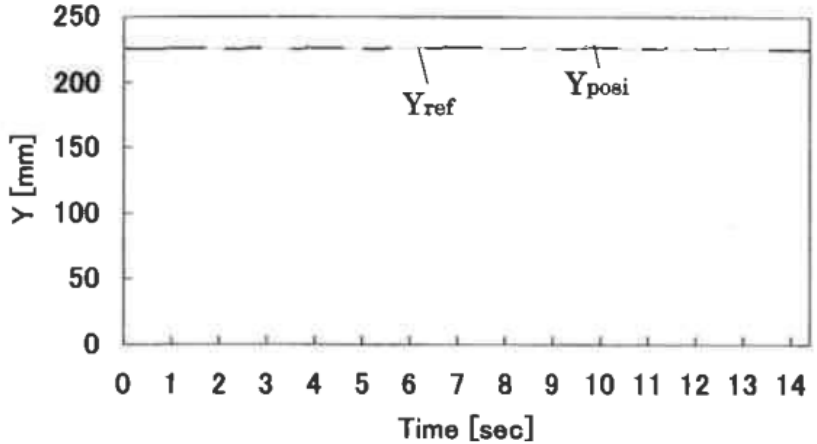

Shortcomings:

- Formulation assumes massless legs.
- Insufficient stability during the walk. The robot fell down after a few steps.
- Different ZMP interval was needed for each step, i.e., the experiment was not satisfactorily repeatable.

Mitobe, K., Capi, G., & Nasu, Y. (2000). Control of walking robots based on manipulation of the zero moment point. *Robotica, 18*(6), 651-657. doi:10.1017/S0263574700002708

Capture Point: A Step toward Humanoid Push Recovery

A humanoid robot can maintain its balance on being pushed in three ways-

- adjust its CoP (mainly ankle torque),
- generate internal angular momentum (hip flexing, windmilling arms etc) and
- taking a step

Simplified model assumptions

- All the assumptions of the 2D inverted pendulum model. The model now has a flywheel at the CoM. No torque at the ankle.

Capture point gives us a principled approach on where to take a step

Recall

Orbital Energy for LIP:

$$E_{LIP} = \frac{1}{2}\dot{x}^2 - \frac{g}{2z_0}x^2$$

On vanishing the Orbital Energy for the next step we get:

$$\dot{x} = \pm x\sqrt{\frac{g}{z_0}}$$

Unique Capture point for LIP:
(No flywheel motion)

$$x_{capture} = \dot{x}\sqrt{\frac{z_0}{g}}$$

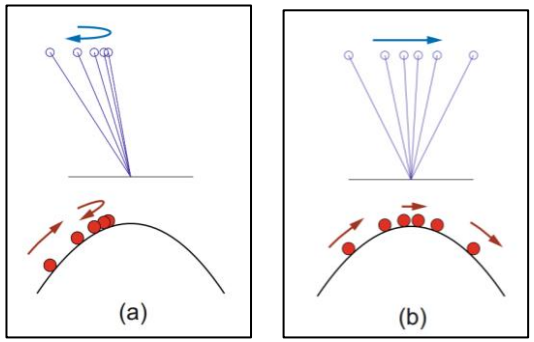

$E_{LIP} < 0$ $E_{LIP} > 0$

Now, consider flywheel + LIP model: The solution is no more unique. It's a region

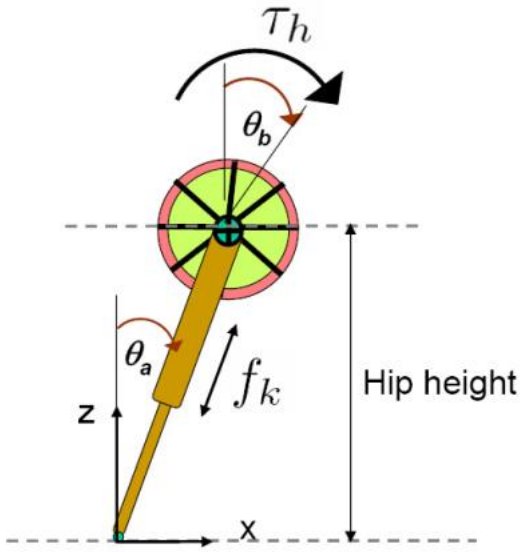

$$m\ddot{x} = f_k \sin\theta_a - \frac{\tau_h}{l}\cos\theta_a$$
$$m\ddot{z} = -mg + f_k\cos\theta_a + \frac{\tau_h}{l}\sin\theta_a$$
$$J\ddot{\theta}_b = \tau_h$$

$$\ddot{x} = \frac{g}{z_0}x - \frac{1}{mz_0}\tau_h$$
$$\ddot{\theta}_b = \frac{1}{J}\tau_h$$

For linear motion of CoM

J. Pratt, J. Carff, S. Drakunov and A. Goswami, "Capture Point: A Step toward Humanoid Push Recovery," *2006 6th IEEE-RAS International Conference on Humanoid Robots*, 2006, pp. 200-207, doi: 10.1109/ICHR.2006.321385.

Capture Point and Divergent Component of Motion (DCM)

Let us start from the equation of motion of the linear inverted pendulum, where all the mass is concentrated at the center of mass $\boldsymbol{p}_G$:

$$\ddot{\boldsymbol{p}}_G = \omega^2(\boldsymbol{p}_G - \boldsymbol{p}_Z)$$

We assume that the robot steps instantly at time $t = 0$ and maintains its ZMP $\boldsymbol{p}_Z$ at a constant location in its new foothold, so that $\boldsymbol{p}_Z$ is stationary. Since the natural frequency ω of the pendulum is also a model constant, we can solve this second-order linear differential equation as:

$$\boldsymbol{p}_G(t) = \boldsymbol{p}_Z + \frac{e^{\omega t}}{2}\left[\boldsymbol{p}_G(0) + \frac{\dot{\boldsymbol{p}}_G(0)}{\omega} - \boldsymbol{p}_Z\right] + \frac{e^{-\omega t}}{2}\left[\boldsymbol{p}_G(0) - \frac{\dot{\boldsymbol{p}}_G(0)}{\omega} - \boldsymbol{p}_Z\right]$$

This function is the sum of a stationary term $\boldsymbol{p}_Z$, a convergent term factored by $e^{-\omega t}$ that vanishes as $t \to \infty$, and a term factored by $e^{\omega t}$ that diverges as $t \to \infty$. Let us define the *capture point* as:

$$\boldsymbol{p}_C \stackrel{\text{def}}{=} \boldsymbol{p}_G + \frac{\dot{\boldsymbol{p}}_G}{\omega}$$

The divergent term in $\boldsymbol{p}_G(t)$ is then $e^{\omega t}/2(\boldsymbol{p}_C(0) - \boldsymbol{p}_Z)$. In particular, the *only* way for the center of mass trajectory to be bounded is for the stationary ZMP to be equal to the instantaneous capture point:

$$\boldsymbol{p}_Z = \boldsymbol{p}_C(0) \implies \boldsymbol{p}_G(t) \underset{t\to\infty}{\longrightarrow} \boldsymbol{p}_C(0)$$

We can thus interpret the capture point as a point where the robot should step (shift its ZMP) in order to come (asymptotically) to a stop.

Recall

$$\ddot{x} = \frac{g}{z}x$$

$$x(t) = x(0)\cosh(t/T_c) + T_c\dot{x}(0)\sinh(t/T_c)$$

$$x_{capture} = \dot{x}\sqrt{\frac{z_0}{g}}$$

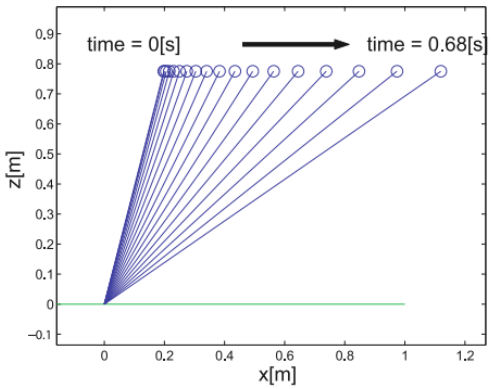

(d) $f = Mg/\cos\theta$: CoM accelerates while keeping the initial height

Source: https://scaron.info/robot-locomotion/capture-point.html

Capture Point: A Step toward Humanoid Push Recovery (contd…)

$$\ddot{x} = \frac{g}{z_0}x - \frac{1}{mz_0}\tau_h$$
$$\ddot{\theta}_b = \frac{1}{J}\tau_h$$

Capture Region based on ideal cases:

Generate Impulsive torque causing an instantaneous angular velocity change

$$\sqrt{\frac{z_0}{g}}(\dot{x} - \frac{J}{mz_0}\Delta\dot{\theta}_{b_{max}}) < x_{capture} < \sqrt{\frac{z_0}{g}}(\dot{x} - \frac{J}{mz_0}\Delta\dot{\theta}_{b_{min}})$$

$$\Delta\dot{x} = -\frac{J}{mz_0}\Delta\dot{\theta}_b$$

Instantaneous change in the angular position of the flywheel

$$\Delta x = -\frac{J}{mz_0}\Delta\theta_b$$

$$\sqrt{\frac{z_0}{g}}\dot{x} - \frac{J}{mz_0}\Delta\theta_{b_{max}} < x_{capture} < \sqrt{\frac{z_0}{g}}\dot{x} - \frac{J}{mz_0}\Delta\theta_{b_{min}}$$

Useful upper bounds to the capture region

Capture Region based on torque-limited and angle-limited flywheel

The bang-bang torque profile gives us the quickest stop:

$$\tau(t) = \tau_{max}u(t) - 2\tau_{max}u(t - T_{R1}) + \tau_{max}u(t - T_{R2})$$

The solution for capture point -x_0 then is

$$x_0 = -\frac{1}{w}\dot{x}_0 + \frac{\tau_{max}}{mg}\left[\frac{(e^{wT_{R2}} - 2e^{w(T_{R2}-T_{R1})} + 1)}{e^{wT_{R2}}}\right]$$

The other boundary of the Capture Region is obtained using the torque limit τ_{min}

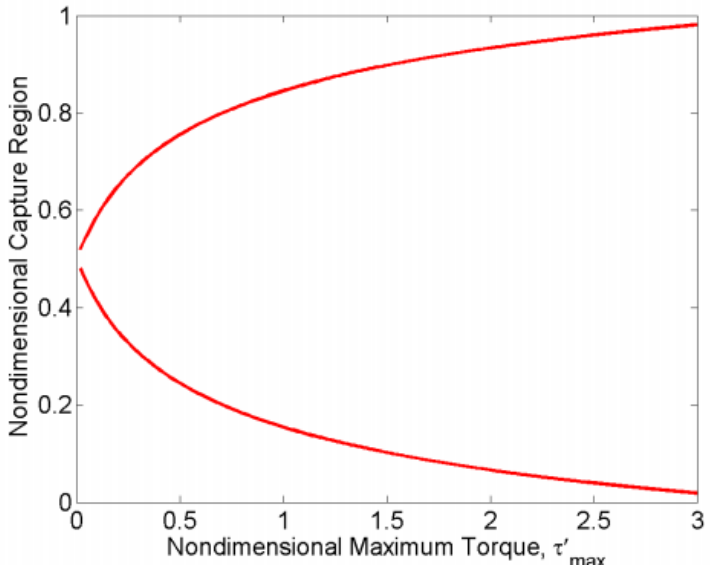

J. Pratt, J. Carff, S. Drakunov and A. Goswami, "Capture Point: A Step toward Humanoid Push Recovery," *2006 6th IEEE-RAS International Conference on Humanoid Robots*, 2006, pp. 200-207, doi: 10.1109/ICHR.2006.321385.

Capture Point: A Step toward Humanoid Push Recovery (contd…)

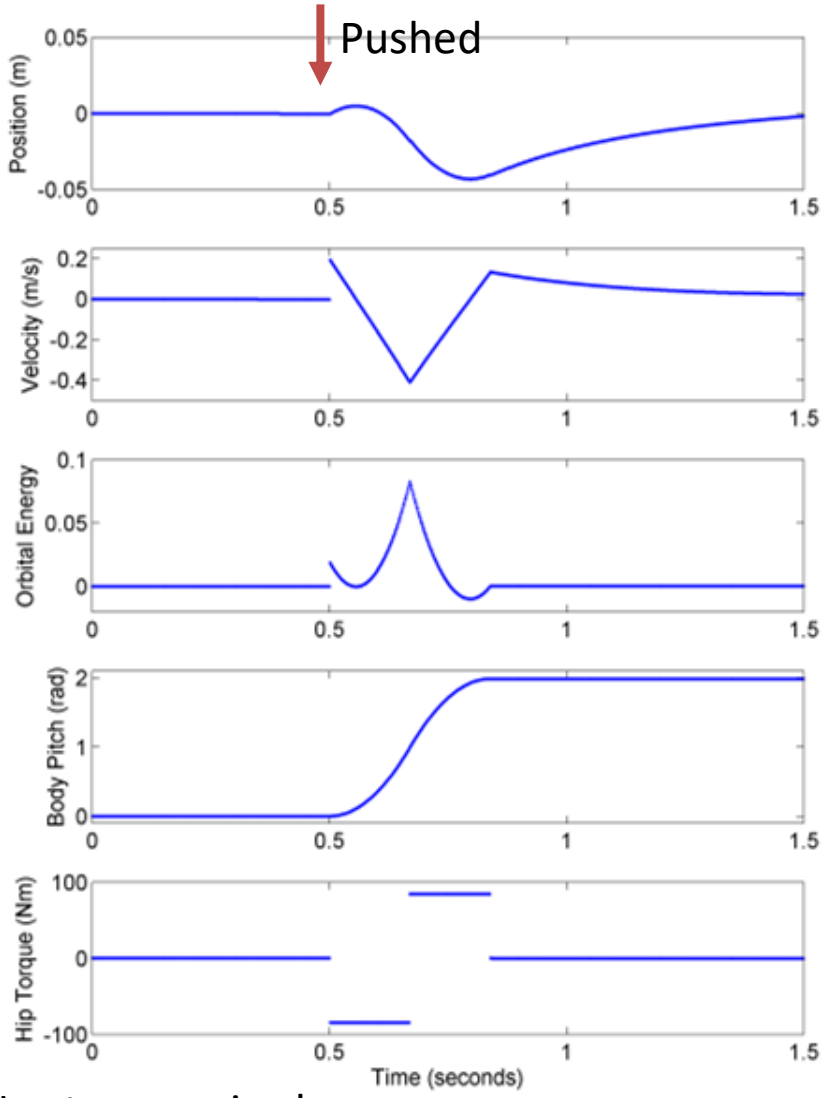

No step required

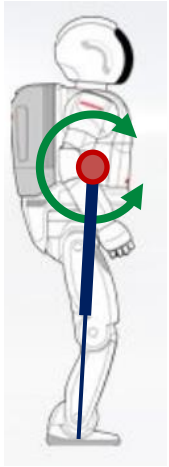

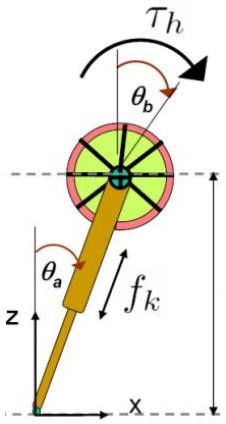

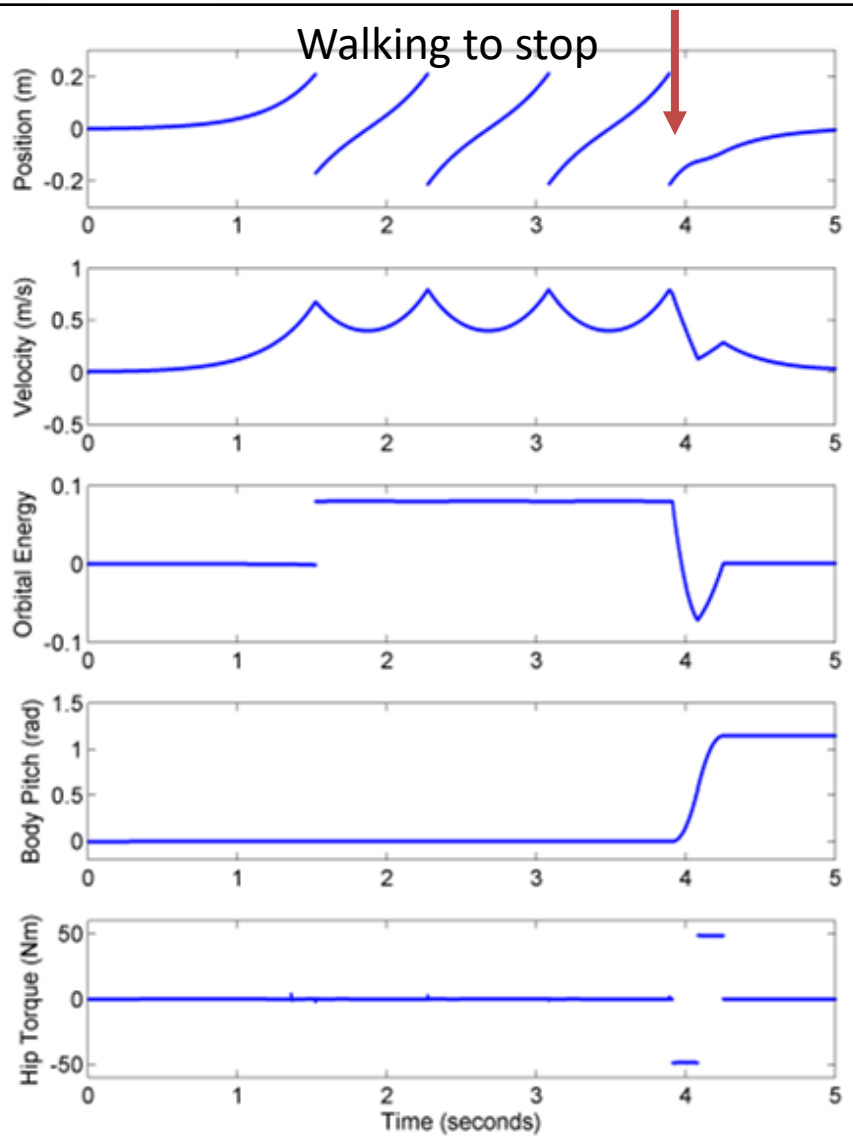

J. Pratt, J. Carff, S. Drakunov and A. Goswami, "Capture Point: A Step toward Humanoid Push Recovery," *2006 6th IEEE-RAS International Conference on Humanoid Robots*, 2006, pp. 200-207, doi: 10.1109/ICHR.2006.321385.

Energy Management Through Footstep Selection For Bipedal Robots

Capture Point based stepping on uneven terrain. Passive planar non-linear inverted pendulum (NIP) model

New concept: Curve of Equal Energy

Continuous dynamics:

$$ml^2\ddot{\theta} = mgl\sin\theta \qquad \Big| \qquad \dot{\mathbf{x}} = \begin{bmatrix} \dot{\theta} \\ \frac{g}{l}\sin\theta \end{bmatrix}$$

Impact Dynamics: $\boldsymbol{L}$ about the touchdown pt. is conserved

Gives us $\boldsymbol{v}^+$ from $\boldsymbol{v}^-$

$$\begin{bmatrix} \theta \\ \phi \\ \dot{\theta} \end{bmatrix}^+ = \begin{bmatrix} 1 & 1 & 0 \\ 0 & -1 & 0 \\ 0 & 0 & \cos\phi^- \end{bmatrix} \begin{bmatrix} \theta \\ \phi \\ \dot{\theta} \end{bmatrix}^-$$

Curve of capture: $E^+ = U^+$

$$\Delta x_{cp} = R_{cp}\left(E^-, \Delta h\right)$$

Curve of Equal Energy: $E^+ = E^-$ or $v_{n+1} = v_n$

$$\Delta x_{\Delta E=0} = R_{\Delta E=0}\left(E^-, \Delta h\right)$$

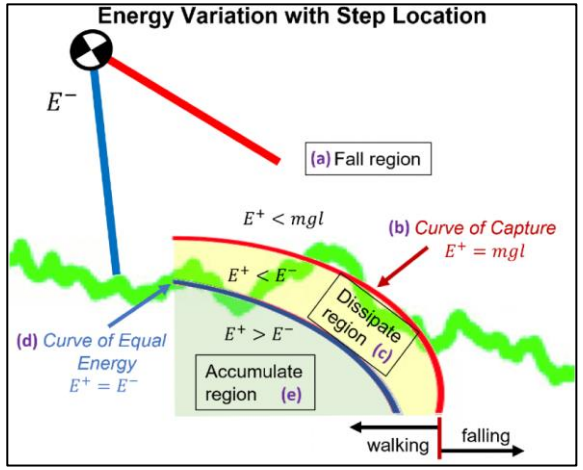

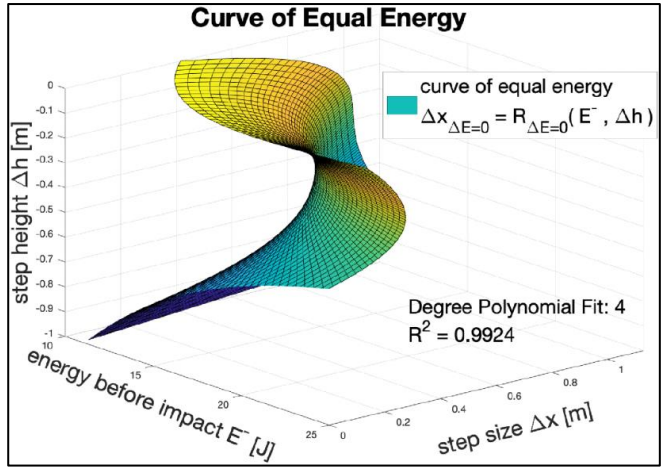

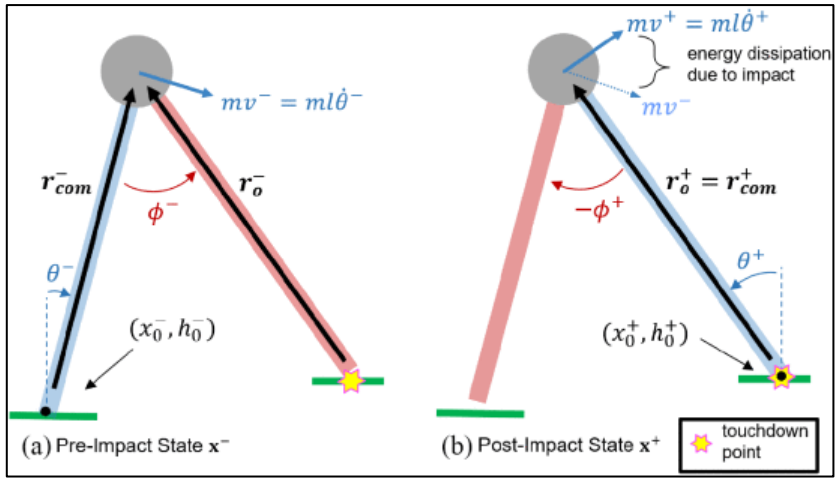

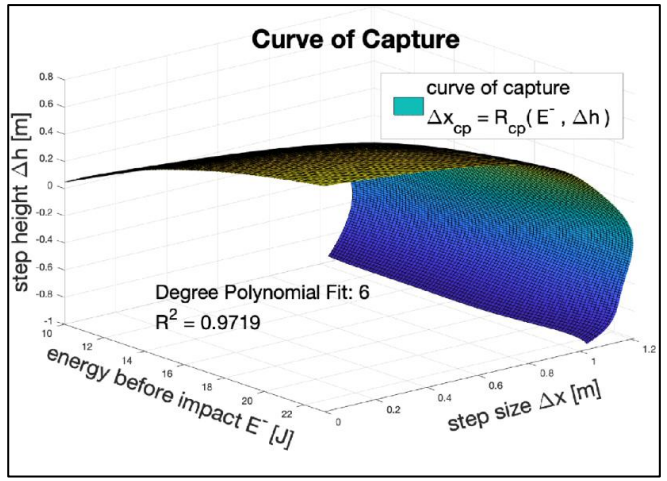

S. Crews and M. Travers, "Energy Management Through Footstep Selection For Bipedal Robots," in *IEEE Robotics and Automation Letters*, vol. 5, no. 4, pp. 5485-5493, Oct. 2020, doi: 10.1109/LRA.2020.3003235.

Energy Management Through Footstep Selection For Bipedal Robots

Results:

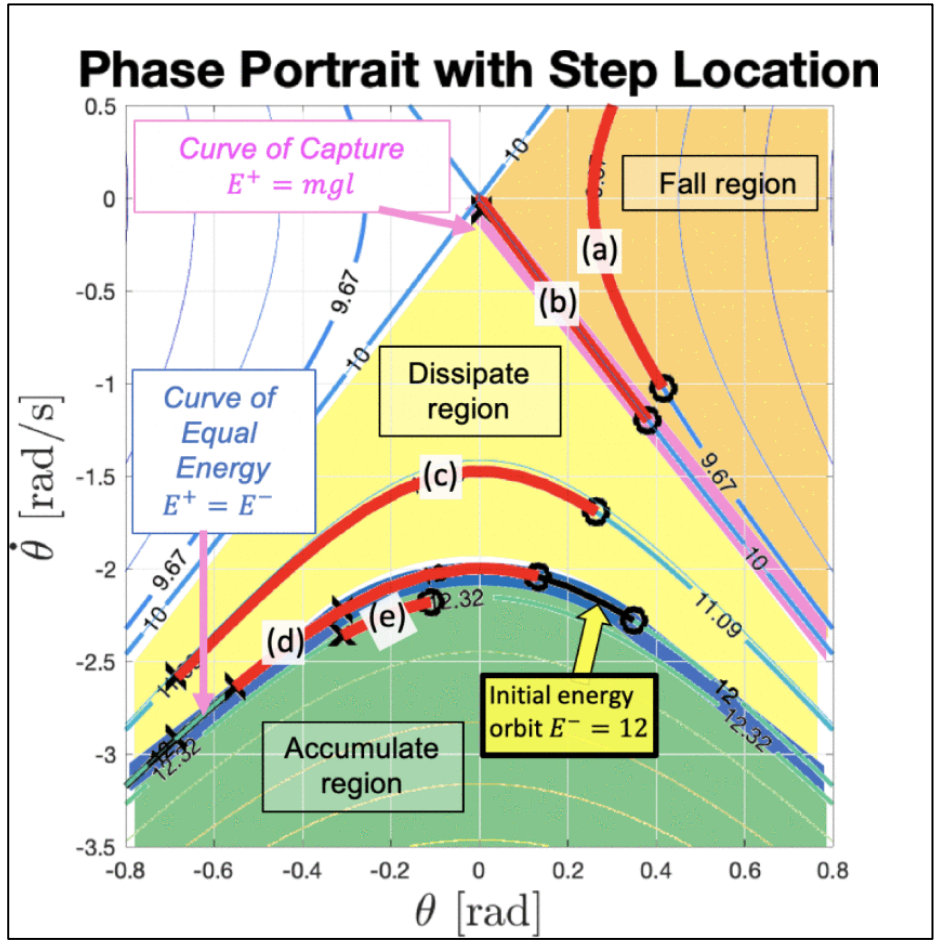

Avenues for further work:

- Extend to 3D walking
- Extend the work to AMPM

S. Crews and M. Travers, "Energy Management Through Footstep Selection For Bipedal Robots," in *IEEE Robotics and Automation Letters*, vol. 5, no. 4, pp. 5485-5493, Oct. 2020, doi: 10.1109/LRA.2020.3003235.

Reaction Mass Pendulum (RMP): An explicit model for centroidal angular momentum of humanoid robots

- Inverted pendulum models ignore the significant centroidal inertia
- Angular momentum control is essential in maintaining the balance of a full-body humanoid robot
- Planar RMP model: five generalized coordinates
- Composite Rigid Body (CRB) inertia $-{}^0\boldsymbol{I}$ (about CoM):

$$
\begin{aligned}
{}^0\boldsymbol{h} &= \sum_i {}^0\boldsymbol{h}_i = \sum_i {}^0\boldsymbol{I}_i {}^0\boldsymbol{v}_i \\
&= {}^0\boldsymbol{I}\boldsymbol{v}_0 + \sum_i \mathrm{Ad}^*_{\boldsymbol{G}_i^{-1}} \boldsymbol{I}_i \boldsymbol{J}_{i,q}\dot{\boldsymbol{q}} \\
&= {}^0\boldsymbol{I}\left(\boldsymbol{v}_0 + \mathbf{A}\dot{\boldsymbol{q}}\right)
\end{aligned}
$$

It is Instantaneous generalized inertia, assuming that all of its joints are frozen.

Physical description	Generalized coordinates (forces)	
	2D	3D
Radial distances of three pairs of point masses forming the ellipsoid and their actuation on linear tracks	r (f)	r_1, r_2, r_3 (f_1, f_2, f_3)
Orientation angles of the ellipsoid body and their actuation	α (τ)	α, β, γ (τ_1, τ_2, τ_3)
Leg length and its actuation	r_l (f_l)	r_l (f_l)
Leg orientation angles and their actuation	θ (τ_θ)	θ, ϕ (τ_θ, τ_ϕ)
CoP position and ground reaction force	x_{CoP} (R_x, R_y)	x_{CoP}, y_{CoP} (R_x, R_y, R_z)

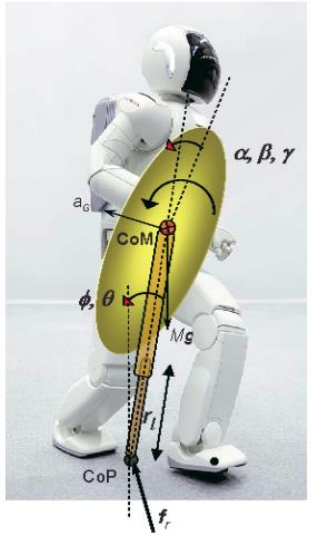

11 DOF

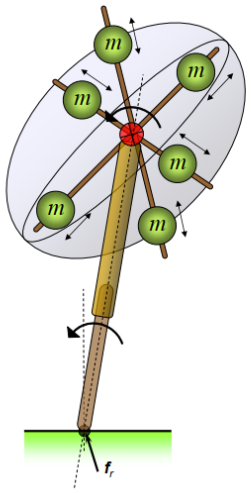

5 DOF

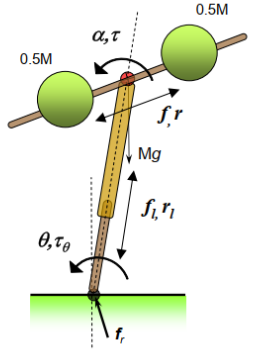

Equations of motion for planar RMP model:

$$
\begin{aligned}
f_l &= M\ddot{r}_l - Mr_l\dot{\theta}^2 + Mg\sin\theta \\
f &= M\ddot{r} - Mr(\dot{\theta} + \dot{\alpha})^2 \\
\tau_\theta &= Mr_l^2\ddot{\theta} + Mr^2(\ddot{\theta} + \ddot{\alpha}) + 2Mr_l\dot{r}_l\dot{\theta} \\
&\quad + 2Mr\dot{r}(\dot{\theta} + \dot{\alpha}) + Mgr_l\cos\theta \\
\tau &= Mr^2(\ddot{\theta} + \ddot{\alpha}) + 2Mr\dot{r}(\dot{\theta} + \dot{\alpha}).
\end{aligned}
$$

S. -H. Lee and A. Goswami, "Reaction Mass Pendulum (RMP): An explicit model for centroidal angular momentum of humanoid robots," *Proceedings 2007 IEEE International Conference on Robotics and Automation*, 2007, pp. 4667-4672, doi: 10.1109/ROBOT.2007.364198.

Reaction Mass Pendulum (RMP): An explicit model for centroidal angular momentum of humanoid robots

Equimomental inertia ellipsoid (about a reference point)

1. Ellipsoid with uniform density = mean density of the robot
2. Rotational inertia about any axis same as that of the robot (at that instant)

Robot → RMP is a mapping to lower dimensions

$$\begin{pmatrix} I_{xx} & I_{xy} & I_{xz} \\ I_{yx} & I_{yy} & I_{yz} \\ I_{zx} & I_{zy} & I_{zz} \end{pmatrix} \xrightarrow{\text{Solve for the eigenvalues \& eigenvectors}} \begin{pmatrix} \sigma_1 & 0 & 0 \\ 0 & \sigma_2 & 0 \\ 0 & 0 & \sigma_3 \end{pmatrix}$$

Rotational inertia of the humanoid

Principle moments of inertia

$$\sigma_1 = \frac{m}{5}(a_2^2 + a_3^2)$$
$$\sigma_2 = \frac{m}{5}(a_1^2 + a_3^2)$$
$$\sigma_3 = \frac{m}{5}(a_1^2 + a_2^2)$$
$$m = \tfrac{4}{3}\pi a_1 a_2 a_3 \rho$$

$$a_1 = \left(\frac{15}{8\pi\rho}\right)^{\frac{1}{5}} \frac{(-\sigma_1+\sigma_2+\sigma_3)^{\frac{2}{5}}}{[(\sigma_1-\sigma_2+\sigma_3)(\sigma_1+\sigma_2-\sigma_3)]^{\frac{1}{10}}}$$
$$a_2 = \left(\frac{15}{8\pi\rho}\right)^{\frac{1}{5}} \frac{(\sigma_1-\sigma_2+\sigma_3)^{\frac{2}{5}}}{[(-\sigma_1+\sigma_2+\sigma_3)(\sigma_1+\sigma_2-\sigma_3)]^{\frac{1}{10}}}$$
$$a_3 = \left(\frac{15}{8\pi\rho}\right)^{\frac{1}{5}} \frac{(\sigma_1+\sigma_2-\sigma_3)^{\frac{2}{5}}}{[(-\sigma_1+\sigma_2+\sigma_3)(\sigma_1-\sigma_2+\sigma_3)]^{\frac{1}{10}}}$$

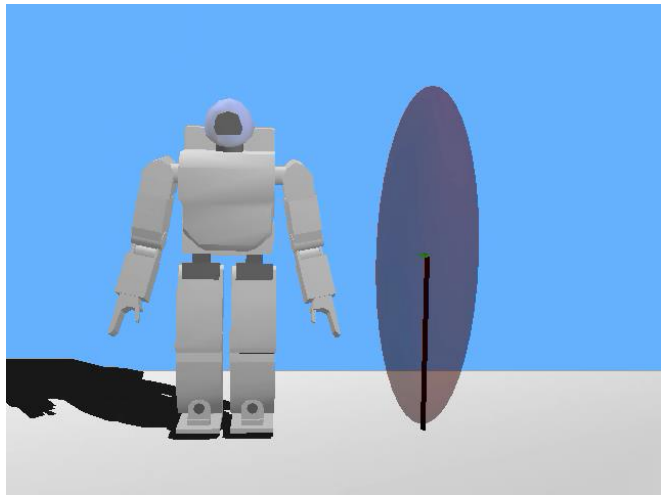

The CRB Inertia Jacobian and Inertia shaping:

Find variation of the inertia w.r.t. the joint coordinates

Control the aggregate dynamics of an articulated chain by controlling its CRB inertia

$$\boldsymbol{\Theta} = (\boldsymbol{T}_0, \boldsymbol{q})$$
$$\delta^s \widehat{\boldsymbol{I}} = \boldsymbol{J}_{\boldsymbol{I}} \delta \boldsymbol{\Theta}$$
$$\delta \widehat{\boldsymbol{I}} = \boldsymbol{J}_{\boldsymbol{I},0}(\boldsymbol{T}_0^{-1}\delta \boldsymbol{T}_0) + \boldsymbol{J}_{\boldsymbol{I},q}\delta \boldsymbol{q}$$

We cannot arbitrarily specify $\boldsymbol{q}$ always

1. The free-floating
2. Single support
3. Double support

Take proper pose while achieving the desired CRB inertia

$$\delta \boldsymbol{\Theta}_I = \boldsymbol{J}_{\boldsymbol{I}}^{\dagger} \delta(\widehat{\boldsymbol{I}}_d - \widehat{\boldsymbol{I}})$$

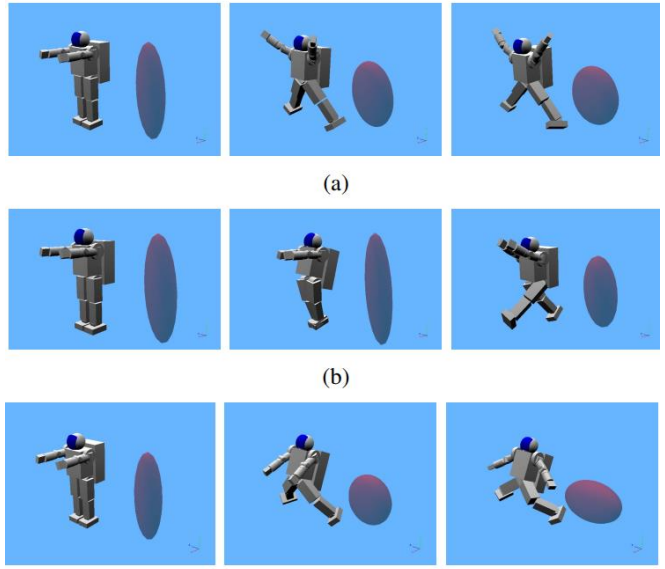

S. -H. Lee and A. Goswami, "Reaction Mass Pendulum (RMP): An explicit model for centroidal angular momentum of humanoid robots," *Proceedings 2007 IEEE International Conference on Robotics and Automation*, 2007, pp. 4667-4672, doi: 10.1109/ROBOT.2007.364198.

A Biomechanically Motivated Two-Phase Strategy for Biped Upright Balance Control

A two-phase control strategy for robust balance maintenance under a force disturbance is presented

- Phase 1: The *reflex phase* in which the body generates a rapid movement to absorb a disturbance force
- Phase 2: The body attempts to recover its original posture in the *recovery phase*

Stability of upright stance/ Home position controllability

- CoP ∈ interior of the foot ⇒ the system has the flexibility to withstand a perturbation
- CoP ∈ boundary ⇒ Loss of a degree of controllability and the system becomes under-actuated

Objective: Maintain x_P while generating internal angular momentum

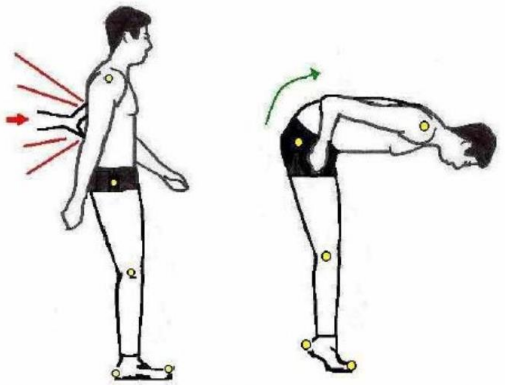

Fig. 1. A typical strategy employed by human beings in response to an external disturbance [16].

Position of CoP-ZMP

$$r_{CP} = \frac{n \times \left(\dot{H}_G + r_{CG} \times m(a_G - g) - r_{CF} \times F\right)}{n \cdot R}$$

Note:

$$n \cdot r_{CP} = 0$$

$$m a_G = F + R + mg$$

$$x_P = x_G + \frac{\dot{H}_G - y_G \dot{L}_x}{d} + \frac{y_F F_{dist}}{d}$$

$$d = \dot{L}_y + mg.$$

$$H_G = A(q)\dot{q}$$

$$L = D(q)\dot{q}.$$

$$\dot{H}_G = A(q)\ddot{q} + \dot{A}(q,\dot{q})\dot{q}$$

$$\dot{L} = D(q)\ddot{q} + \dot{D}(q,\dot{q})\dot{q}.$$

$$\dot{L}_x = D_x\ddot{q} + \dot{D}_x\dot{q}.$$

Momentum controller:

Produce H_G and regulate L_x

$$\dot{H}_G^* = k_1(x_P - x_G)$$

$$\dot{L}_x^* = -k_2 L_x$$

$$\ddot{q} = \begin{bmatrix} A \\ D_x \end{bmatrix}^+ \begin{pmatrix} \dot{H}_G^* - \dot{A}\dot{q} \\ \dot{L}_x^* - \dot{D}_x\dot{q} \end{pmatrix}$$

Absorbing the disturbance: The reflex phase

$$\tau = M(q)\ddot{q} + C(q,\dot{q}) + G(q).$$

Find required Joint torques

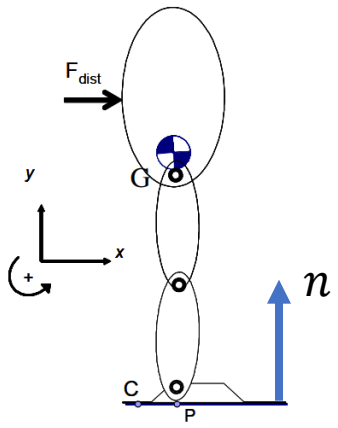

M. Abdallah and A. Goswami, "A Biomechanically Motivated Two-Phase Strategy for Biped Upright Balance Control," Proceedings of the 2005 IEEE International Conference on Robotics and Automation, 2005, pp. 1996-2001, doi: 10.1109/ROBOT.2005.1570406.

A Biomechanically Motivated Two-Phase Strategy for Biped Upright Balance Control

Going back to the home position: The recovery phase

- Minimize the joint torques due to gravity in the home position, i.e., minimize $\|G\|$, which also means finding a stationary point of V – maximizing V

$$\boldsymbol{G} = \frac{\partial V}{\partial \boldsymbol{q}}^T \qquad \boldsymbol{\tau} = \boldsymbol{M}(\boldsymbol{q})\ddot{\boldsymbol{q}} + \boldsymbol{C}(\boldsymbol{q},\dot{\boldsymbol{q}}) + \boldsymbol{G}(\boldsymbol{q}).$$

The Gradient method: maximize the potential energy

$$\dot{\boldsymbol{q}} = k\boldsymbol{G}$$

The Hessian method: minimize the gradient (is zero at an extremum)

$$\dot{\boldsymbol{q}} = -k[\tfrac{\partial \boldsymbol{G}}{\partial \boldsymbol{q}}]^{-1}\boldsymbol{G}$$

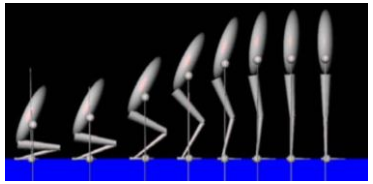

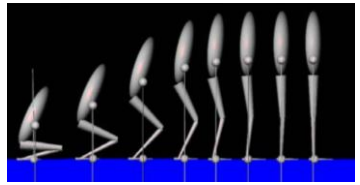

Full simulation:

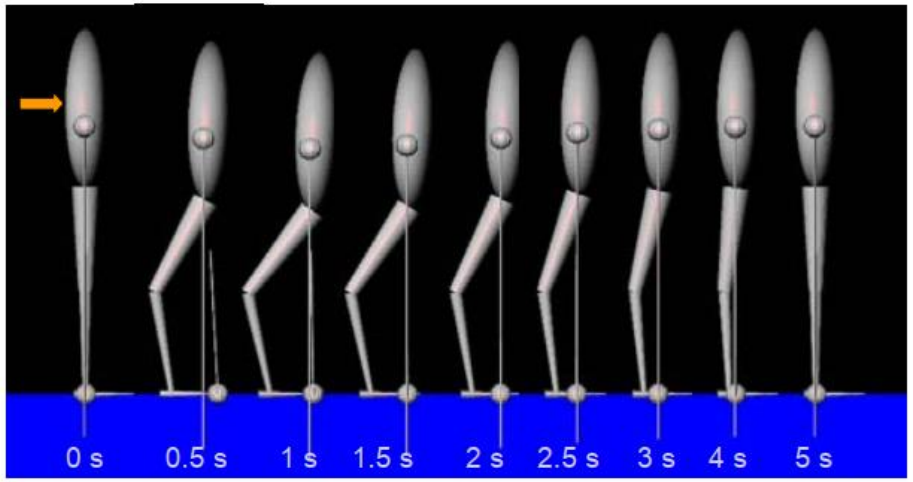

Fig. 9. A disturbance force of 300 N was applied to the robot for 0.1 seconds. The full *Reflex-Recovery Strategy* was used. The controller absorbed the disturbance during the first 0.1 seconds and then recovered the natural posture.

- Toppling force for the stiff robot: 96 N.
- Toppling force with the controller: 300 N for a duration of 0.1 seconds

Shortcomings and avenues for extension:

- The concept has been illustrated on a very low-DOF robot without applying realistic joint and torque limits.
- The controller starts right at the moment disturbance force is applied. There would be a lag in a real system.
- The concept can be tested further on a three-dimensional high-DOF robot.
- The control strategy can be expanded further to analyse the usefulness of including an active toe link in the humanoid (refer to prev. slide)

M. Abdallah and A. Goswami, "A Biomechanically Motivated Two-Phase Strategy for Biped Upright Balance Control," Proceedings of the 2005 IEEE International Conference on Robotics and Automation, 2005, pp. 1996-2001, doi: 10.1109/ROBOT.2005.1570406.

Centroidal dynamics of a humanoid robot

- Refocus attention to *centroidal dynamics*, i.e. write quantities like linear & angular momentum of the robot in the CoM frame
- Introduction of novel concept: Average Spatial Velocity
- Develop $O(N)$ algorithm to compute quantities associated with centroidal dynamics such as Centroidal Momentum Matrix
- **Momentum-based balance control that directly employs CMM and its advantages**

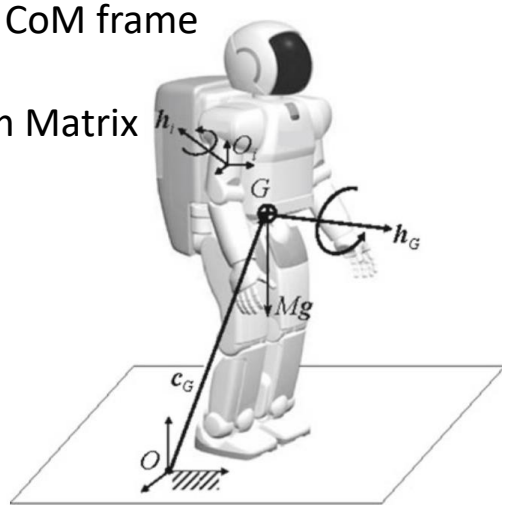

$$\mathbf{v}_i = \begin{bmatrix} \boldsymbol{\omega}_i \\ \mathbf{v}_i \end{bmatrix} = {}^i\mathbf{X}_{p(i)}\, \mathbf{v}_{p(i)} + \boldsymbol{\Phi}_i\, \dot{\mathbf{q}}_i$$

$${}^i\mathbf{X}_{p(i)} = \begin{bmatrix} {}^i\mathbf{R}_{p(i)} & \mathbf{0} \\ {}^i\mathbf{R}_{p(i)}\, \mathbf{S}({}^{p(i)}\mathbf{p}_i)^T & {}^i\mathbf{R}_{p(i)} \end{bmatrix}$$

$$\boldsymbol{h}_i = \begin{bmatrix} \mathbf{k}_i \\ \mathbf{l}_i \end{bmatrix} = \mathbf{I}_i\, \mathbf{v}_i$$

$$\mathbf{I}_i = \begin{bmatrix} \bar{\mathbf{I}}_i & m_i\, \mathbf{S}(\mathbf{c}_i) \\ m_i\, \mathbf{S}(\mathbf{c}_i)^T & m_i\, \mathbf{1} \end{bmatrix}$$

$$\bar{\mathbf{I}}_i = \bar{\mathbf{I}}_i^{cm} + m_i\, \mathbf{S}(\mathbf{c}_i)\, \mathbf{S}(\mathbf{c}_i)^T$$

System space

$$\mathbf{v} = \left[\mathbf{v}_1^T, \mathbf{v}_2^T, \ldots \mathbf{v}_i^T, \ldots \mathbf{v}_N^T\right]^T$$

$$\dot{\mathbf{q}} = \left[\dot{\mathbf{q}}_1^T, \dot{\mathbf{q}}_2^T, \ldots \dot{\mathbf{q}}_i^T, \ldots \dot{\mathbf{q}}_N^T\right]^T$$

$$\boldsymbol{J} = \left[\mathbf{J}_1^T, \mathbf{J}_2^T, \ldots \mathbf{J}_i^T, \ldots \mathbf{J}_N^T\right]^T$$

$$\mathbf{v} = \boldsymbol{J}\, \dot{\mathbf{q}}$$

$$\boldsymbol{h} = \left[\boldsymbol{h}_1^T, \boldsymbol{h}_2^T, \ldots \boldsymbol{h}_i^T, \ldots \boldsymbol{h}_N^T\right]^T$$

$$\boldsymbol{I} = \mathrm{diag}\left[\mathbf{I}_1, \mathbf{I}_2, \ldots \mathbf{I}_i, \ldots \mathbf{I}_N\right]$$

$$\boldsymbol{h} = \boldsymbol{I}\, \mathbf{v}$$

$$\boldsymbol{h} = \boldsymbol{I}\, \mathbf{v}$$

$$\boldsymbol{h} = \boldsymbol{A}\, \dot{\mathbf{q}}.$$

$$\boldsymbol{A} = \boldsymbol{I}\, \boldsymbol{J}$$

$$\mathbf{X}_G = \left[{}^1\mathbf{X}_G^T, {}^2\mathbf{X}_G^T, \ldots {}^i\mathbf{X}_G^T, \ldots {}^N\mathbf{X}_G^T\right]^T$$

$$\boxed{\boldsymbol{A}_G = \mathbf{X}_G^T\, \boldsymbol{A} = \mathbf{X}_G^T\, \boldsymbol{I}\, \boldsymbol{J}}$$

$$\boldsymbol{h}_G = \mathbf{X}_G^T\, \boldsymbol{A}\, \dot{\mathbf{q}}$$

$$\boldsymbol{h}_G = \mathbf{X}_G^T\, \boldsymbol{I}\, \mathbf{v}\,.$$

$$\boldsymbol{h}_G = \mathbf{X}_G^T\, \boldsymbol{I}\, \mathbf{v}^c = \mathbf{X}_G^T\, \boldsymbol{I}\, \mathbf{X}_G\, \mathbf{v}_G$$

$$\boldsymbol{h}_G = \sum_{i=1}^{N} {}^i\mathbf{X}_G^T\, \boldsymbol{h}_i = \mathbf{X}_G^T\, \boldsymbol{h}$$

$$\boxed{\boldsymbol{h}_G = \boldsymbol{A}_G(\mathbf{q})\, \dot{\mathbf{q}}}$$

$$\boldsymbol{h}_G = \begin{bmatrix} \mathbf{k}_G \\ \mathbf{l}_G \end{bmatrix} = \mathbf{I}_G\, \mathbf{v}_G = \begin{bmatrix} \bar{\mathbf{I}}_G & \mathbf{0} \\ \mathbf{0} & M\, \mathbf{1} \end{bmatrix} \begin{bmatrix} \boldsymbol{\omega}_G \\ \mathbf{v}_G \end{bmatrix}$$

$$\boldsymbol{I}_G = \mathbf{X}_G^T\, \boldsymbol{I}\, \mathbf{X}_G$$ Centroidal CRBI

$$\boxed{\mathbf{v}_G = (\boldsymbol{I}_G)^{-1}\, \boldsymbol{h}_G}$$

$$T = \frac{1}{2}\, \mathbf{v}^T\, \boldsymbol{I}\, \mathbf{v}$$

$$\mathbf{v} = \mathbf{v}^c + \mathbf{v}' = \mathbf{X}_G\, \mathbf{v}_G + \mathbf{v}'$$

$$T = \frac{1}{2}\, \mathbf{v}_G^T\, \boldsymbol{I}_G\, \mathbf{v}_G + \frac{1}{2}\, (\mathbf{v}')^T\, \boldsymbol{I}\, \mathbf{v}'$$

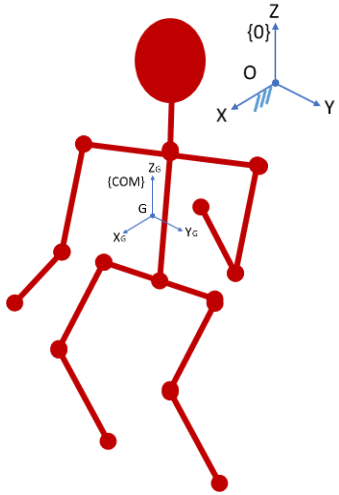

Transformation Diagram

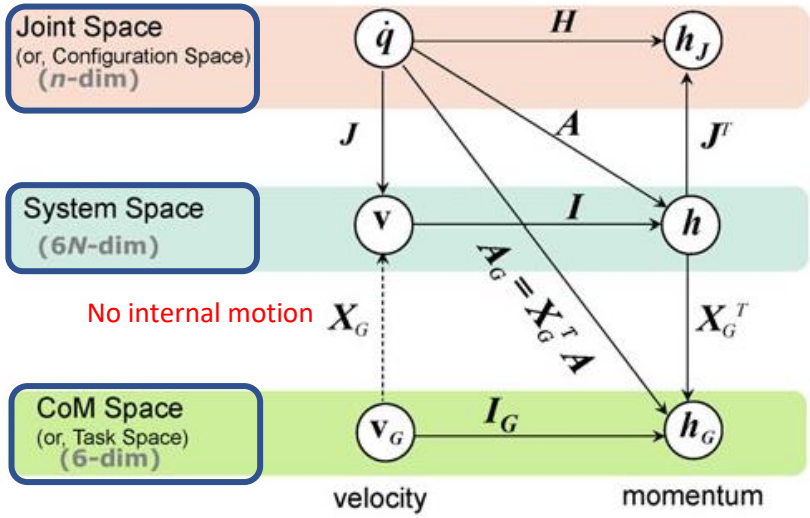

Orin, D.E., Goswami, A. & Lee, SH. Centroidal dynamics of a humanoid robot. *Auton Robot* **35,** 161–176 (2013). https://doi.org/10.1007/s10514-013-9341-4

Centroidal dynamics of a humanoid robot

$O(N)$ Algorithm for computation of CMM

N = d.o.f

inputs: *model*, $\mathbf{\Phi}_i$, ${}^i\mathbf{X}_{p(i)}$, $\dot{\mathbf{q}}_i$
output: $\boldsymbol{A}_G$, $\boldsymbol{h}_G$, $\mathbf{I}_G$, $\mathbf{v}_G$
model data: N, $p(i)$, $\mathbf{I}_i$

$\mathbf{I}_0^C = \mathbf{0}$
for $i = 1$ **to** N **do**
  $\mathbf{I}_i^C = \mathbf{I}_i$
end
for $i = N$ **to** 1 **do**
  $\mathbf{I}_{p(i)}^C = \mathbf{I}_{p(i)}^C + {}^i\mathbf{X}_{p(i)}^T\, \mathbf{I}_i^C\, {}^i\mathbf{X}_{p(i)}$
end
$\boldsymbol{h}_G = \mathbf{0}$
for $i = 1$ **to** N **do**
  ${}^i\mathbf{X}_G = {}^i\mathbf{X}_{p(i)}\, {}^{p(i)}\mathbf{X}_G$
  $(\boldsymbol{A}_G)_i = {}^i\mathbf{X}_G^T\, \mathbf{I}_i^C\, \mathbf{\Phi}_i$
  $\boldsymbol{h}_G = \boldsymbol{h}_G + (\boldsymbol{A}_G)_i\, \dot{\mathbf{q}}_i$
end
$\mathbf{I}_G = {}^0\mathbf{X}_G^T\, \mathbf{I}_0^C\, {}^0\mathbf{X}_G$
$\mathbf{v}_G = (\mathbf{I}_G)^{-1}\, \boldsymbol{h}_G$

The process does not seem to be of $O(N)$ for constrained dynamics (which is the most encountered case!)

Writing centroidal momentum of the robot in presence of constraints

$$\mathbf{L}_S\, \dot{\mathbf{q}}_S + \mathbf{L}_P\, \dot{\mathbf{q}}_P = \mathbf{0}\,,$$

$$\boldsymbol{h}_G = \boldsymbol{A}_G\, \dot{\mathbf{q}} = \boldsymbol{A}_G\, \mathbf{Q} \begin{bmatrix} \dot{\mathbf{q}}_S \\ \dot{\mathbf{q}}_P \end{bmatrix} = \mathbf{A}_{GS}\, \dot{\mathbf{q}}_S + \mathbf{A}_{GP}\, \dot{\mathbf{q}}_P$$

$$\boldsymbol{h}_G = \left(\mathbf{A}_{GP} - \mathbf{A}_{GS}\, \mathbf{L}_S^{-1}\, \mathbf{L}_P\right) \dot{\mathbf{q}}_P = \mathbf{A}_G^c\, \dot{\mathbf{q}}_P$$

Postural balance control using **Centroidal Momentum**

Set point regulation problem:

Maintain position & spatial (6D) velocity of the CoM

- dim(ctrl inputs) = dim($\boldsymbol{q_P}$) > dim(states to be controlled) = 6
- Balancing against external disturbances or balancing on non-stationary ground problem is tackled via momentum control instead of directly controlling the CoM pose.

$$\dot{\mathbf{h}}_{G,d} = \begin{bmatrix} \dot{\mathbf{k}}_{G,d} \\ \dot{\mathbf{l}}_{G,d} \end{bmatrix},$$

$$\dot{\mathbf{l}}_{G,d}/M = \boldsymbol{\Gamma}_{11}\,(\mathbf{v}_{G,d} - \mathbf{v}_G) + \boldsymbol{\Gamma}_{12}(\mathbf{c}_{G,d} - \mathbf{c}_G)$$

$$\dot{\mathbf{k}}_{G,d} = \boldsymbol{\Gamma}_{21}\,(\mathbf{k}_{G,d} - \mathbf{k}_G)\,,$$

- Optimal control problem- minimize the following qty:

$$w||\dot{\mathbf{h}}_{G,a} - \mathbf{A}_G^c\, \ddot{\mathbf{q}}_P - \dot{\mathbf{A}}_G^c\, \dot{\mathbf{q}}_P|| + (1-w)||\ddot{\mathbf{q}}_{U,d} - \ddot{\mathbf{q}}_U||$$

Further details on control strategy are discussed in another article

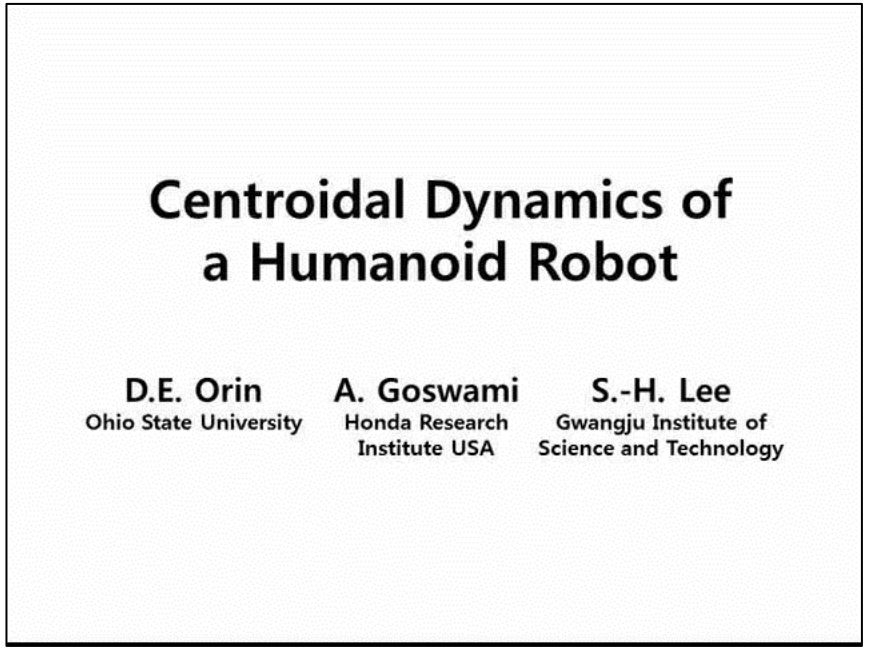

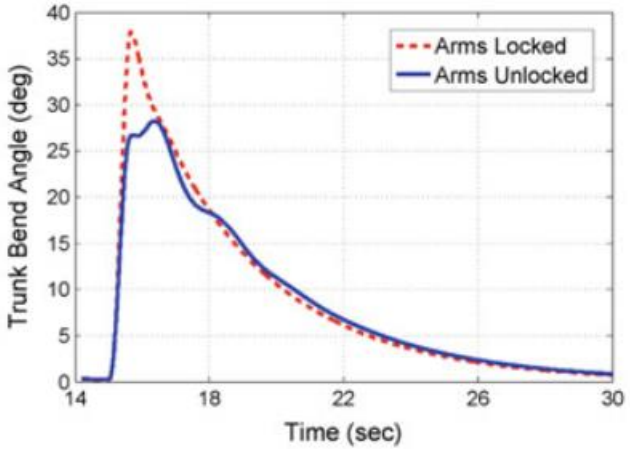

Orin, D.E., Goswami, A. & Lee, SH. Centroidal dynamics of a humanoid robot. *Auton Robot* **35,** 161–176 (2013). https://doi.org/10.1007/s10514-013-9341-4

A momentum-based balance controller for humanoid robots on non-level and non-stationary ground

Gap: Robust controller that can deal with:

- Discrete and non-level foot support
- Large unexpected and unknown disturbance
- Moving support
- Slip and trip

A specified rate of change of **spatial momentum** is used to define the control objectives

The motion is adheres to these constraints:

1. *ZMP ∈ the interior of the support region*
2. Normal GRF is always non-negative
3. Tangential GRF satisfies the friction limit

GRFs and CoP are computed for each leg separately

Equations of motion:

$$\boldsymbol{\tau} = \boldsymbol{H}(Q)\ddot{\boldsymbol{q}} + \boldsymbol{C}(Q,\dot{\boldsymbol{q}})\dot{\boldsymbol{q}} + \boldsymbol{\tau}_g(Q) - \boldsymbol{J}^T \boldsymbol{f}_c$$

$$\boldsymbol{0} = \boldsymbol{H}_0\ddot{\boldsymbol{q}} + \boldsymbol{C}_0\dot{\boldsymbol{q}} + \boldsymbol{\tau}_{g,0} - \boldsymbol{J}_0^T \boldsymbol{f}_c$$ CoM dynamics

$$\boldsymbol{\tau}_s = \boldsymbol{H}_s\ddot{\boldsymbol{q}} + \boldsymbol{C}_s\dot{\boldsymbol{q}} + \boldsymbol{\tau}_{g,s} - \boldsymbol{J}_s^T \boldsymbol{f}_c$$

$$\boldsymbol{0} = \boldsymbol{J}(Q)\dot{\boldsymbol{q}}$$ Loop closure constraints

$$\boldsymbol{0} = \boldsymbol{J}\ddot{\boldsymbol{q}} + \dot{\boldsymbol{J}}\dot{\boldsymbol{q}}$$

Control Strategy:

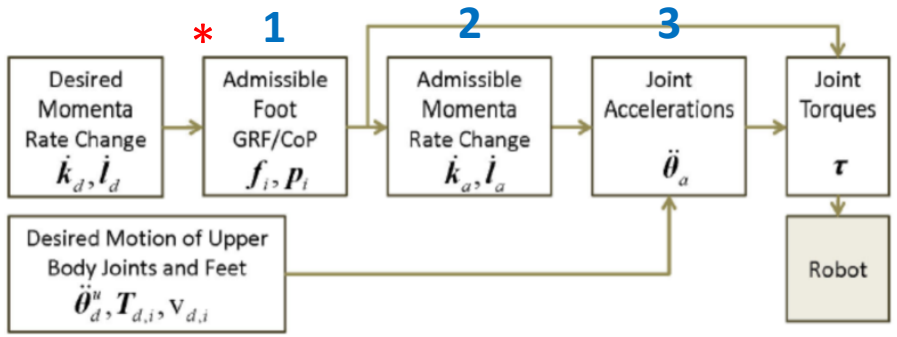

*In the double support phase, since the robot becomes redundantly actuated, the **ankle torques are minimized** while retaining all the other constraints

Feedback control policy:

$$\dot{\boldsymbol{k}}_d = \boldsymbol{\Gamma}_{11}(\boldsymbol{k}_d - \boldsymbol{k})$$

$$\dot{\boldsymbol{l}}_d/m = \boldsymbol{\Gamma}_{21}(\dot{\boldsymbol{r}}_{G,d} - \dot{\boldsymbol{r}}_G) + \boldsymbol{\Gamma}_{22}(\boldsymbol{r}_{G,d} - \boldsymbol{r}_G)$$

Postural balance: desired momenta set zero.

What happens when one of the said constraints is violated? P.T.O.

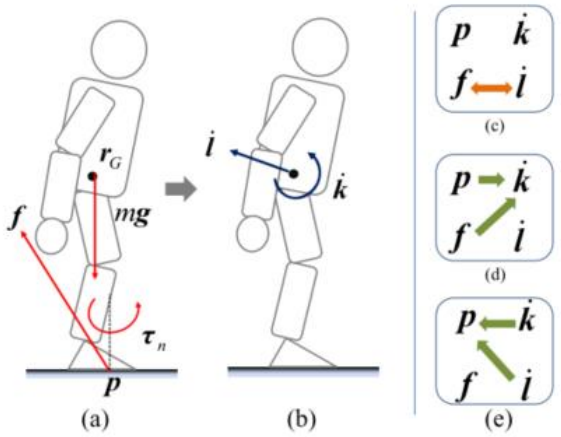

$$\dot{\boldsymbol{k}} = (\boldsymbol{p} - \boldsymbol{r}_G) \times \boldsymbol{f} + \boldsymbol{\tau}_n$$

$$\dot{\boldsymbol{l}} = m\boldsymbol{g} + \boldsymbol{f}$$

$$\boldsymbol{f} \in \mathbb{R}^3 \quad \boldsymbol{p} \in \mathbb{R}^2 \quad \boldsymbol{\tau}_n \in \mathbb{R} \qquad (\boldsymbol{k}^{\mathrm{T}}, \boldsymbol{l}^{\mathrm{T}})^{\mathrm{T}} \in \mathbb{R}^6$$

One to one correspondence bet^n **Spatial momentum** and **GRF-CoP**

Lee, SH., Goswami, A. A momentum-based balance controller for humanoid robots on non-level and non-stationary ground. *Auton Robot* **33,** 399–414 (2012).
https://doi.org/10.1007/s10514-012-9294-z

A momentum-based balance controller for humanoid robots on non-level and non-stationary ground

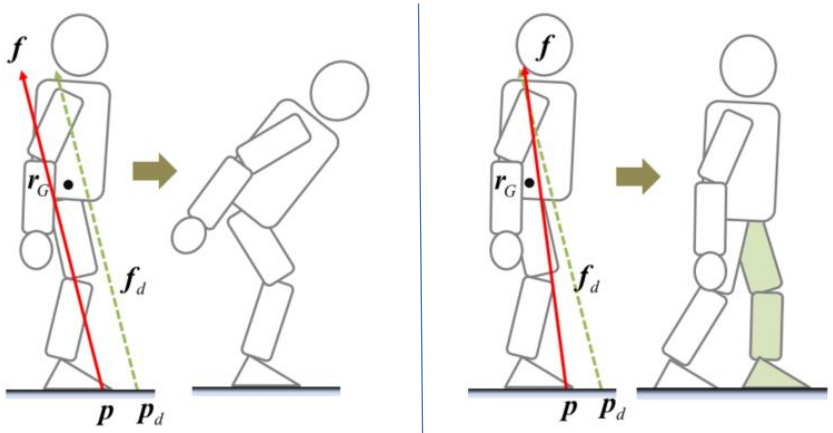

$\boldsymbol{k_d}$ compromized $\qquad$ $\boldsymbol{l_d}$ compromized

A case where $\dot{\boldsymbol{h}}_d = (\dot{\boldsymbol{k}}_d, \dot{\boldsymbol{l}}_d)$ leads to a fall:

In this paper preservation of $\dot{\boldsymbol{l}}_d$ is given higher priority as it allows for posture maintenance without stepping.

Gap: Design a smart controller take appropriate decision based on

- Environment conditions
- Status of the robot

1 Admissible foot **GRF** and **CoP**

A. Single support case:

i. Find the GRF-- $\boldsymbol{f}$

ii. Solve for (p_x, p_y)

$$\dot{\boldsymbol{k}} = (\boldsymbol{p} - \boldsymbol{r}_G) \times \boldsymbol{f} + \boldsymbol{\tau}_n$$

$$\dot{\boldsymbol{l}} = m\boldsymbol{g} + \boldsymbol{f}$$

B. Double support case:

Find GRF-CoP separately for each foot

Split the contributions due to GRF and ankle torque

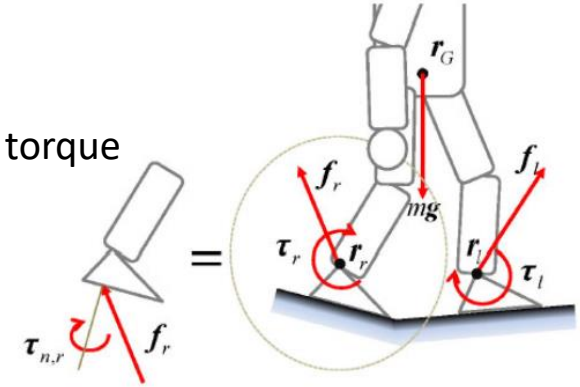

$$\dot{\boldsymbol{k}} = \dot{\boldsymbol{k}}_f + \dot{\boldsymbol{k}}_\tau$$

$$\boxed{\begin{aligned} \dot{\boldsymbol{k}}_f &= (\boldsymbol{r}_r - \boldsymbol{r}_G) \times \boldsymbol{f}_r + (\boldsymbol{r}_l - \boldsymbol{r}_G) \times \boldsymbol{f}_l \\ \dot{\boldsymbol{k}}_\tau &= \boldsymbol{\tau}_r + \boldsymbol{\tau}_l \end{aligned}}$$

$$\dot{\boldsymbol{l}} = m\boldsymbol{g} + \boldsymbol{f}_r + \boldsymbol{f}_l$$

$$\boldsymbol{\tau}_i = -[\boldsymbol{f}_i]_\times \boldsymbol{R}_i \boldsymbol{d}_i + \boldsymbol{R}_i \boldsymbol{\tau}_{n,i}$$

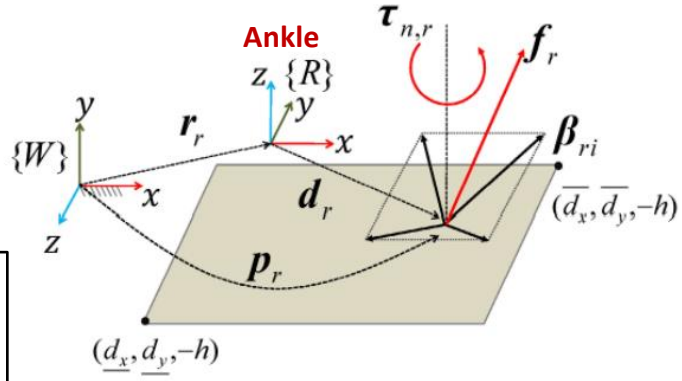

Minimize:

$$\boxed{\begin{aligned} & w_l \left\| \dot{\boldsymbol{l}}_d - \dot{\boldsymbol{l}}(\boldsymbol{f}_r, \boldsymbol{f}_l) \right\|^2 + w_k \left\| \dot{\boldsymbol{k}}_d - \dot{\boldsymbol{k}}(\boldsymbol{f}_r, \boldsymbol{f}_l, \boldsymbol{\tau}_r, \boldsymbol{\tau}_l) \right\|^2 \\ & + w_f \left(\|\boldsymbol{f}_r\|^2 + \|\boldsymbol{f}_l\|^2 \right) + w_\tau \left(\|\boldsymbol{\tau}_r\|^2 + \|\boldsymbol{\tau}_l\|^2 \right) \end{aligned}}$$

Lee, SH., Goswami, A. A momentum-based balance controller for humanoid robots on non-level and non-stationary ground. *Auton Robot* **33,** 399–414 (2012).
https://doi.org/10.1007/s10514-012-9294-z

A momentum-based balance controller for humanoid robots on non-level and non-stationary ground

Admissible joint accelerations are determined based on allowable limits

$$\ddot{\boldsymbol{\theta}}_a = \underset{\ddot{\boldsymbol{\theta}}}{\operatorname{argmin}}\ w_b \|\dot{\boldsymbol{h}}_a - \boldsymbol{A}\ddot{\boldsymbol{q}} - \dot{\boldsymbol{A}}\dot{\boldsymbol{q}}\| + (1 - w_b)\left\|\ddot{\boldsymbol{\theta}}_d^u - \ddot{\boldsymbol{\theta}}^u\right\|$$

$$\text{s.t.} \quad \boldsymbol{J}\ddot{\boldsymbol{q}} + \dot{\boldsymbol{J}}\dot{\boldsymbol{q}} = \boldsymbol{a}_d \quad \text{and} \quad \ddot{\boldsymbol{\theta}}_l \leq \ddot{\boldsymbol{\theta}} \leq \ddot{\boldsymbol{\theta}}_u,$$

Simulation:

- Software: Locomote simulator, based on software package Webots, which uses ODE (open dynamics engine) solver
- 50kg robot, 6 DOF per leg
- Arms are locked

Avenues open for research

- Setting the desired angular momentum for complex motions such as locomotion
- Balance maintenance through stepping (in all directions)

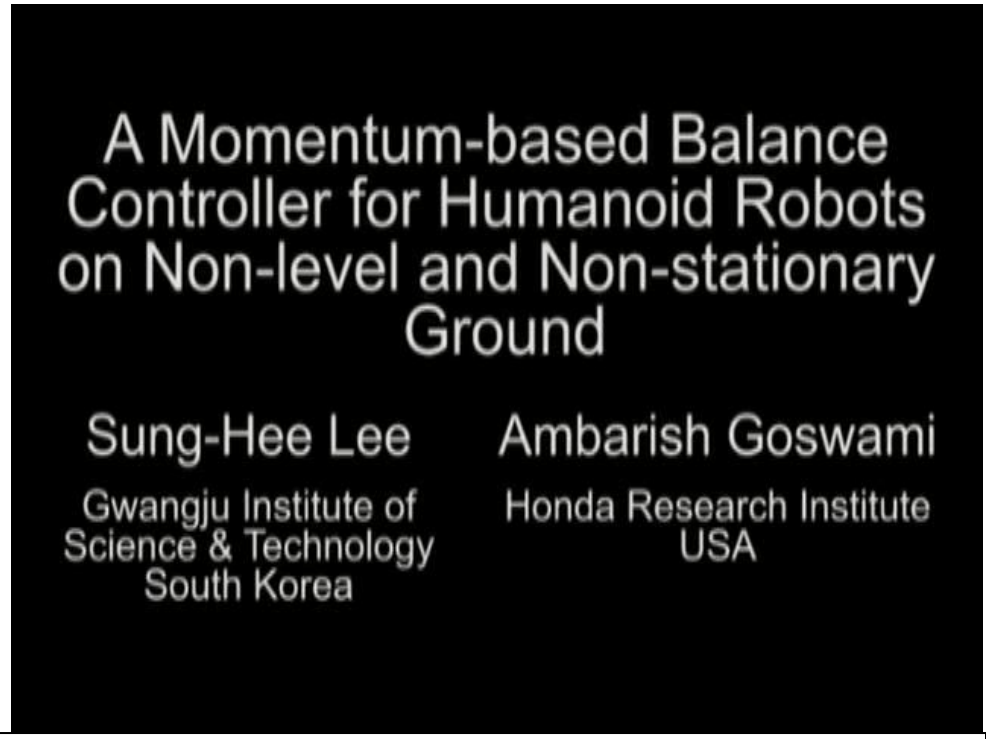

Lee, SH., Goswami, A. A momentum-based balance controller for humanoid robots on non-level and non-stationary ground. *Auton Robot* **33,** 399–414 (2012). https://doi.org/10.1007/s10514-012-9294-z

Effects of constraints on standing balance control of a biped with toe joints

- Importance of toe-joint torque in preventing rollover
- Effect of toe-link length on standing balance control

- **The biped is stabilized only by the ankle and the toe torque**
- Satisfaction of the following three constraints => balance
  - No lift-off (and penetration in the ground)
  - No rollover toe or heel
  - No slipping
- Above constraints also impose bounds on the control torques
- Beyond a critical angular velocity $\dot{\theta}$, the robot falls regardless of control torques

- Importance of active toe-joint:
  - Adds to the stability margin
  - Smoother and energy-efficient walking
  - Better distribution of GRFs

$$\begin{cases} F_{hy} > 0 \\ F_{ty} > 0 \\ -L_t < X_{ct} < 0 \\ |F_x| < \mu F_y \end{cases} \quad \begin{cases} B_1\tau_a + B_2\tau_t + B_3 > 0 \\ C_1\tau_a + C_2\tau_t + C_3 > 0 \\ -L_t < \dfrac{D_1 - \tau_t}{C_1\tau_a + C_2\tau_t + C_3} < 0 \\ |A_1\tau_a + A_2| < \mu[(B_1 + C_1)\tau_a + (B_2 + C_2)\tau_t + (B_3 + C_3)] \end{cases}$$

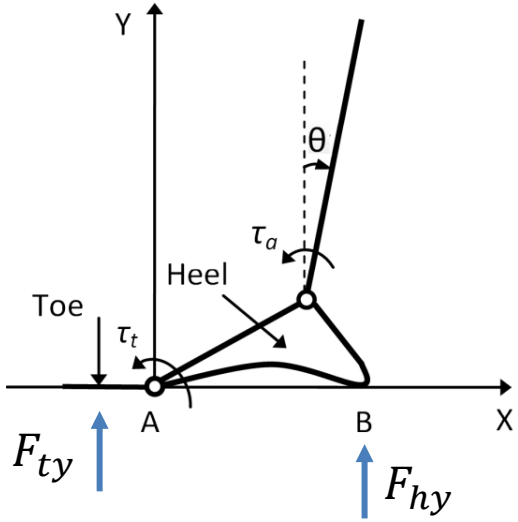

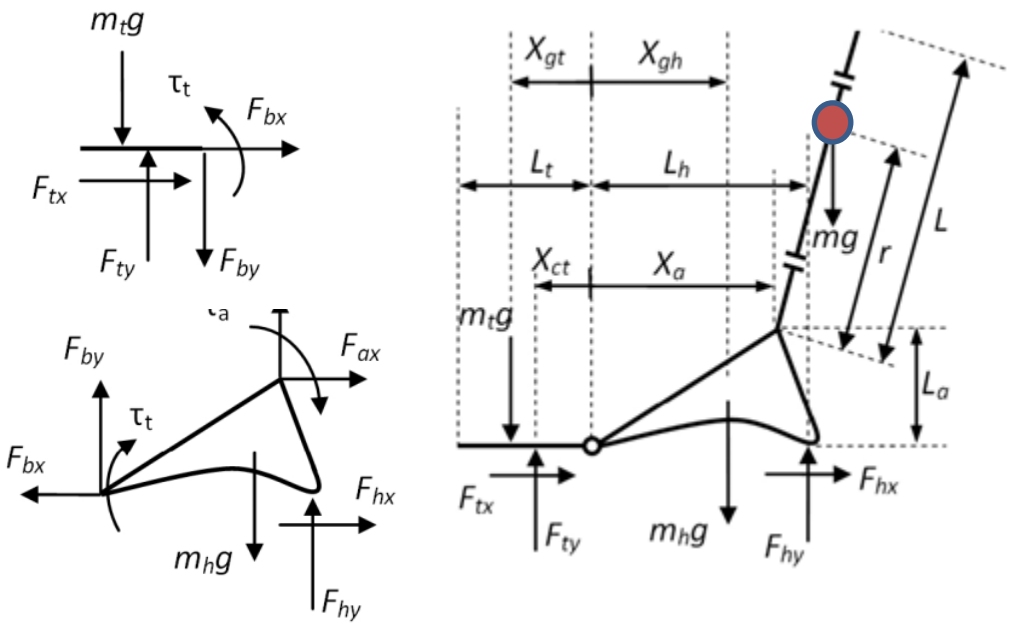

$$F_{ax} = mr\dot{\theta}^2 \sin\theta - mr\ddot{\theta}\cos\theta$$

$$F_{ay} = mr\dot{\theta}^2 \cos\theta + mr\ddot{\theta}\sin\theta - mg$$

$$\tau_a = mgr\sin\theta - (I + mr^2)\ddot{\theta}$$

$$F_{hx} + F_{tx} + F_{ax} = 0$$

$$F_{hy} + F_{ty} - m_t g - m_h g + F_{ay} = 0$$

$$\tau_t + F_{ty}X_{ct} - m_t g X_{gt} = 0$$

$$\tau_t + \tau_a - F_{hy}L_h + m_h g X_{gh} + F_{ax}L_a - F_{ay}X_a = 0$$

Kouchaki, E., Wu, C. Q., & Sadigh, M. J. (2012). Effects of constraints on standing balance control of a biped with toe-joints. *International Journal of Humanoid Robotics*, *9*(03), 1250016. https://doi.org/10.1142/S0219843612500168

Effects of constraints on standing balance control of a biped with toe joints

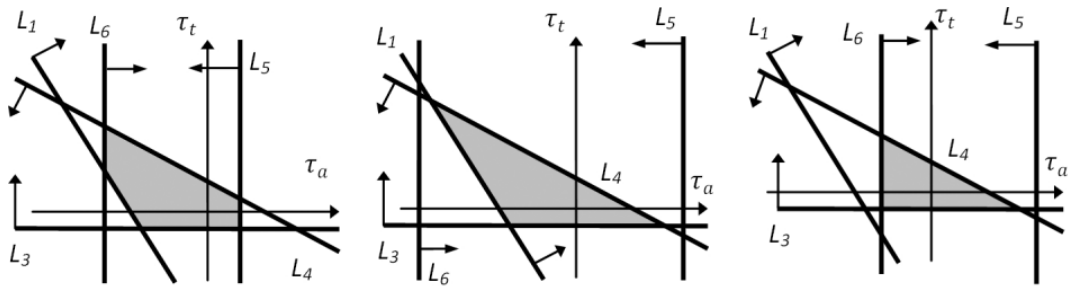

Area between L_i and L_j shows the range of torques τ_a and τ_t satisfying the constraints as follows:

L_1 and L_2: The gravity constraint

L_3 and L_4: The COP constraint (L_4 is always more conservative than L_2)

L_5 and L_6: The friction constraint

Results

- The role of the toe torque on standing balance has also been examined.
- The toe torque gives the biped a better capability to keep standing balance and prevents the anterior tipping over as compared to the case that the foot is simplified as one rigid link.
- However, this torque cannot help the system significantly to prevent posterior tipping over.

Avenues for extension:

- Simplified model of humanoid is used wherein angular momentum characterization is missing (hip strategy)
- How does toe help when forward/ backward stepping is used for balancing against a large external disturbance?
- Perform the same analyses where the foot is partially in contact with the ground

Results

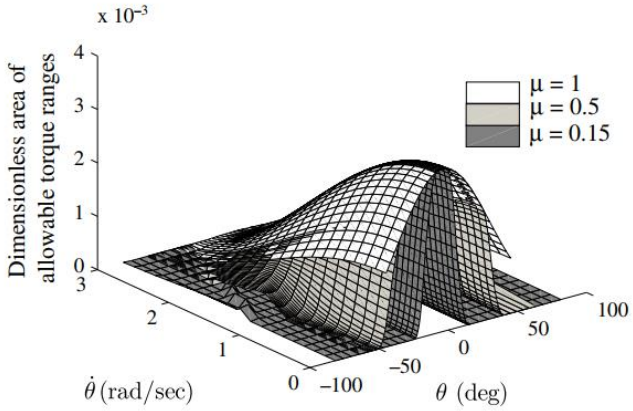

Effects of the friction coefficient on area of the allowable torque range

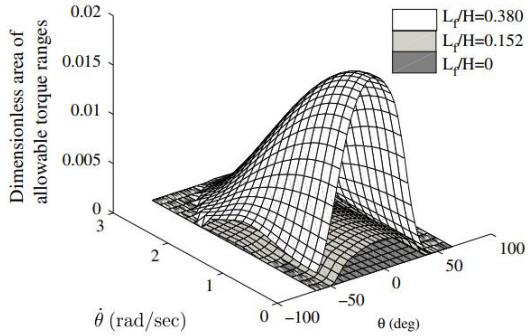

Fig. 15. Effects of length of foot on area of the allowable torque ranges.

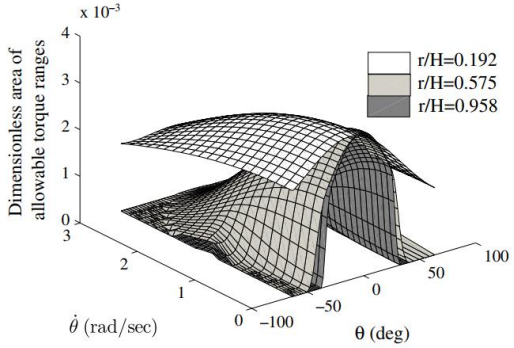

Fig. 17. Effects of center of mass position on area of the allowable torque ranges.

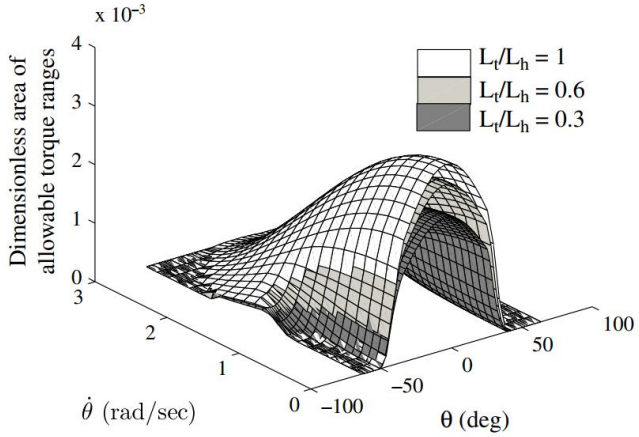

Fig. 19. Effects of length of toe-link on area of the allowable torque ranges.

Kouchaki, E., Wu, C. Q., & Sadigh, M. J. (2012). Effects of constraints on standing balance control of a biped with toe-joints. *International Journal of Humanoid Robotics*, *9*(03), 1250016. https://doi.org/10.1142/S0219843612500168

Making feasible walking motion of humanoid robots from human motion capture data

- Adaptation of Human Motion Capture Data for driving a 40 DOF humanoid robot
  - Kinematic inconsistencies: Require joint angle correction
  - Dynamic inconsistencies and underactuation: An optimisation problem is solved to match a desired ZMP trajectory with the actual one. Design variables are two joint angles at the torso.

Euler's equation about ZMP:

$$\sum_i(\boldsymbol{r}_i\times m_i\boldsymbol{a}_i+\boldsymbol{I}_i\boldsymbol{\alpha}_i+\boldsymbol{\omega}_i\times\boldsymbol{I}_i\boldsymbol{\omega}_i)=\sum_i\boldsymbol{r}_i\times m_i\boldsymbol{g}+\boldsymbol{r}_L\times\boldsymbol{f}_L+\boldsymbol{r}_R\times\boldsymbol{f}_R+\boldsymbol{n}_L+\boldsymbol{n}_R$$

Solve for ZMP: $-\sum_i(\boldsymbol{r}_i\times m_i\boldsymbol{a}_i+\boldsymbol{I}_i\boldsymbol{\alpha}_i+\boldsymbol{\omega}_i\times\boldsymbol{I}_i\boldsymbol{\omega}_i)+\sum_i(\boldsymbol{r}_i\times m_i\boldsymbol{g})=(0,0,*)^{\mathrm{T}}$

Net CoP: $\boldsymbol{r}_L\times\boldsymbol{f}_L+\boldsymbol{r}_R\times\boldsymbol{f}_R+\boldsymbol{n}_L+\boldsymbol{n}_R=(0,0,*)^{\mathrm{T}}$

Adaptation of HMCD

1. Set the desired ZMP trajectory based on foot motion data in the HMCD
2. Apply periodic joint motion correction at selected joints

Corrective motion at ith joint

$$\delta\theta_i=\sum_n a_{in}\sin n\omega_{\omega i}t+b_{in}\cos n\omega_{\omega i}t$$

$$\text{Minimize } \mathcal{J}=\int\left\|\boldsymbol{p}_{zmp}-\boldsymbol{p}^d_{zmp}\right\|^2\mathrm{d}t$$

- $\boldsymbol{p}_{ZMP}$ is computed using the EoM
- GRFs are needed for joint torque computations

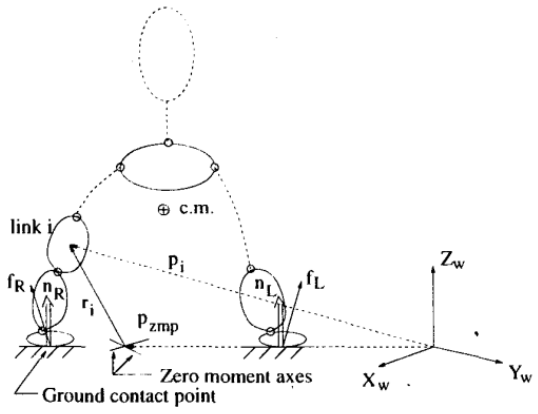

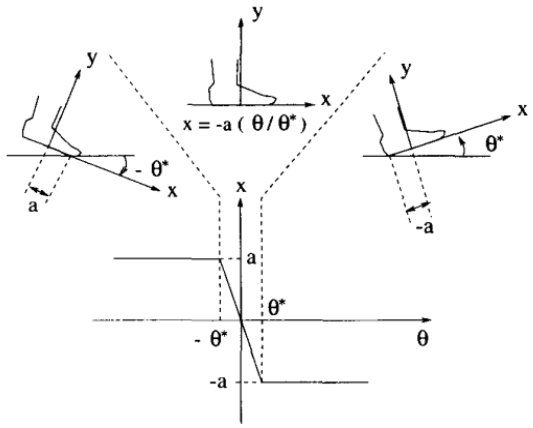

Model of the robot foot to accommodate the rolling action of the human foot

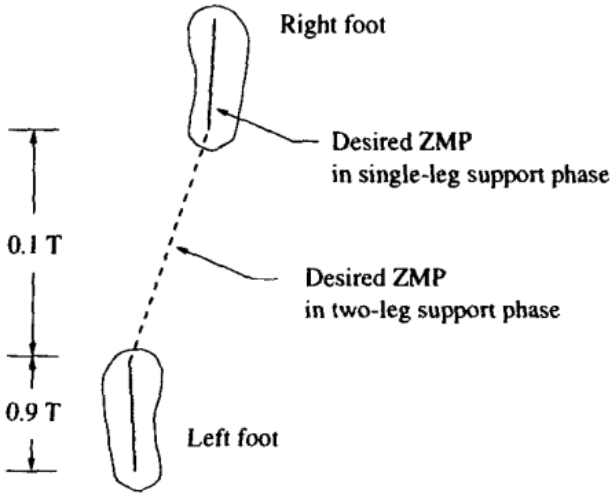

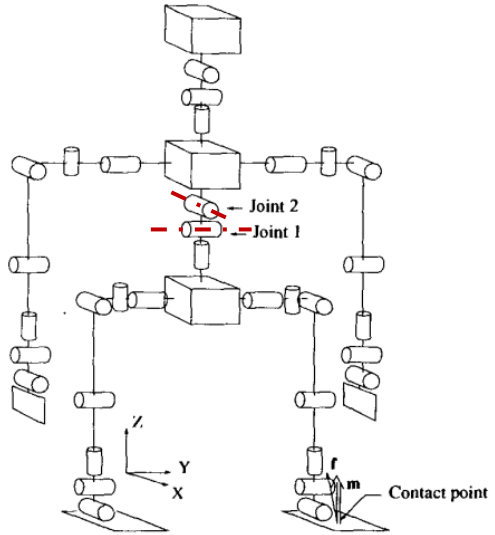

A. Dasgupta and Y. Nakamura, "Making feasible walking motion of humanoid robots from human motion capture data," *Proceedings 1999 IEEE International Conference on Robotics and Automation (Cat. No.99CH36288C)*, 1999, pp. 1044-1049 vol.2, doi: 10.1109/ROBOT.1999.772454.

Making feasible walking motion of humanoid robots from human motion capture data

Computation of Ground Reaction Forces:
Why? Avoid slipping

$$m_{cm}\boldsymbol{a}_{cm} = \boldsymbol{f}_L + \boldsymbol{f}_R + m_{cm}\boldsymbol{g}$$

SSP:

- One of $\boldsymbol{f}_L$ or $\boldsymbol{f}_R$ is zero. The other one computed directly

DSP:

- The z-component, i.e., $\boldsymbol{f}_{L3}$ and $\boldsymbol{f}_{R3}$ are derived from:

$$\boldsymbol{r}_L \times \boldsymbol{f}_L + \boldsymbol{r}_R \times \boldsymbol{f}_R + \boldsymbol{n}_L + \boldsymbol{n}_R = (0, 0, *)^{\mathrm{T}}$$

$$y_L f_{L3} + y_R f_{R3} = y_{zmp}(f_{L3} + f_{R3})$$

$$x_L f_{L3} + x_R f_{R3} = x_{zmp}(f_{L3} + f_{R3})$$

- The x and y components are computed by solving an optimisation problem
  - stability margin $\boldsymbol{d_1}$ is maximized, and
  - $\boldsymbol{d_2}$ (inversely proportional to the internal forces of the closed-loop mechanism) is minimized

$$\begin{aligned}
\text{Min} \quad & -d_1 - d_2 \\
\text{subject to} \quad & f_{L1} + f_{R1} = m_{cm} a_{cm1} \\
& f_{L2} + f_{R2} = m_{cm} a_{cm2}
\end{aligned}$$

Friction constraint:

$$\mathbf{P}[f_{L1}, f_{L2}, f_{R1}, f_{R2}]^{\mathrm{T}} + d_1 \mathbf{1} < \mathbf{b}$$

Internal force constraints:

$$\frac{(\boldsymbol{p}_L - \boldsymbol{p}_R)^{\mathrm{T}}}{\|\boldsymbol{p}_L - \boldsymbol{p}_R\|}(\boldsymbol{f}_L - \boldsymbol{f}_R) + d_2 < 0$$

$$-\frac{(\boldsymbol{p}_L - \boldsymbol{p}_R)^{\mathrm{T}}}{\|\boldsymbol{p}_L - \boldsymbol{p}_R\|}(\boldsymbol{f}_L - \boldsymbol{f}_R) + d_2 < 0$$

$$d_1, d_2 > 0$$

$$\mathbf{P} = \begin{bmatrix} 1 & 0 & 0 & 0 \\ -1 & 0 & 0 & 0 \\ 0 & 1 & 0 & 0 \\ 0 & -1 & 0 & 0 \\ 0 & 0 & 1 & 0 \\ 0 & 0 & -1 & 0 \\ 0 & 0 & 0 & 1 \\ 0 & 0 & 0 & -1 \end{bmatrix} \text{ and } \mathbf{b} = \begin{bmatrix} -\mu f_{L3} \\ -\mu f_{L3} \\ -\mu f_{L3} \\ -\mu f_{L3} \\ -\mu f_{R3} \\ -\mu f_{R3} \\ -\mu f_{R3} \\ -\mu f_{R3} \end{bmatrix},$$

A. Dasgupta and Y. Nakamura, "Making feasible walking motion of humanoid robots from human motion capture data," *Proceedings 1999 IEEE International Conference on Robotics and Automation (Cat. No.99CH36288C)*, 1999, pp. 1044-1049 vol.2, doi: 10.1109/ROBOT.1999.772454.

Making feasible walking motion of humanoid robots from human motion capture data

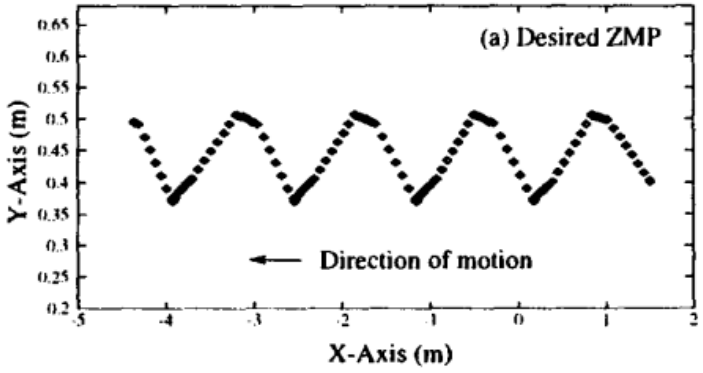

Planned ZMP trajectory

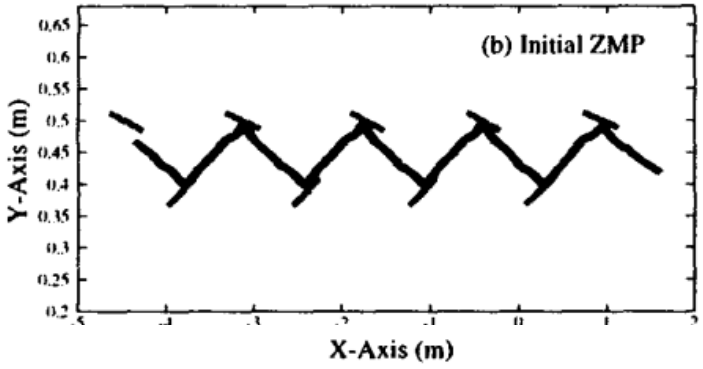

ZMP trajectory w/o any correction

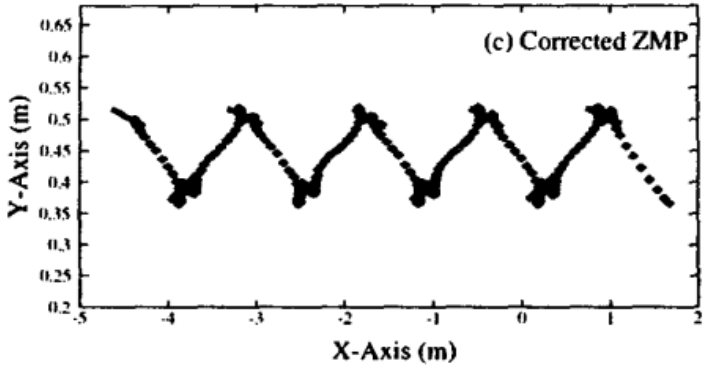

Corrected ZMP trajectory

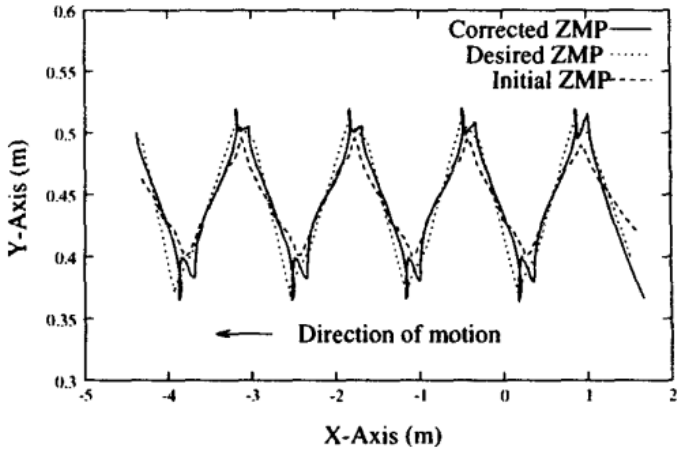

Shortcomings and avenues for extension:

- Coarse kinematic mapping using markers only
- No comments on the resulting optimum- global or local
- The technique works best for repeated motions only, such as walking.
- The model cannot handle multi-contact phases
- Capture Point or DCM based walking can be used for trajectory planning, instead of ZMP

A. Dasgupta and Y. Nakamura, "Making feasible walking motion of humanoid robots from human motion capture data," *Proceedings 1999 IEEE International Conference on Robotics and Automation (Cat. No.99CH36288C)*, 1999, pp. 1044-1049 vol.2, doi: 10.1109/ROBOT.1999.772454.

Overview of the torque-controlled humanoid robot TORO

This article describes the mechanical design, sensors & electronics, and the computer hardware of TORO
Also provides an introduction to walking and multi-contact balancing algorithms

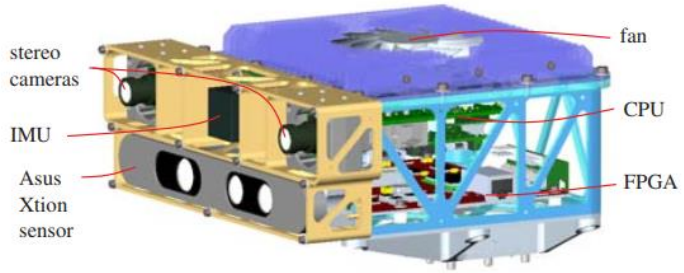

Introduction

- Aim: an experimental platform for evaluating torque based control approaches
- Off the shelf LWR units are used. Both position control and torque control possible
- Torque control allows robust interaction with the environment and self collisions
- Torque control methods: Inverse dynamics control, impedance control, SEA, etc.

Mechanical design

- 174cm, 76.4kg, 25 + 2 joints, electrical prosthesis for grasping, 19 x 9.5cm foot
- LWR drive: BLDC motor + Harmonic drive + torque sensor (1kHz) + encoders + brake
- Shell structure for the limbs-- machined and cast aluminium, shoulders- carbon fiber, aluminium plates + tube weldment for the thorax
- Each arm can lift up to 5 kg

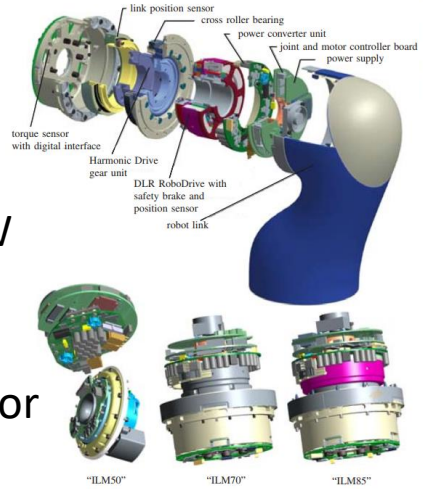

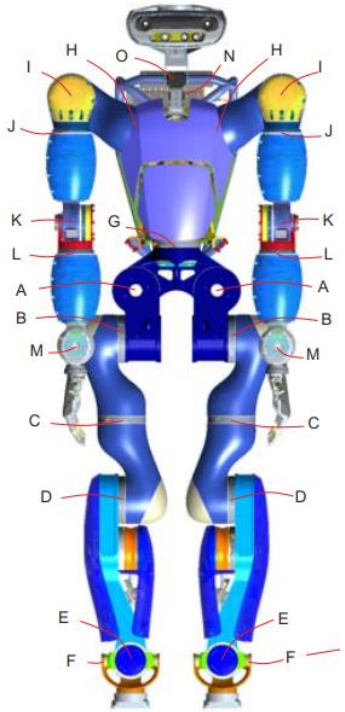

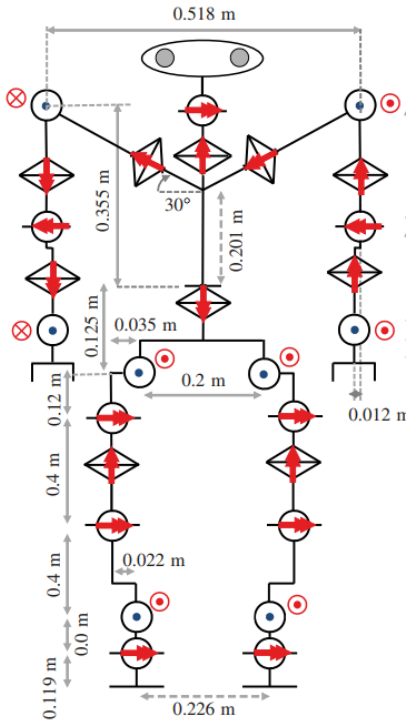

Electronics and sensors

- 48V 6.6Ah $LiFePO_4$ x 2 batteries, steady-state power draw: 250W
- Partially automated recalibration of joint angles.
- Feet: 6 DOF force-torque sensors (FTS) 1000N and 100Nm
- IMU in thorax, stereo cameras + Asus Xtion Pro depth image sensor
- Visual information processed on FPGA @ 15Hz, FTS @ 500Hz

J. Englsberger *et al.*, "Overview of the torque-controlled humanoid robot TORO," *2014 IEEE-RAS International Conference on Humanoid Robots*, 2014, pp. 916-923, doi: 10.1109/HUMANOIDS.2014.7041473.

Overview of the torque-controlled humanoid robot TORO

Computer hardware and software

- Sercos II ring bus connection, glass fibers used for galvanic isolation of all the LWR drives. Each LWR controls a joint at 3kHz
- Intel Core i7 computers x 2 mounted on compactPCI rack
- One for real-time control of joints and the second for motion planning and communication
- Motion estimation and (terrain) mapping are done using Core2Duo and ARM7.
- Hardware abstraction layer and a proprietary middleware is used
- OS: Real Time Linux based on kernel 3.0. Control loop updated at 1kHz
- Real-time control software developed in Simulink. Exported in C, compiled and uploaded to the robot

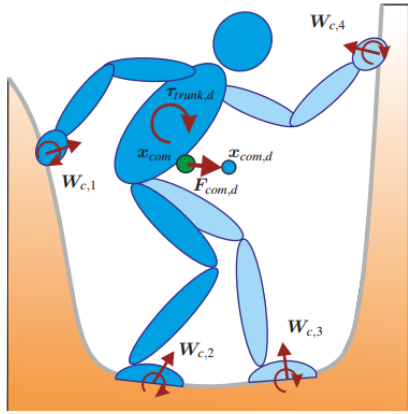

DCM-based walking

- Walking algorithms are based on Divergent Component of Motion- a generalization of Capture Point to 3D
- Walking algorithms that guarantee continuous leg forces during DSP and heel-to-toe shift are derived
- The walking algorithm is based on admittance control

Multi-contact balancing

- Given the desired position of CoM and orientation of the hip, the desired wrench to be applied is computed according to a compliance control law:

$$\boldsymbol{W}_d = \begin{bmatrix} m\boldsymbol{g} \\ 0 \end{bmatrix} - \boldsymbol{D} \begin{bmatrix} \dot{\boldsymbol{x}}_{com} \\ \boldsymbol{\omega} \end{bmatrix} - \begin{bmatrix} \boldsymbol{K}(\boldsymbol{x}_{com} - \boldsymbol{x}_{com,d}) \\ \boldsymbol{\tau}_k(\boldsymbol{R}, \boldsymbol{R}_d) \end{bmatrix}$$

- The wrench distribution at the contact points is done based on optimizing certain quantities while adhering to constraints such as friction, CoP limit and unilaterality of contact forces

J. Englsberger *et al.*, "Overview of the torque-controlled humanoid robot TORO," *2014 IEEE-RAS International Conference on Humanoid Robots*, 2014, pp. 916-923, doi: 10.1109/HUMANOIDS.2014.7041473.

Three dimensional bipedal walking control using Divergent Component of Motion

Contributions:

- Extend DCM (Capture Point) to 3D
- Method for real-time planning and control of DCM trajectories in 3D
- Feasibility of the commanded leg forces is guaranteed (the problem of underactuated is addressed)
- The basic DCM trajectory generator is extended to produce continuous leg force profiles and to facilitate the use of toe-off motion during double support.

$$\ddot{\boldsymbol{x}} = \frac{1}{m}\boldsymbol{F} = \frac{1}{m}(\boldsymbol{F}_g + \boldsymbol{F}_{\text{ext}}) = \boldsymbol{g} + \frac{1}{m}\boldsymbol{F}_{\text{ext}}$$

Centroidal dynamics

$$\boldsymbol{\xi} = \boldsymbol{x} + b\dot{\boldsymbol{x}} \quad \Rightarrow \quad \dot{\boldsymbol{x}} = -\frac{1}{b}(\boldsymbol{x} - \boldsymbol{\xi})$$

CoM follows DCM
Stable dynamics

$$\dot{\boldsymbol{\xi}} = -\frac{1}{b}\boldsymbol{x} + \frac{1}{b}\boldsymbol{\xi} + \frac{b}{m}\boldsymbol{F}$$

DCM dynamics

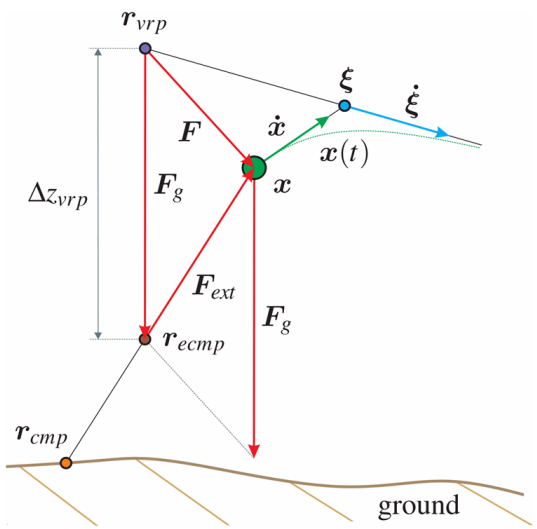

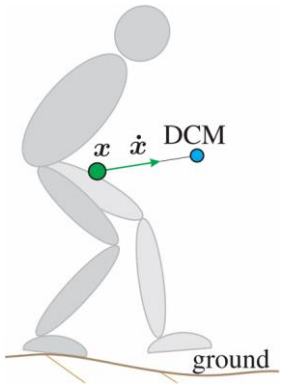

Let $\boldsymbol{F}_{ext} = s\,(\boldsymbol{x} - \boldsymbol{r}_{ecmp}) \Rightarrow \boldsymbol{F} = \boldsymbol{F}_{ext} + \boldsymbol{F}_g = s\,(\boldsymbol{x} - \boldsymbol{r}_{ecmp}) + m\boldsymbol{g}$

Substituting ***F*** in DCM dynamics we get:

$$\dot{\boldsymbol{\xi}} = \left(\frac{bs}{m} - \frac{1}{b}\right)\boldsymbol{x} + \frac{1}{b}\boldsymbol{\xi} - \frac{bs}{m}\boldsymbol{r}_{ecmp} + b\,\boldsymbol{g}$$

$$\dot{\boldsymbol{\xi}} = \frac{1}{b}\boldsymbol{\xi} - \underbrace{\frac{1}{b}\boldsymbol{r}_{ecmp} + b\,\boldsymbol{g}} = \frac{1}{b}(\boldsymbol{\xi} - \boldsymbol{r}_{vrp})$$

$$\begin{bmatrix}\dot{\boldsymbol{x}} \\ \dot{\boldsymbol{\xi}}\end{bmatrix} = \begin{bmatrix}-1/b & 1/b \\ 0 & 1/b\end{bmatrix}\begin{bmatrix}\boldsymbol{x} \\ \boldsymbol{\xi}\end{bmatrix} + \begin{bmatrix}0 \\ -1/b\end{bmatrix}\boldsymbol{r}_{vrp}$$

The virtual repellent point (VRP) encodes the effect of gravity and external forces in a single point

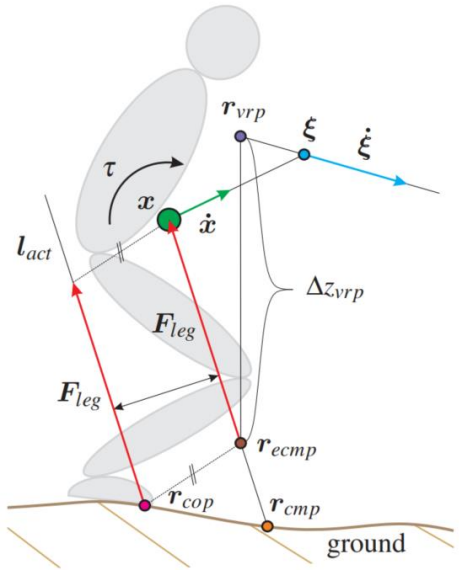

J. Englsberger, C. Ott and A. Albu-Schäffer, "Three-dimensional bipedal walking control using divergent component of motion", Proc. IEEE/RSJ Int. Conf. Intell. Robots Syst., pp. 2600-2607, 2013.
J. Englsberger, C. Ott and A. Albu-Schäffer, "Three-Dimensional Bipedal Walking Control Based on Divergent Component of Motion," in IEEE Transactions on Robotics, vol. 31, no. 2, pp. 355-368, April 2015, doi: 10.1109/TRO.2015.2405592.

Flashback..

Let us start from the equation of motion of the linear inverted pendulum, where all the mass is concentrated at the center of mass $\boldsymbol{p}_G$:

$$\ddot{\boldsymbol{p}}_G = \omega^2(\boldsymbol{p}_G - \boldsymbol{p}_Z)$$

We assume that the robot steps instantly at time $t = 0$ and maintains its ZMP $\boldsymbol{p}_Z$ at a constant location in its new foothold, so that $\boldsymbol{p}_Z$ is stationary. Since the natural frequency ω of the pendulum is also a model constant, we can solve this second-order linear differential equation as:

$$\boldsymbol{p}_G(t) = \boldsymbol{p}_Z + \frac{e^{\omega t}}{2}\left[\boldsymbol{p}_G(0) + \frac{\dot{\boldsymbol{p}}_G(0)}{\omega} - \boldsymbol{p}_Z\right] + \frac{e^{-\omega t}}{2}\left[\boldsymbol{p}_G(0) - \frac{\dot{\boldsymbol{p}}_G(0)}{\omega} - \boldsymbol{p}_Z\right]$$

This function is the sum of a stationary term $\boldsymbol{p}_Z$, a convergent term factored by $e^{-\omega t}$ that vanishes as $t \to \infty$, and a term factored by $e^{\omega t}$ that diverges as $t \to \infty$. Let us define the *capture point* as:

$$\boldsymbol{p}_C \stackrel{\text{def}}{=} \boldsymbol{p}_G + \frac{\dot{\boldsymbol{p}}_G}{\omega}$$

The divergent term in $\boldsymbol{p}_G(t)$ is then $e^{\omega t}/2(\boldsymbol{p}_C(0) - \boldsymbol{p}_Z)$. In particular, the *only* way for the center of mass trajectory to be bounded is for the stationary ZMP to be equal to the instantaneous capture point:

$$\boldsymbol{p}_Z = \boldsymbol{p}_C(0) \implies \boldsymbol{p}_G(t) \xrightarrow[t\to\infty]{} \boldsymbol{p}_C(0)$$

We can thus interpret the capture point as a point where the robot should step (shift its ZMP) in order to come (asymptotically) to a stop.

Recall

$$\ddot{x} = \frac{g}{z}x$$

$$x(t) = x(0)\cosh(t/T_c) + T_c\dot{x}(0)\sinh(t/T_c)$$

$$x_{capture} = \dot{x}\sqrt{\frac{z_0}{g}}$$

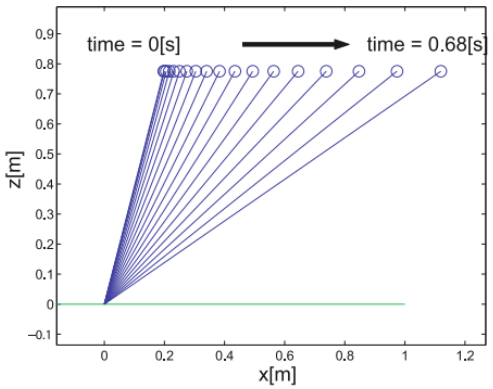

(d) $f = Mg/\cos\theta$: CoM accelerates while keeping the initial height

Source: https://scaron.info/robot-locomotion/capture-point.html

Three dimensional bipedal walking control using Divergent Component of Motion

Generation of DCM trajectory

Assumptions:

- Point feet
- No angular momentum variation about CoM
- No DSP
- No impacts during the transition

This means the stepping point, CoP and CMP are all coincident, and the kick force passes through CoM

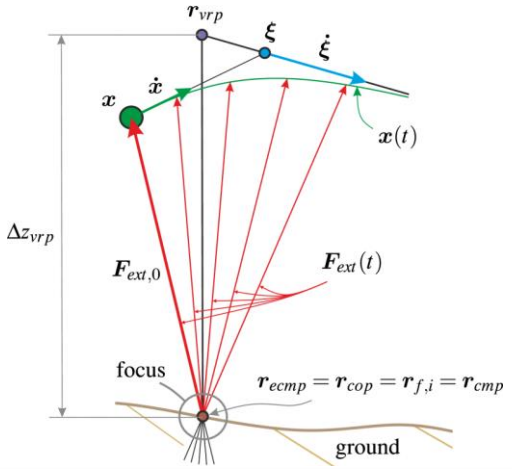

1. Define an average eCMP--VRP height difference: $r_{vrp} = r_{ecmp} + \left[0\ 0\ b^2 g\right]^T = r_{ecmp} + \left[0\ 0\ \Delta z_{vrp}\right]^T$

2. Define stepping points (over the given 3D terrain) and hence the VRPs

3. For a given step integrate to find the DCM trajectory: $\xi(t) = r_{vrp} + e^{t/b}\left(\xi_0 - r_{vrp}\right)$

4. Define the DCM position at the end of the step

$$\xi_{d,eos,i-1} = \xi_{d,ini,i} = r_{vrp,d,i} + e^{-\frac{t_{step}}{b}}\left(\xi_{d,eos,i} - r_{vrp,d,i}\right)$$

5. End step:

$$\xi_{d,eos,N-1} = r_{vrp,d,N}$$

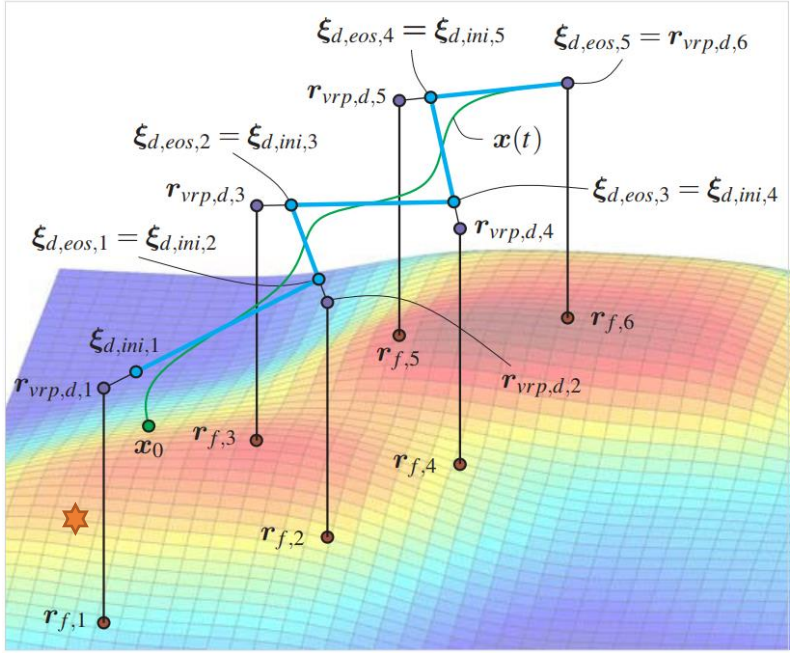

J. Englsberger, C. Ott and A. Albu-Schäffer, "Three-dimensional bipedal walking control using divergent component of motion", Proc. IEEE/RSJ Int. Conf. Intell. Robots Syst., pp. 2600-2607, 2013.
J. Englsberger, C. Ott and A. Albu-Schäffer, "Three-Dimensional Bipedal Walking Control Based on Divergent Component of Motion," in IEEE Transactions on Robotics, vol. 31, no. 2, pp. 355-368, April 2015, doi: 10.1109/TRO.2015.2405592.

Torque-Based Balancing for a Humanoid Robot Performing High-Force Interaction Tasks

- Use of gravito-inertial wrench cone to guarantee the feasibility of the balancing forces
- Balancing control should account for unknown perturbation forces that might destabilize the robot when performing the intended tasks

Dynamic Model

- Total of Ψ end effectors are split– balancing end effectors (bal) and interaction end effectors (int)

$$M \underbrace{\begin{pmatrix} \dot{\boldsymbol{v}}_c \\ \ddot{\boldsymbol{q}} \end{pmatrix}}_{\dot{\boldsymbol{\nu}}} + C \underbrace{\begin{pmatrix} \boldsymbol{v}_c \\ \dot{\boldsymbol{q}} \end{pmatrix}}_{\boldsymbol{\nu}} + \underbrace{\begin{pmatrix} m\boldsymbol{g}_0 \\ \boldsymbol{0} \end{pmatrix}}_{\boldsymbol{g}} = \begin{pmatrix} \boldsymbol{0} \\ \boldsymbol{\tau} \end{pmatrix} + \boldsymbol{\tau}_{\text{ext}}$$

(6+n) x 1

Equations of motion

$$\boldsymbol{v} = \begin{pmatrix} \boldsymbol{v}_{\text{bal}} \\ \boldsymbol{v}_{\text{int}} \end{pmatrix} = \begin{bmatrix} \boldsymbol{J}_{\text{bal}} \\ \boldsymbol{J}_{\text{int}} \end{bmatrix} \boldsymbol{\nu} = \boldsymbol{J}\boldsymbol{\nu}$$

Cartesian velocity of end effectors

$$\boldsymbol{\tau}_{\text{ext}} = \boldsymbol{J}^T \boldsymbol{F}_{\text{ext}}$$

Joint torques

(Old design) Controller based on cartesian compliance:

$$\boldsymbol{F}_{\text{bal}}^{\text{opt}} = \underset{\boldsymbol{F}_{\text{bal}}}{\operatorname{argmin}} \left(\boldsymbol{F}_{\text{bal}} - \boldsymbol{F}_{\text{bal}}^{\text{def}}\right)^T \boldsymbol{Q} \left(\boldsymbol{F}_{\text{bal}} - \boldsymbol{F}_{\text{bal}}^{\text{def}}\right)$$

$(1 \text{ x } 6\Psi)$

while satisfying CoP, friction and unilaterality of contact forces

$$\boldsymbol{\tau} = -\left[\bar{\boldsymbol{J}}_{\text{bal}}^T \quad \bar{\boldsymbol{J}}_{\text{int}}^T\right] \begin{pmatrix} \boldsymbol{F}_{\text{bal}}^{\text{opt}} \\ \boldsymbol{F}_{\text{int}} \end{pmatrix}$$

Joint torques can be determined from the optimized contact wrenches

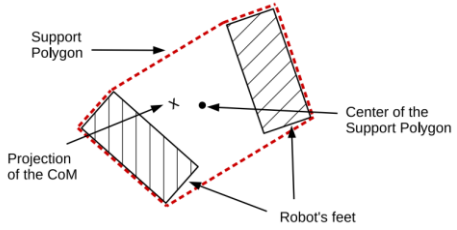

(New) Controller Design based on GIWC (an object of dimension 6)

Why? Support polygon computation in a multi-(out-of-plane)-contact scenario is complicated.

GIWC is a set of wrenches that the balancing end-effectors can apply for a particular pose $\boldsymbol{\Gamma}$

$$\boldsymbol{\xi}_i = \{\boldsymbol{F}_{\text{bal,i}} : \boldsymbol{A}_i \boldsymbol{F}_{\text{bal,i}} \leq \boldsymbol{b}_i\} \xrightarrow{\text{Minkowski-Sum}} \boldsymbol{\xi} = \{{}^w\boldsymbol{F}_{\text{bal,t}} : \boldsymbol{A}\,{}^w\boldsymbol{F}_{\text{bal,t}} \leq \boldsymbol{b}\}$$

ξ_i are the faces of the polyhedron

All quantities written in world frame

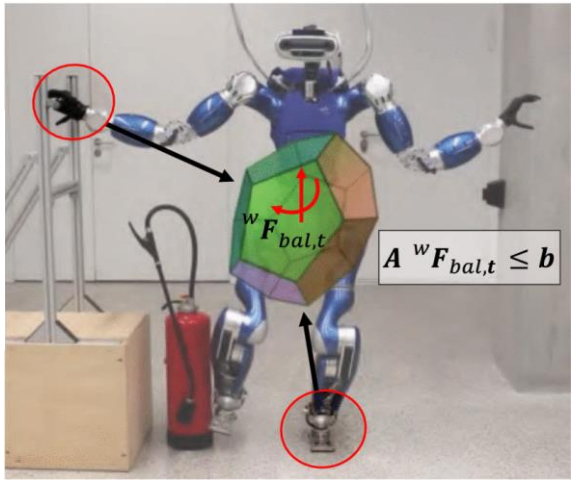

A schematic of a polyhedron of feasible wrenches

F. Abi-Farraj, B. Henze, C. Ott, P. R. Giordano and M. A. Roa, "Torque-Based Balancing for a Humanoid Robot Performing High-Force Interaction Tasks," in *IEEE Robotics and Automation Letters*, vol. 4, no. 2, pp. 2023-2030, April 2019, doi: 10.1109/LRA.2019.2898041.

Torque-Based Balancing for a Humanoid Robot Performing High-Force Interaction Tasks

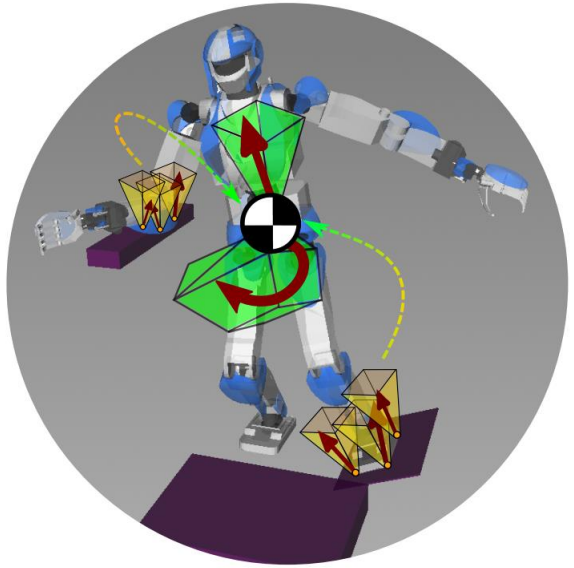

More on GIWC…

- Problems of ZMP criterion
  - Cannot handle non-coplanar supports
  - Only the tilting moments are constrained by ZMP criterion. New conditions are required for constraining M_z and F_X, F_Y, and F_z. These are significant in low friction scenarios.
- GIWC can be thought of as a general contact stability criterion-- a "ZMP for non-coplanar contacts"
- It needs to be computed only once per pose.

Contact switching

- An autonomous contact-switching algorithm that handles the weight shifting process in the wrench space (when the end effectors are already in position)

$$
{}^{w}\boldsymbol{F}_{\mathrm{bal},d} = {}^{w}\boldsymbol{F}_{\mathrm{opt},1} \xrightarrow{\star}
\begin{array}{l}
\textbf{while } \alpha < 1 \textbf{ do} \\
\quad {}^{w}\boldsymbol{F}_{\mathrm{bal},d} = (1-\alpha)\,{}^{w}\boldsymbol{F}_{\mathrm{opt},1} + \alpha\,{}^{w}\boldsymbol{F}_{\mathrm{opt},2} \\
\quad \boldsymbol{F}_c = \boldsymbol{F}_{c,cs}({}^{w}\boldsymbol{F}_{\mathrm{bal},d}) \\
\quad \alpha = \alpha + \epsilon_\alpha \\
\textbf{end while}
\end{array}
\xrightarrow{\star} {}^{w}\boldsymbol{F}_{\mathrm{bal},d} = {}^{w}\boldsymbol{F}_{\mathrm{opt},2}
$$

Experiments

- Carrying a heavy box, Pushing a table, Interaction with the right foot, Automatic contact switching

https://ieeexplore.ieee.org/ielx7/7083369/8581687/8637046/RAL_video_FirasRoa.mp4?arnumber=8637046

Next step:

- The end effectors that are not stationary. Example of a task: Opening a spring-loaded door.

F. Abi-Farraj, B. Henze, C. Ott, P. R. Giordano and M. A. Roa, "Torque-Based Balancing for a Humanoid Robot Performing High-Force Interaction Tasks," in *IEEE Robotics and Automation Letters*, vol. 4, no. 2, pp. 2023-2030, April 2019, doi: 10.1109/LRA.2019.2898041.

Caron, S., Pham, Q. C., & Nakamura, Y. (2015, July). Leveraging Cone Double Description for Multi-contact Stability of Humanoids with Applications to Statics and Dynamics. In Robotics: science and systems (Vol. 11, pp. 1-9).

An impact dynamics model and sequential optimization to generate impact motions for a humanoid robot

Impulsive motions enable the application of forces higher than actuator limits

Propose a way to generate impact motions for a humanoid robot while keeping a balance

The equation of motion for the humanoid: (Including the actuator dynamics)

$$\begin{bmatrix} \boldsymbol{H}_b & \boldsymbol{H}_{bm} \\ \boldsymbol{H}_{bm}^{\mathrm{T}} & \widehat{\boldsymbol{H}}_m \end{bmatrix} \begin{bmatrix} \dot{\boldsymbol{v}}_b \\ \ddot{\boldsymbol{q}} \end{bmatrix} + \begin{bmatrix} \boldsymbol{c}_b \\ \boldsymbol{c}_m \end{bmatrix} = \begin{bmatrix} \boldsymbol{F}_b \\ \boldsymbol{G}\boldsymbol{\tau}_m \end{bmatrix} + \sum_j^{N_{cp}} \begin{bmatrix} \boldsymbol{J}_{bhj}^{\mathrm{T}} \\ \boldsymbol{J}_{mhj}^{\mathrm{T}} \end{bmatrix} \boldsymbol{F}_{hi} + \begin{bmatrix} \boldsymbol{g}_b \\ \boldsymbol{g}_m \end{bmatrix}$$

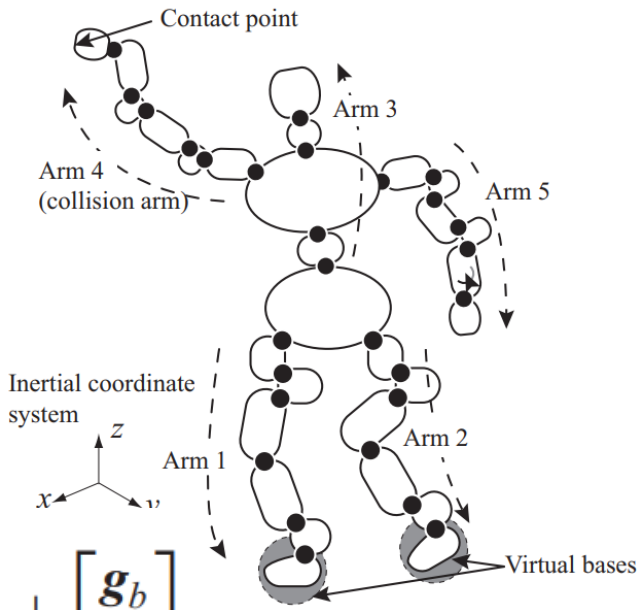

Impact dynamics:

Assumptions:

A single impact occurs only at a single point (on either of the arms say)

The motor torque is constant at the moment of impact

$$\begin{bmatrix} \boldsymbol{H}_b & \boldsymbol{H}_{bm} \\ \boldsymbol{H}_{bm}^{\mathrm{T}} & \widehat{\boldsymbol{H}}_m \end{bmatrix} \begin{bmatrix} \dot{\boldsymbol{v}}_b \\ \ddot{\boldsymbol{q}} \end{bmatrix} + \begin{bmatrix} \boldsymbol{c}_b \\ \boldsymbol{c}_m \end{bmatrix} = \begin{bmatrix} \boldsymbol{F}_{b\delta} \\ \boldsymbol{\tau}_{res} \end{bmatrix} + \begin{bmatrix} \boldsymbol{J}_{bh}^{\mathrm{T}} \\ \boldsymbol{J}_{mh}^{\mathrm{T}} \end{bmatrix} \boldsymbol{F}_{h\delta} \quad \Bigg| \quad \begin{bmatrix} \boldsymbol{0} \\ \boldsymbol{0} \end{bmatrix} = \begin{bmatrix} \boldsymbol{F}_{b0} \\ \boldsymbol{\tau}_0 \end{bmatrix} + \sum_j^{N_{cp}} \begin{bmatrix} \boldsymbol{J}_{bhj}^{\mathrm{T}} \\ \boldsymbol{J}_{mhj}^{\mathrm{T}} \end{bmatrix} \boldsymbol{F}_{hi0} + \begin{bmatrix} \boldsymbol{g}_b \\ \boldsymbol{g}_m \end{bmatrix}$$

$$\begin{bmatrix} \boldsymbol{H}_b & \boldsymbol{H}_{bm} \\ \boldsymbol{H}_{bm}^{\mathrm{T}} & \widehat{\boldsymbol{H}}_m \end{bmatrix} \begin{bmatrix} \Delta\boldsymbol{v}_b \\ \Delta\dot{\boldsymbol{q}} \end{bmatrix} = \int_{t_0}^{t_0+\Delta t} \left\{ \begin{bmatrix} \boldsymbol{F}_{b\delta} \\ \boldsymbol{\tau}_{res} \end{bmatrix} + \begin{bmatrix} \boldsymbol{J}_{bh}^{\mathrm{T}} \\ \boldsymbol{J}_{mh}^{\mathrm{T}} \end{bmatrix} \boldsymbol{F}_{h\delta} - \begin{bmatrix} \boldsymbol{c}_b \\ \boldsymbol{c}_m \end{bmatrix} \right\} dt$$

Big matrix to invert!

$$= \begin{bmatrix} \overline{\boldsymbol{F}}_{b\delta}\Delta t \\ \boldsymbol{\tau}_{res}\cancel{\Delta t} \end{bmatrix} + \begin{bmatrix} \boldsymbol{J}_{bh}^{\mathrm{T}} \\ \boldsymbol{J}_{mh}^{\mathrm{T}} \end{bmatrix} \overline{\boldsymbol{F}}_{h\delta}\Delta t - \begin{bmatrix} \boldsymbol{c}_b\cancel{\Delta t} \\ \boldsymbol{c}_m\cancel{\Delta t} \end{bmatrix},$$

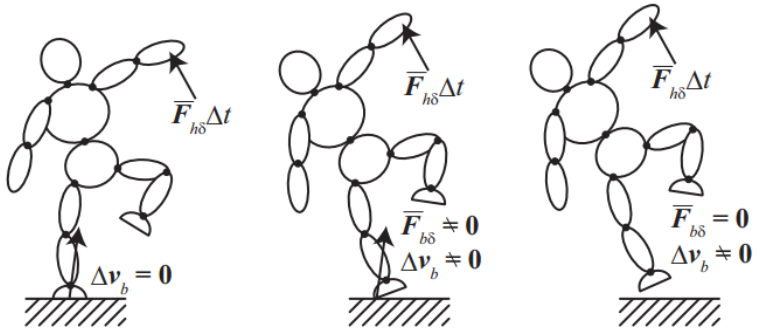

The concept of virtual mass (defined a pervious publication) is used to estimate the impulsive forces to reduce the computational load.

The maximum error of impulse is estimated about 6% for HRP-2 during a hammering operation. Further details are skipped at the moment.

A. Konno, T. Myojin, T. Tsujita and M. Uchiyama, "Optimization of impact motions for humanoid robots," *2008 IEEE/RSJ International Conference on Intelligent Robots and Systems*, 2008, pp. 647-652, doi: 10.1109/IROS.2008.4650751.

An impact dynamics model and sequential optimization to generate impact motions for a humanoid robot

An optimum impact motion is expected to maximize the impact force as well as stability margin.

Example under study: Karate chop motion

Motion plan:

1. Find appropriate pose and velocity required for the impact.
2. Initial and final positions are generated as a result of decelerations from the impact position

Minimize angular momentum of the humanoid, maximize the impact:

$$J_A = w_A\left(1 - \frac{M_{eq}V_n}{(M_{eq}V_n)_{max}}\right)^2 + (1 - w_A)\left(\frac{L_y}{L_{y,max}}\right)^2$$

$$J_{BC} = w_{BC}\widehat{\dot{\boldsymbol{q}}}^T\widehat{\dot{\boldsymbol{q}}} + (1 - w_{BC})\left(\frac{L_y}{L_{y,max}}\right)^2$$

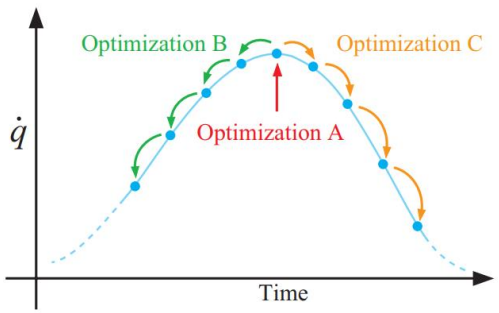

Conceptual sketch of the proposed motion generation.

Experiment and results: Higher impulses applied, 5mm board was broken 90% of times as compared to 10%

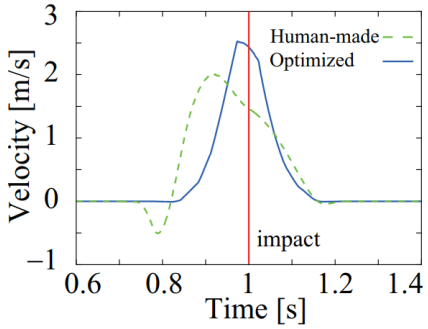

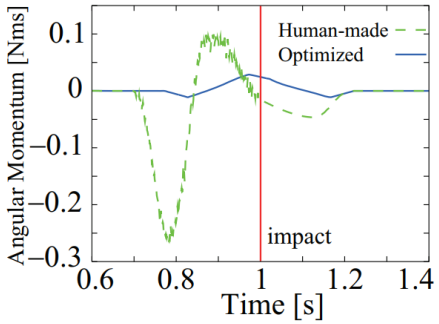

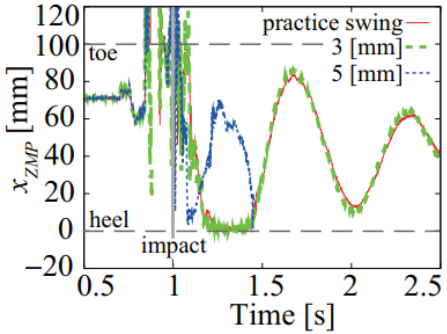

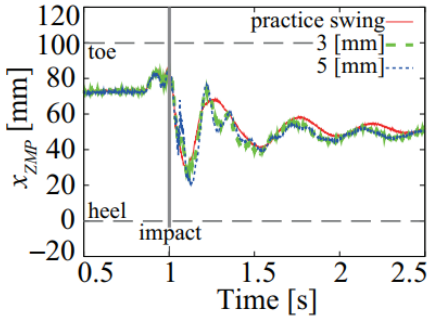

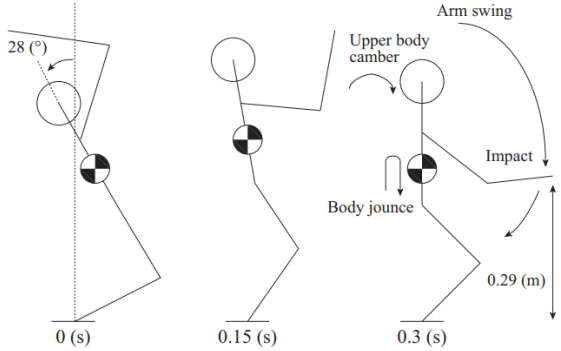

Avenues to extension

- Balancing strategy for impulsive (unplanned) disturbances
- Applying impulsive force with one arm while using a support with another
- Same application with humanoid standing on uneven terrain

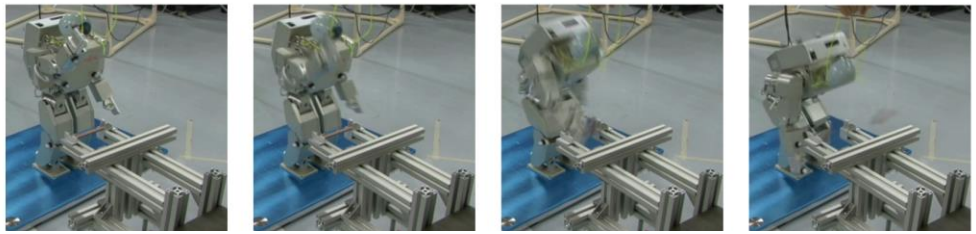

A. Konno, T. Myojin, T. Tsujita and M. Uchiyama, "Optimization of impact motions for humanoid robots," *2008 IEEE/RSJ International Conference on Intelligent Robots and Systems*, 2008, pp. 647-652, doi: 10.1109/IROS.2008.4650751.

Tools for simulating humanoid robot dynamics: A survey based on user feedback

- Codes used for robot simulations have their origins in computer graphics community mainly built for video-games.
- As the graphics of video-games got more and more realistic, kinematics based motions evolved to physics based motions requiring real-time dynamics simulations.
- Today, still there exist unrealistic accelerations in games.

Challenges/ Needs for robotics simulation and control:

- Fast integration of equations of motion (simulation) with guaranteed convergence
- Kinematic collision detection
- Accurate computation of contact forces. Otherwise physically unfeasible forces lead to unrealistic behaviour
- Capability to simulate variable impedance or soft actuators

Physics Engines

1. ODE
2. PhysX
3. Bullet
4. DART
5. MuJoCo
6. MOBY

System simulators

1. Gazebo
2. ARGoS
3. V-Rep
4. SimBody
5. OpenHRP

Speciality

1. Robotran: closed form equations
2. OpenRave: motion planner

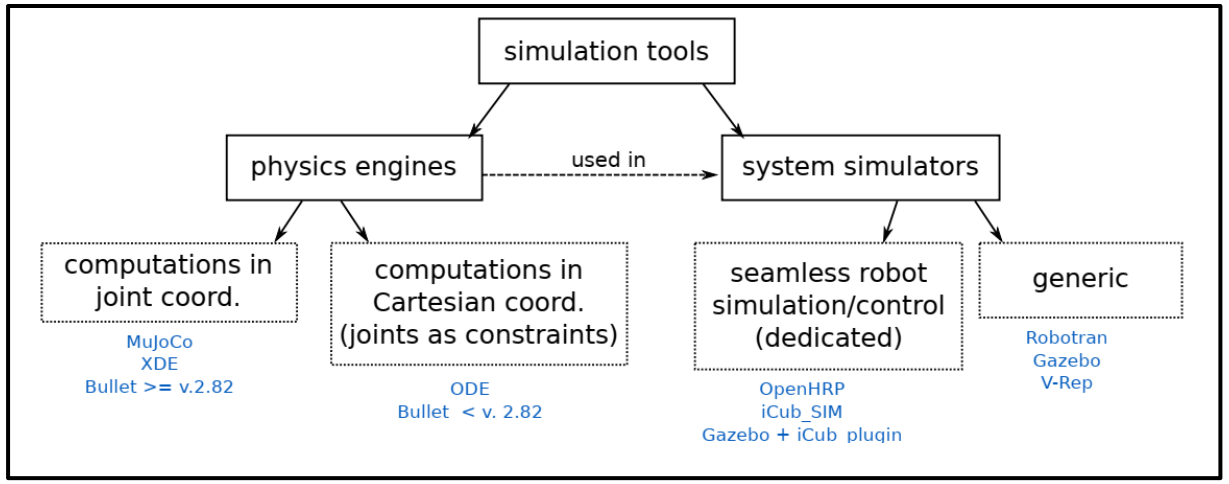

Physics engines (libraries)

- ODE
  - With all joints and contacts modelled as constraints, system-level information like inertia matrix, velocity jacobians etc., is not available.
- Bullet
  - Version 2.82 and later support joint coordinates, implement Featherstone's Articulated Body algorithm and have an LCP solver for contacts with the environment
- MuJoCo
  - Tailored for robot simulation and implementing control
  - Supports variable impedance actuators
  - Has a solver for computing contact forces (impulsive incl.)

S. Ivaldi, J. Peters, V. Padois and F. Nori, "Tools for simulating humanoid robot dynamics: A survey based on user feedback," 2014 IEEE-RAS International Conference on Humanoid Robots, 2014, pp. 842-849, doi: 10.1109/HUMANOIDS.2014.7041462.

Tools for simulating humanoid robot dynamics: A survey based on user feedback

Research area	Users	Most used software	Other used software
Humanoid Robotics	32	(4) ODE, (3) Gazebo, Robotran, OpenRave, Arboris-Python, (2) XDE, iCub_SIM	(1) Drake, MapleSim, MuJoCo, OpenSIM, RoboticsLab, SL, Vortex, V-Rep, Webots, own code

Robot	Users	Most used software	Other used software
Wheeled vehicle	28 (24%)	(4) Gazebo, V-Rep	(3) ARGoS, (2) Morse, Webots, Vortex, (1) Autodesk, Matlab/Simulink, Adams, trep, XDE, SIMPACK, Autolev, RCIS, Bullet, RoboticsLab, own code
Multi-legged robot	18 (15%)	(4) ODE	(2) SL, Bullet, Webots, (1) V-Rep, Adams, Drake, trep, MuJoCo, SIMPACK, Autolev, RoboticsLab
Quadrotor/quadcopter	17 (14%)	(4) Gazebo, ARGoS	(2) V-Rep, (1) Morse, Matlab/Simulink, Drake, ODE, trep, Webots, RoboticsLab
PR2	14 (12%)	(3) OpenRave	(2) Gazebo, MuJoCo, (1) Bullet, V-Rep, Drake, Morse, ODE, RoboticsLab, own code
iCub	13 (11%)	(3) Arboris-Python	(2) ODE, Robotran, iCub_SIM, (1) Bullet, Gazebo, OpenSim, XDE
Atlas	10 (8%)	**(6) Gazebo**	(2) MuJoCo, (1) Autolev, Drake
Nao	8 (7%)	(3) V-Rep	(2) MuJoCo, (1) ODE, OpenRave, Webots
HRP2/4	6 (5%)	(2) MuJoCo	(2) own code, (1) ODE, Drake
Hubo	3 (3%)		(1) RoboticsLab, ODE, Drake
Asimo	3 (3%)		(1) Arboris-Python, V-Rep, own code
Reem-C	1 (1%)	(1) Gazebo	

TABLE IX: Some of the most simulated robots - the colored cells indicate humanoid robots.

A few stats of the survey:

- >62% PhD holders, from US -19%, France-17%, Italy-10%, Germany-9%
- 66% use GNU/Linux systems
- 26% working on humanoid projects
- Aim to simulate robot interaction with environment, locomotion and navigation. Test controllers on virtual robots before implementing physically.

Other points:

- A lot of in-demand open source tools were also the most abandoned software after test use. Either due to poor support or availability of better ones.
- 29% of the times, a tool was chosen based on laboratory inheritance.
- Use case for iCub humanoid suggests ODE does not perform well in contact problems.

S. Ivaldi, J. Peters, V. Padois and F. Nori, "Tools for simulating humanoid robot dynamics: A survey based on user feedback," 2014 IEEE-RAS International Conference on Humanoid Robots, 2014, pp. 842-849, doi: 10.1109/HUMANOIDS.2014.7041462.

Recursive Dynamics Simulator (ReDySim)

- A MATLAB-based recursive solver for dynamic analysis of robotic and multibody systems
- Consists of efficient inverse and forward dynamics algorithms for open as well as closed-loop multi-body systems
- ReDySim has the capability to incorporate any control algorithm and trajectory planner with utmost ease

- The library consists for three modules
  1. **Basic module: fixed base systems**
     - Open loop and closed loop multi-body systems
     - Also has a GUI version
  2. **Specialized module: floating base systems**
     - Sub-module for space robots
     - Sub-module for legged robots
       - For systems frequently interacting with environment
  3. **Symbolic module:** Open loop fixed and floating base systems
     - Generate closed form equations of motion only for open loop mechanisms

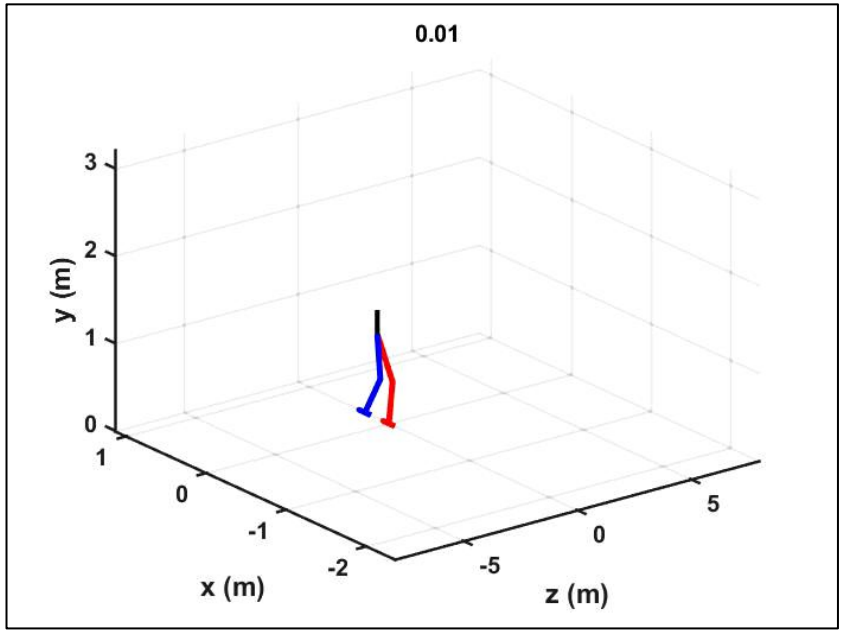

Two second forward dynamics simulation of a planar biped walking on hard ground. This is an inbuilt example in ReDySim . It took 15 sec on an Intel® Core™ i7 7500U CPU @ 2.7-3.4 GHz!

http://redysim.weebly.com/

Shah S. V., Saha S. K., and Dutt J. K., "Dynamics of Tree-type Robotic Systems," Intelligent Systems, Control and Automation: Science and Engineering Bookseries, Springer, Netherlands (ISBN 978-94-007-5005-0).

Analysis, gaps, and avenues for research

Broad topic:

- Full body humanoids performing some activity
- Dynamics simulation and control strategy

Approach:

- The task should be useful in our context, it may not be just about pushing the state-of-the-art capabilities. △
- Take up tasks that can be implemented on robot hardware available to us. ○

Areas thoroughly studied:

- Walking on flat ground, mildly uneven rigid and compliant terrain
- Simple manipulations of objects
- Balancing in presence of external disturbances while standing on flat ground, moving ground
- Multi-contact balancing while standing on flat ground

Avenues for research:

- Tasks involving impact
  - Use the robot to apply forces greater than actuators' stalling force/torque limits △
  - Strategies to minimize the effect of external impacts on actuators △ ○
- Performing tasks on uneven terrain
  - <u>Standing up from fallen position</u> △ ○
  - Locomotion while taking support of the environment
- <u>Improvising pre-planned tasks in case of an actuator failure</u> △ ○
- Tasks involving multiple contacts
  - Interaction with dynamic environment. E.g. opening/ closing a door △
  - Performing a task such as lifting a box along with human △

Kinematic walking simulation of a 8 DOF biped

```
Show[{12, 13, 141, 142, 15, 16, ground}, PlotRange → {{-1, 4}, {-0.5,
{{u, 1}, 1, Length[allthlist], 1}, AnimationRepetitions → 1, Animati
```

Out[80]=

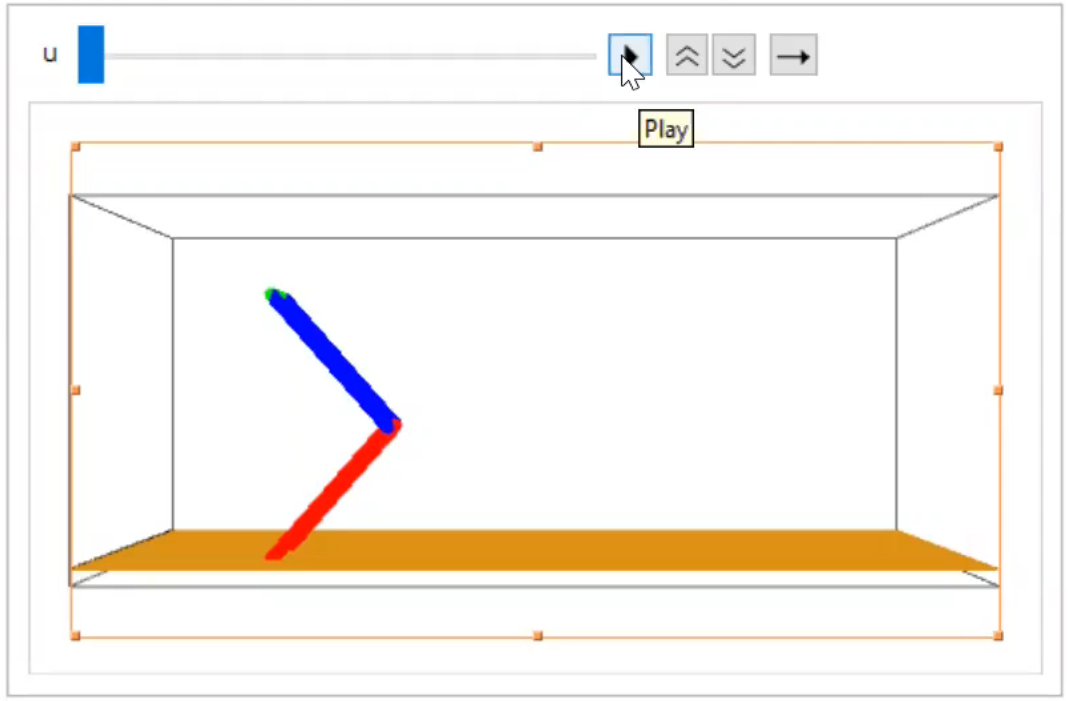

Hardware for experiments

22 DOF robot
400 mm height, ~2.2 kg
INR 2L

Acknowledgements

I would like to thank Sunil for helping me understand concepts in the dynamics of humanoids.

Thank you, Sushant and James for helping me understand the format of the SOTA presentation.

I would like to thank my supervisor, Prof Ashish Dutta for the fruitful discussions.

References

1. Saeedvand, S., Jafari, M., Aghdasi, H., & Baltes, J. (2019). A comprehensive survey on humanoid robot development. *The Knowledge Engineering Review, 34*, E20. doi:10.1017/S0269888919000158
2. Ficht, G., Behnke, S. Bipedal Humanoid Hardware Design: a Technology Review. *Curr Robot Rep* **2,** 201–210 (2021). https://doi.org/10.1007/s43154-021-00050-9
3. Ghosal. (2006) Robotics: Fundamental Concepts and Analysis (pp. 151-219), New Delhi, Oxford University Press.
4. Greenwood, D. T. (1988). *Principles of dynamics* (pp. 239-298). Englewood Cliffs, NJ: Prentice-Hall.
5. Sarkar, A., & Dutta, A. (2015). 8-DoF biped robot with compliant-links. Robotics and Autonomous Systems, 63, 57-67.
6. Kajita S., Hirukawa H., Harada K., Yokoi K. (2014) Generation of Whole Body Motion Patterns. In: Introduction to Humanoid Robotics. Springer Tracts in Advanced Robotics, vol 101. Springer, Berlin, Heidelberg. https://doi.org/10.1007/978-3-642-54536-8_5
7. Kajita S., Hirukawa H., Harada K., Yokoi K. (2014) Biped Walking. In: Introduction to Humanoid Robotics. Springer Tracts in Advanced Robotics, vol 101. Springer, Berlin, Heidelberg. https://doi.org/10.1007/978-3-642-54536-8_4
8. S. Kajita, K. Tani and A. Kobayashi, "Dynamic walk control of a biped robot along the potential energy conserving orbit," *EEE International Workshop on Intelligent Robots and Systems, Towards a New Frontier of Applications*, 1990, pp. 789-794 vol.2, doi: 10.1109/IROS.1990.262497.
9. S. Kajita and K. Tani, "Study of dynamic biped locomotion on rugged terrain-derivation and application of the linear inverted pendulum mode," *Proceedings. 1991 IEEE International Conference on Robotics and Automation*, 1991, pp. 1405-1411 vol.2, doi: 10.1109/ROBOT.1991.131811.
10. S. Kajita, F. Kanehiro, K. Kaneko, K. Yokoi and H. Hirukawa, "The 3D linear inverted pendulum mode: a simple modeling for a biped walking pattern generation," Proceedings 2001 IEEE/RSJ International Conference on Intelligent Robots and Systems. Expanding the Societal Role of Robotics in the the Next Millennium (Cat. No.01CH37180), 2001, pp. 239-246 vol.1, doi: 10.1109/IROS.2001.973365.
11. S. Kajita, F. Kanehiro, K. Kaneko, K. Fujiwara, K. Yokoi and H. Hirukawa, "A realtime pattern generator for biped walking," *Proceedings 2002 IEEE International Conference on Robotics and Automation (Cat. No.02CH37292)*, 2002, pp. 31-37 vol.1, doi: 10.1109/ROBOT.2002.1013335.
12. J. Pratt, J. Carff, S. Drakunov and A. Goswami, "Capture Point: A Step toward Humanoid Push Recovery," 2006 6th IEEE-RAS International Conference on Humanoid Robots, 2006, pp. 200-207, doi: 10.1109/ICHR.2006.321385.
13. M. A. Ali, H. Andy Park and C. S. G. Lee, "Closed-form inverse kinematic joint solution for humanoid robots," *2010 IEEE/RSJ International Conference on Intelligent Robots and Systems*, 2010, pp. 704-709, doi: 10.1109/IROS.2010.5649842.
14. S. Crews and M. Travers, "Energy Management Through Footstep Selection For Bipedal Robots," in IEEE Robotics and Automation Letters, vol. 5, no. 4, pp. 5485-5493, Oct. 2020, doi: 10.1109/LRA.2020.3003235.
15. Miyazaki, F., and Arimoto, S. (December 1, 1980). "A Control Theoretic Study on Dynamical Biped Locomotion." ASME. *J. Dyn. Sys., Meas., Control*. December 1980; 102(4): 233–239.
16. Luh, J. Y. S., Walker, M. W., and Paul, R. P. C. (June 1, 1980). "On-Line Computational Scheme for Mechanical Manipulators." ASME. *J. Dyn. Sys., Meas., Control*. June 1980; 102(2): 69–76. https://doi.org/10.1115/1.3149599
17. Featherstone R. (2008) Dynamics of Rigid Body Systems. In: Rigid Body Dynamics Algorithms. Springer, Boston, MA. https://doi.org/10.1007/978-1-4899-7560-7_3

P.T.O.

References

18. Featherstone R. (2008) Dynamics of Rigid Body Systems. In: Rigid Body Dynamics Algorithms. Springer, Boston, MA. https://doi.org/10.1007/978-1-4899-7560-7_3
19. Shah S.V., Saha S.K., Dutt J.K. (2013) Dynamics of Robotic Systems. In: Dynamics of Tree-Type Robotic Systems. Intelligent Systems, Control and Automation: Science and Engineering, vol 62. Springer, Dordrecht. https://doi.org/10.1007/978-94-007-5006-7_2
20. M. Abdallah and A. Goswami, "A Biomechanically Motivated Two-Phase Strategy for Biped Upright Balance Control," Proceedings of the 2005 IEEE International Conference on Robotics and Automation, 2005, pp. 1996-2001, doi: 10.1109/ROBOT.2005.1570406.
21. Orin, D.E., Goswami, A. & Lee, SH. Centroidal dynamics of a humanoid robot. *Auton Robot* **35,** 161–176 (2013). https://doi.org/10.1007/s10514-013-9341-4
22. Lee, SH., Goswami, A. A momentum-based balance controller for humanoid robots on non-level and non-stationary ground. Auton Robot 33, 399–414 (2012). https://doi.org/10.1007/s10514-012-9294-z
23. S. -H. Lee and A. Goswami, "Reaction Mass Pendulum (RMP): An explicit model for centroidal angular momentum of humanoid robots," Proceedings 2007 IEEE International Conference on Robotics and Automation, 2007, pp. 4667-4672, doi: 10.1109/ROBOT.2007.364198.
24. A. Dasgupta and Y. Nakamura, "Making feasible walking motion of humanoid robots from human motion capture data," Proceedings 1999 IEEE International Conference on Robotics and Automation (Cat. No.99CH36288C), 1999, pp. 1044-1049 vol.2, doi: 10.1109/ROBOT.1999.772454.
25. S. Ivaldi, J. Peters, V. Padois and F. Nori, "Tools for simulating humanoid robot dynamics: A survey based on user feedback," *2014 IEEE-RAS International Conference on Humanoid Robots*, 2014, pp. 842-849, doi: 10.1109/HUMANOIDS.2014.7041462.
26. Vukobratović, Miomir, and Branislav Borovac. "Zero-moment point—thirty five years of its life." International journal of humanoid robotics 1, no. 01 (2004): 157-173.
27. P. Sardain and G. Bessonnet, "Forces acting on a biped robot. Center of pressure-zero moment point," in IEEE Transactions on Systems, Man, and Cybernetics - Part A: Systems and Humans, vol. 34, no. 5, pp. 630-637, Sept. 2004, doi: 10.1109/TSMCA.2004.832811.
28. Mitobe, K., Capi, G., & Nasu, Y. (2000). Control of walking robots based on manipulation of the zero moment point. Robotica, 18(6), 651-657. doi:10.1017/S0263574700002708
29. Kouchaki, E., Wu, C. Q., & Sadigh, M. J. (2012). Effects of constraints on standing balance control of a biped with toe-joints. International Journal of Humanoid Robotics, 9(03), 1250016.
30. J. Englsberger *et al*., "Overview of the torque-controlled humanoid robot TORO," *2014 IEEE-RAS International Conference on Humanoid Robots*, 2014, pp. 916-923, doi: 10.1109/HUMANOIDS.2014.7041473.
31. J. Englsberger, C. Ott and A. Albu-Schäffer, "Three-Dimensional Bipedal Walking Control Based on Divergent Component of Motion," in IEEE Transactions on Robotics, vol. 31, no. 2, pp. 355-368, April 2015, doi: 10.1109/TRO.2015.2405592.
32. F. Abi-Farraj, B. Henze, C. Ott, P. R. Giordano and M. A. Roa, "Torque-Based Balancing for a Humanoid Robot Performing High-Force Interaction Tasks," in IEEE Robotics and Automation Letters, vol. 4, no. 2, pp. 2023-2030, April 2019, doi: 10.1109/LRA.2019.2898041.
33. A. Konno, T. Myojin, T. Tsujita and M. Uchiyama, "Optimization of impact motions for humanoid robots," *2008 IEEE/RSJ International Conference on Intelligent Robots and Systems*, 2008, pp. 647-652, doi: 10.1109/IROS.2008.4650751.
34. https://robots.ieee.org/robots/
35. https://scaron.info

Thank you!

www.mad4machines.com

vyankatesh20@iitk.com